INCORPORATING SPATIAL AND TEMPORAL VARIATION OF WATERSHED RESPONSE IN A GIS-BASED HYDROLOGIC MODEL

by
Mohammad Al-Smadi

Thesis submitted to the Faculty of the Virginia Polytechnic Institute and State University
in partial fulfillment of the requirement for the degree of

Master of Science
In
Biological Systems Engineering

Dr. Conrad D. Heatwole, Chair
Dr. Mary Leigh Wolfe
Dr. Laurence W. Carstensen Jr.
Dr. John V. Perumpral, Department Head

November 20, 1998
Blacksburg, VA

INCORPORATING SPATIAL AND TEMPORAL VARIATION OF WATERSHED RESPONSE IN A GIS-BASED HYDROLOGIC MODEL

by
Mohammad Al-Smadi

(ABSTRACT)

The hydrograph at the watershed outlet was simulated using the time-area curve concept implemented in a geographic information system (GIS). The goal of this study was to determine if hydrograph prediction accuracy would be improved by accounting for spatial and temporal variation of excess rainfall. Three models with different methods of estimating excess rainfall were developed: the Distributed Curve Number (DCN) model uses a CN for each cell, generating spatially distributed excess rainfall using the Soil Conservation Services curve number method (SCS, 1972); the Uniform Curve Number (UCN) model uses a single "average" CN for the whole watershed, thus generating a uniform excess rainfall; the Phi (Φ) index model which uses the Φ-index method to generate uniform excess rainfall.

With the aid of a GIS, the cumulative flow time to the watershed outlet is estimated for each cell in the watershed and the isochrones of equal travel time are developed. The time-area curve is developed in the form of an S curve. The spatially distributed 1-hr unit hydrograph is derived from the S curve as the difference between the S curve and its value lagged by 1-hr. The models used in this study describe the physical processes and flow mechanisms. They also reflect effects of watershed characteristics (slope, landuse, soil drainage potential) and excess rainfall intensity on the resulting hydrograph at the watershed outlet. Surface flow is divided into channel flow and

overland flow based on the upstream drainage area. Flow is routed to the watershed outlet through a channel network derived from the watershed Digital Elevation Model (DEM).

The models developed were tested against observed rainfall-runoff data from the 1153-ha Virginia Piedmont watershed (Owl Run). A total of 30 storms were simulated, with statistical comparison of peak flow rate, time to peak flow rate, and the hydrograph shape. The hydrograph shape was compared both visually and statistically. Results indicated that the two models which account for temporal variation in excess rainfall (DCN and UCN) predicted the output hydrograph much more accurately than the Phi model which lacks the ability to capture the temporal variation of excess rainfall. For this watershed, results showed that the spatial variability in excess rainfall which was accounted for by the DCN model did not improve the prediction accuracy over the UCN model which lacks that ability. However, a sensitivity analysis for the effect of the spatial distribution of the excess rainfall indicated that can be a significant effect of spatial distribution on the predicted hydrograph.

Keywords: *peak flow rate, time to peak flow rate, geographic information system, time-area curve, hydrograph shape, hydrologic modeling, spatial variability, temporal variability, excess rainfall.*

In the memory of my mother

Acknowledgments

First of all, thanks to Allah for making this possible. I would like also to thank Dr. Heatwole for his knowledge and support both academically and financially while serving as my major advisor. Thanks also go to my other committee members, Dr. Wolfe and Dr. Carstensen for their suggestions and support. I would also like to thank our department head Dr. Perumpral for making sure that, we, the graduate students in the Biological Systems Engineering Department are provided with adequate resources to conduct our research and the excellent education it provides.

Thanks also goes to the source of data I used in my study. The Virginia Department of Conservation and Recreation, Division of Soil and Water Conservation, Richmond, Virginia. Thanks also to the department's personnel who maintain the data and make it available, Jan Carr and Phil McClellan.

My father, thank you for being a great source of support and encouragement. Thanks to all my family, especially brother Yassein. Without you, this wouldn't have been possible. All my friends and fellow graduate students, thank you.

Table of Contents

List of Figures

List of Tables

1 Introduction

1.1 Background

Hydrologists and engineers have always been concerned with discharge rates resulting from rainfall. Not only measuring total volume of rainfall and resulting runoff is of interest, but also the process of transforming the rainfall history (hyetograph) into the streamflow history (hydrograph).

Two important hydrograph characteristics are the peak discharge rate and the time to peak. Information about these two parameters is needed to correctly design various hydraulic structures such as spillways, dams, levees, and culverts (Ajward, 1996). Unfortunately, the classic problem of predicting the previously mentioned parameters is usually difficult to resolve because many rivers and streams are ungaged, especially those in underdeveloped regions or remote areas. Even in the cases where watersheds are gaged, the period of record is often too short to allow accurate estimation of different hydraulic parameters (Muzik, 1993). Historical flow data is necessary to conduct flood frequency analysis. This type of analysis enables the user to predict flow rates with certain return periods. In cases where the historical flow records are not available, it becomes necessary to utilize another tool such as hydrologic models that incorporates watershed characteristics to predict flow rates at a given location in the watershed. The model proposed in this study is one such a model.

Extrapolation is sometimes done to estimate hydraulic parameters beyond the record length. Extrapolation is mainly done when the hydraulic structure's service life under study is longer than record length. Since precipitation records are generally more extensive than the streamflow records both in the number of rain gage locations and the length of records, synthetic flow records can be generated using rainfall-runoff models with the more available rainfall data (Ajward, 1996).

Standard methods of analysis usually take the form of empirical and/or statistical approaches. Simulation is a tool for predicting flow characteristics. In simulation, the response of a given watershed to a certain event is described using mathematical operations. The degree of complexity of the hydrological simulation model is greatly affected by the availability of data.

Hydrological simulation models can take the form of theoretical linkage between the geomorphology and hydrology. The geomorphological instantaneous unit hydrograph (GIUH) is one approach of this kind of model. The GIUH focuses on finding the watershed response given its geomorphological features. Another form of these hydrological simulation models is the physically based model, which can provide realistic estimates because, to a large extent, it represents the "real world" if the hydrological parameters are properly defined and used.

Hydrological models are also classified as either lumped or distributed. Lumped models ignore the spatial variability of precipitation, excess rainfall generation, and other related processes. The input, output, and parameter values of lumped models are spatially averaged. Even though lumped models are unable to account for internal variation of hydrological processes, they have the advantage of simplicity. Distributed hydrological

models on the other hand account for spatial variation of hydrological processes and parameters. This type of model has the potential to give more accurate results but is computationally intensive. These models also require a vast amount of data. While the intensive computational requirements of spatially distributed models can be met by the advancement in computer hardware and software, the lack of spatially distributed hydrologic data remains a constraint.

The spatially distributed input and analysis required by spatially distributed models can be met by incorporating a system that can manage data on a grid basis. An approach to handle this problem lies in using a raster-based geographic information system (GIS). During the 1980's and up to the present, using GIS in hydrology has become an important issue. The capabilities available in GISs enable the user to handle and analyze hydrological data more efficiently. Moreover, different scenarios of analysis can now be modeled in a relatively shorter time.

One method of transforming the rainfall volume into runoff volume is the US Department of Agriculture, Soil Conservation Services (SCS) runoff curve number (CN) method (SCS, 1972). This method is known for its simplicity. The CN is an index based on physical parameters of the watershed. It can be applied to gaged as well as ungaged watersheds. This method is able to reflect the effect of changes in landuse on runoff. The CN is determined from a combination of landuse and soil runoff potential (hydrologic soil group). CN values range between zero and 100. A value of 100 indicates that all rainfall is transformed into runoff (no abstractions), while for CN equal to zero, no direct runoff is generated.

Maidment (1993b) suggested the use of raster-based GIS to derive a spatially distributed unit hydrograph (SDUH) using the time-area diagram method. Maidment's conceptual procedure can be summarized as follows. Starting with the digital elevation model (DEM) of the watershed, flow direction is determined from each cell to one of its eight neighboring cells and is taken to be the direction of the maximum downhill slope. By estimating the flow velocity through each cell, the flow time through each cell can be obtained by dividing the flow distance by the flow velocity. The grid of the cumulative travel time to the watershed outlet can then be obtained by tracing the time grid from the watershed outlet to each upstream cell and storing the resulting value in each cell. From the cumulative travel time map the isochrones of the flow time for intervals of width Δt can be obtained. The time-area diagram is then determined by finding the incremental areas of cells between isochrones.

While several studies have used Maidment's concept, none of them provided a comparison between using spatially distributed excess rainfall versus uniformly distributed excess rainfall and the effect of this distribution on the output hydrographs obtained. Kilgore (1997) applied the SDUH concept to a watershed in Virginia. She used a spatially uniform excess rainfall as an input to her model. The results obtained by Kilgore using the SDUH model were "comparable" to those obtained using traditional synthetic unit hydrographs. In this study, the same watershed and some of the storms modeled by Kilgore (1997) were used.

1.2 Objectives

The overall objective of this study was to determine if the hydrograph prediction accuracy would be improved by accounting for spatial and temporal variation of excess rainfall.

Specific objectives of the study were:

[1] To determine the most appropriate model to be used to predict data for the watershed under study.

[2] To determine whether model's prediction accuracy is a function of storm size or season when storm occurred.

2 Literature Review

2.1 Introduction

Predicting runoff for ungaged watersheds is and has been a big concern for hydrologists and engineers. The proper design of a hydraulic structure to control floods and make use of water requires certain hydrologic data. Two necessary parameters are the peak flow rate and the time to peak resulting from a specific rainfall event. In many cases this kind of data is either entirely not available or not enough records are available both in time and space to enable predicting infrequent (extreme) events.

Generally, records for precipitation are more extensive in both the number of gages and the length of these records than are the records for flow. Knowing that rainfall and runoff can be related using mathematical functions, the lack of runoff data can be overcome by utilizing a rainfall-runoff relationship along with the more available rainfall data. The relationship between rainfall and the resulting runoff has been extensively studied, and many prediction methods of varying complexity have been developed. These mathematical functions are necessary to:

[1] design and manage hydraulic structures and projects ,

[2] predict future discharges, and,

[3] predict watershed response associated with changes in topography, landuse, and land cover (e.g. urbanization).

Wilson (1983) defined two kinds of factors affecting rainfall-runoff relationships. The first is climatic factors like intensity and duration of rainfall, form of precipitation, movement of the storm, and temperature. The second is physiographic factors like watershed area, slope and slope orientation, shape, length of water course, soil moisture conditions, land cover, and landuse. A certain degree of difficulty therefore, should be anticipated when making any attempt to accurately model such a complex relationship.

2.2 Model Selection

It should be kept in mind that no model can exactly represent the real world. Hydrologic models are no exception. So, any proposed model is an attempt to simplify the real world. Ajward (1996) stated that:

> *" In presenting an approximate view of reality, a model must remain simple enough to understand and easy to use, and yet complex enough to be representative of the system being modeled."*

A highly complex model might produce accurate and representative results. On the other hand such a model requires intensive input data and calibration and its mathematical complexity might result in making the problem formulation intractable. Conversely, a highly simplified model might be satisfied with minimum data, but the representation and results will most probably be inaccurate. As a result, the hydrologic model selected has to be a compromise between model complexity and input data availability (Overton and Meadows, 1976). Muzik (1996) stated that "it is widely held view among hydrologists that distributed modeling will not often yield superior results to

lumped modeling if not supported by data of sufficient quantity and quality". According to Linsley (1981), a hydrologic model should retain some properties such as accuracy, applicability, generality, and ease of use. Hydrologic models can be classified into three categories: empirical models; physical models; and conceptual models.

2.2.1 Empirical Models

Empirical models do not utilize physical laws to relate input to output. They are developed by conducting measurements on both inputs and outputs. In empirical models, the variation within the watershed characteristics is not accounted for directly. However, the mathematical formulas used implicitly represent the physical system within the range of data they were developed from. Regression analysis and the classical unit hydrograph developed by Sherman (1932) are two examples of empirical models. Since this type of model is not based on physical characteristics of the watershed, empirical models can not be generalized to other locations and scenarios without reducing their accuracy (Wood and O'Connell, 1985).

2.2.3 Physical Models

Physical models are those based on complex physical laws and theories. The "real world" is simplified to different degrees in space and time. Physical models have logical structures which are similar to the real hydrologic process in the field. Since these models describe the hydrologic processes in more detail, it is expected that the data requirement is greater than that with using empirical models, for example. Such models offer a full description of the hydrograph and not just give estimates for the important hydrograph

parameters (i.e. time to peak and peak flow rate). Another advantage that these models offer is the ability to reflect the effect(s) of changes happening in the watershed.

In a physical model, the inputs are related to the outputs in a physical manner, and also the effect of changes in the input parameters (which have physical meaning) on resulting hydrograph can be assessed. These models, therefore, can improve understanding of hydrological systems (Singh, 1988).

2.2.2 Conceptual Models

Conceptual models fall in a category between physical models and empirical models. They usually represent physical formulas in a simplified form. Singh (1988) noted that these models are able to provide useful results efficiently and economically for some problems. These models are capable of reflecting changes in the watershed characteristics if the parameters used are physically based.

2.3 Synthetic Unit Hydrographs

2.3.1 Introduction

Since watershed characteristics such as the slope, area, and shape are constant, it is expected that the watershed response to storms having similar rainfall characteristics will be similar. This similarity in response is the basis of the unit hydrograph theory (Linsley et al., 1982). The concept of the unit hydrograph was first introduced by Sherman (1932). Sherman defined the unit hydrograph as follows:

"If a given one-day rainfall produced a 1-in depth of runoff over a given drainage area, the hydrograph showing the rates at which the runoff occurred can be considered a unit graph for that watershed."

Chow et al. (1988) described the assumptions behind the unit hydrograph theory:

[1] *The excess rainfall has a constant intensity within the effective duration.*

[2] *The excess rainfall is uniformly distributed throughout the entire drainage area.*

[3] *The base time of direct runoff hydrograph is constant for a given duration of rainfall.* [This assumption implies that regardless of the rainfall intensities, storms with the same duration produce direct runoff hydrographs with the same time base.]

[4] *The hydrograph resulting from excess rainfall reflects the unique characteristics of the watershed.*

[5] *The ordinates of all direct runoff hydrographs with the same base time are proportional to the total amount of direct runoff represented by each hydrograph.*

It can be noticed that to derive a unit hydrograph for a watershed, flow records must be available. But since only a relatively small portion of catchments are gaged, it became necessary to develop a means for deriving unit hydrographs for ungaged catchments (Linsley et al., 1982). Different approaches have been used to derive synthetic unit hydrographs.

Chow et al., (1988) described three types of synthetic unit hydrographs:

[1] Formulas relating hydrograph features (peak discharge, time to peak, time base) to basin characteristics (area, slope) (e.g. Synder, 1938; Gray, 1961; and James et al., 1987);

[2] Those based on dimensionless unit hydrograph (e.g. SCS, 1972); and

[3] Those based on storage routing (e.g. Clark, 1945).

The first synthetic unit hydrograph procedure was presented by Synder (1938). Synder developed his procedure by studying several basins located in the Appalachian Mountains region. In his model, discharge properties were determined empirically from the drainage basin physical characteristics such as area and length.

According to Watt and Chow (1985), the time parameter is a key variable in estimating the peak discharge and the complete hydrograph resulting from a specific storm. Inaccurate estimates of the time parameter result in an inaccurate design based on that time parameter. Bondelid et al. (1982) obtained the unit peak discharge as a function of the time of concentration of the watershed. Their results showed that the error in the time of concentration accounted for as much as 75% of the total error in the unit peak discharge. Recognizing the importance of time parameters in hydrology, hydrologists developed various methods to estimate time parameters such as the time of concentration, the time to peak, and the lag time (McCuen et al., 1984).

2.3.2 Time-area Method

2.3.2.1 General

The basis of the time-area method is the time-area diagram that represents the relationship between runoff travel time and the portion of the watershed area that contributes to runoff during that time period (McCuen, 1989). In this method, the watershed is divided into sub-areas separated by isochrones. The travel time required for a rain drop falling on any location in a sub-area is the same as that for any other drop falling on the same sub-area. An isochrone is a contour line connecting all points that share the same travel time. Isochrones can not cross one another, can not close, and can only originate and terminate at the watershed boundaries (Dooge, 1959). Figure 2.1 shows the watershed isochrone map drawn by classifying a grid of time of flow to the watershed outlet. According to Linsley et al. (1982), the time-area approach is a lag-and-route method in which the inflow (excess rainfall) is lagged by dividing the watershed into zones by isochrones of travel time from the outlet. The fundamental assumption of the traditional time-area method is that it accounts for translation and does not account for storage effects. Neglecting the storage effect results in lack of attenuation and therefore predicts higher peak flow rates (Ajward, 1996). However, neglecting storage effect can be overcome by adjusting the hydrograph resulting from the time-area method by routing it through a linear reservoir with the appropriate storage coefficient (Bedient and Huber, 1992). For the sake of simplicity, Muzik (1996) computed the travel times from the equilibrium flow conditions and later empirically adjusted them for neglected effects of storage and unsteady flow.

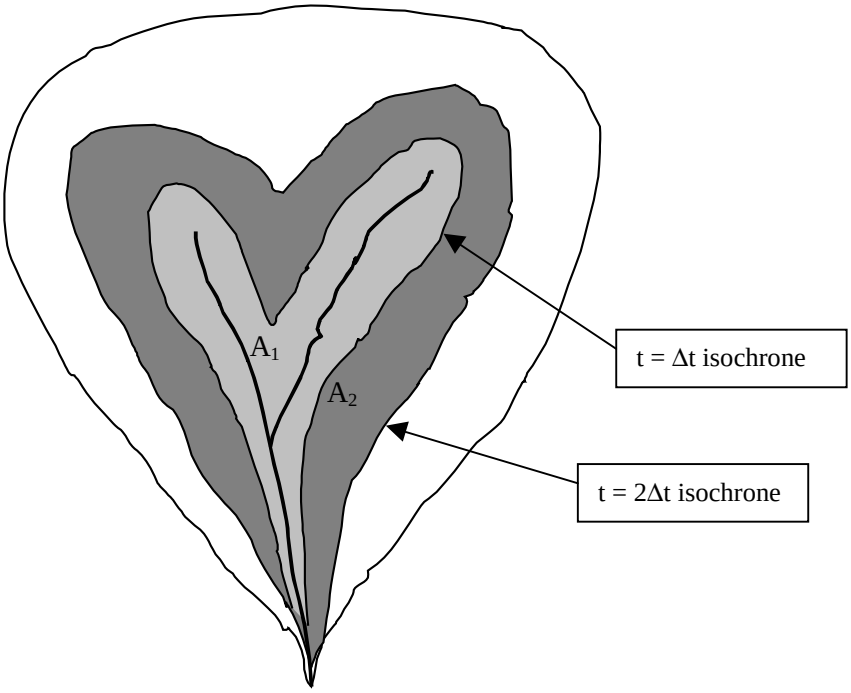

Figure 2.1. Watershed isochrone map drawn by classifying a grid of time of flow to the outlet.

2.3.2.2 Mathematical Representation of the Time-area Method

The time-area method is based on the fact that the unit hydrograph ordinate can be represented by the derivative of the time-area diagram (Maidment, 1993b). Consider an excess rainfall occurring at a rate I over the watershed, the runoff at the watershed outlet can then be represented by:

$$Q(t) = I\,A(t) \tag{2.1}$$

which is the S-hydrograph tending to an equilibrium flow of IA where A is the total area of the watershed (Maidment, 1993b). Figure 2.2a shows the incremental time-area diagram which is a discrete function of time that has a single value over each time interval Δt. On the other hand, the cumulative time-area diagram (Figure 2.2b) is a continuous function of time. Taking into account a rainfall pulse of duration Δt and intensity I, the runoff response can be represented as:

$$Q(t) = I\,A(t) - I\,A(t - \Delta t) \tag{2.2}$$

This expression can be viewed as the difference between the S-Hydrograph at time t and its value lagged by Δt time units. Knowing that the amount of excess rainfall falling during the Δt time period is $I\Delta t$, it follows that the corresponding unit hydrograph ordinate U(t) to this unit pulse of rainfall is given by:

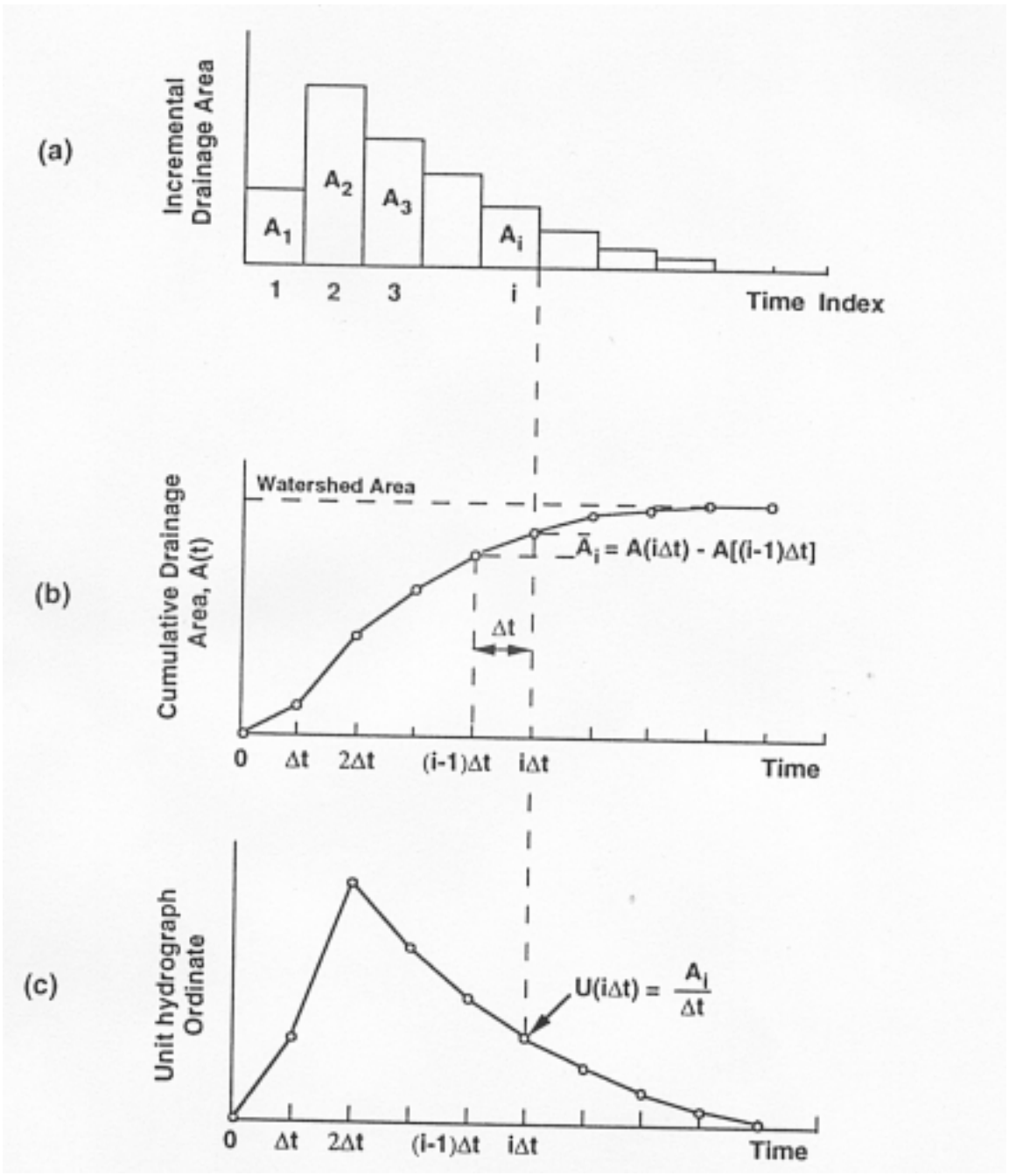

Figure 2.2. The time-area diagram and the unit hydrograph: (a) incremental drainage area; (b) the cumulative time-area diagram; (c) unit hydrograph found as the slope of the time-area diagram (Maidment, 1993b with permission).

$$U(t) = \frac{Q(t)}{I\Delta t} = \frac{A(t) - A(t - \Delta t)}{\Delta t} \qquad (2.3)$$

This relationship between the cumulative time-area diagram and the unit hydrograph ordinates is illustrated in Figure 2.2c.

2.4 Use of Geographic Information Systems in Hydrology

2.4.1 History

Geographic Information Systems can be defined as computer based tools that display, store, analyze, retrieve, and generate spatial data. GISs are being more and more involved in hydrology and water resources and showing promising results. However, there has not been a widespread use of GIS in most circles. Unfortunately, most existing standard GISs do not include procedures that are necessary for hydrologic modeling. Nevertheless, there are some hydrologically oriented GISs which have made use of the cell based analysis.

Solomon (1968) showed that meteorological and hydrological data can be combined using a square grid cell based system to estimate temperature, precipitation, and runoff distribution. Lee (1985) concluded that GIS is an efficient tool for compiling input data for use in hydrologic investigations and best suited distributed hydrologic models. Berry and Sailor (1987) noted some of the advantages of GIS in hydrology and

water resources. According to them, GIS provides a powerful tool for expressing complex spatial relationships. It provides an opportunity to fully incorporate spatial conditions into hydrologic inquiries. Different proposed levels of development can be made rapidly and the resulting hydrologic effects easily communicated to decision-makers. The technology can also handle tremendous amounts of spatial data and complex analysis considerations can be processed effectively. Following are examples of using GIS in hydrology.

Maidment (1993a) summarized the different levels of hydrologic modeling in association with GIS as follows: hydrologic assessment; hydrologic parameter estimation; hydrologic modeling inside GIS; and linking GIS and hydrologic models. Maidment (1993a) suggested that the major limitation for applying hydrologic modeling directly within GIS is the time variability of the hydrologic processes.

Hill et al. (1987) used GIS with remotely sensed data and other different data sources. They used a model called Watershed Hydrology Simulation (WAHS) developed by Singh and Aminian (1985). LANDSAT MSS satellite information was used to produce land cover and landuse map layers and the SCS CNs were generated for a 1542 km^2 basin at Louisiana and Mississippi using the raster-based GIS, GRASS. In this application, GIS was used as a tool to store and prepare the input data. This type of use of GIS was also conducted by Wolfe and Neale (1988). They used the raster-based GIS GRASS to provide input data to a distributed parameter model called Finite Element Storm Hydrograph Model (FESHM). In this study, the hydrologically homogeneous areas or “hydrologic response units” were detected by overlaying maps of soil and land cover. Moeller (1991) used a GIS to derive spatially weighted hydrologic parameters to be used

in the HEC-1 hydrologic model. Weighted percent imperviousness and CN values were derived.

Stuebe and Johnston (1990) estimated runoff using the SCS CN method manually and using GRASS. They found that using a GIS made estimations much easier especially when dealing with large areas. The GIS was advantageous when many repetitions were made and different scenarios of land cover landuse were modeled.

Bhaskar et al. (1992) simulated watershed runoff using the Geomorphological Instantaneous Unit Hydrograph (GIUH) with the Arc-Info GIS to compile the required data. They used the hydrological model WAHS. In their study, total volumes of runoff showed good agreement but the predicted values for peak flow rate occurred much later than the observed ones. The average delay was 46% with a maximum of 76%. Peak values were off by an average of 47%. Arc-Info GIS was utilized successfully for runoff modeling by Terstriep and Lee (1989), DeBarry and Carrington (1990), and Lee and Terstriep (1991).

Zollweg et al. (1996) successfully incorporated a hydrologic model called The Soil Moisture-based Runoff Model (SMORMOD) into GRASS to predict daily stream flow amounts.

2.4.2 Spatially Distributed Unit Hydrograph Modeling with GIS

Maidment (1993b) was the first to propose the promising concept of using GIS to derive a unit hydrograph that reflects the spatially distributed flow characteristics of the watershed. He suggested the name “spatially distributed unit hydrograph” (SDUH) to distinguish it from the traditional concept for a unit hydrograph that requires a uniform

spatial distribution of excess rainfall. He used a hypothetical 36 grid-cell watershed. Each cell had an area of 1 km^2. Maidment's results were inconclusive in the sense that he could not generate the proper shape of the S-Hydrograph. He attributed that to the possibility that "the example grid is just too small to give realistic results".

Muzik (1996) applied the SDUH concept on a mostly forested, 229 km^2 watershed located on the eastern slopes of the Rocky Mountains in Alberta, Canada. The watershed was divided into 1 km^2 grid cells. The SCS CN method was used to estimate excess rainfall with a uniform rainfall intensity of equal one-hour intervals. Each cell was assigned a CN value and hence the excess rainfall generated was spatially distributed. The incremental one-hour spatially distributed excess rainfalls were then spatially averaged to obtain a representative uniform excess hyetograph for the watershed. Muzik's results were very good considering that no parameter optimization was used.

Johnson et al. (1997) developed a distributed hydrologic model, known as the Terrestrial Hydrologic Model (THM) to utilize rasterized databases to simulate runoff. In this model, three options were available for estimating the hydrologic abstractions: a constant infiltration rate (Φ-index), the SCS CN method, and the Green-Ampt equation. The kinematic wave routing technique (Woolhiser and Liggett, 1967; Morries and Woolhiser, 1980) was used for modeling overland flow in each cell. A modified Muskingum-Cunge (Cunge, 1969) channel routing technique was used to simulate channel flow in each channel cell. Rainfall data could be entered as a uniform value for the whole study area or by supplying a gridded rainfall coverage which changes for each cell over time. Johnson et al. (1997) showed that the THM model was able to simulate successfully the surface runoff.

Kilgore (1997) incorporated the SDUH concept to model runoff from a mostly agricultural, 1153ha watershed located in Fauquier County, Virginia. Excess rainfall was considered to be uniformly distributed over the entire watershed area. Based on the visual comparison, hydrographs generated using the SDUH model were closer to the observed runoff hydrograph than those generated by using other types of synthetic unit hydrographs. However, the peak flow rates predicted by the SDUH model were comparable to the results of other synthetic hydrograph techniques. Moreover, the SDUH model under-predicted the time to peak 90% of the time.

3. Methodology

3.1 Study overview

In this study, the time-area curve method was used to obtain the output hydrograph at the watershed outlet. A raster GIS, namely, the Spatial Analyst Extension in ArcView GIS was used. The time-area method involves obtaining the travel time of excess rainfall through each cell and then accumulating the travel time from each cell to the watershed outlet by summing the time of travel along the flow path for each cell. Flow direction, slope, and channel network were derived from the digital elevation model (DEM) for the watershed. Each cell has a unique value for each physiographic property. The DEM is an ordered array of numbers that represents the spatial distribution of elevation above an arbitrary fixed datum in the land surface. A cell size of 900 m^2 was used in this study.

Three different models were used. [Uniform curve number model (UCN), distributed curve number model (DCN), and a Φ-index model.] The procedure of routing the excess rainfall to the watershed outlet is the same in the three models. The difference between them lies in the method of excess rainfall generation for a given storm. While the excess rainfall is spatially distributed in the DCN, it is uniformly distributed in the other two models. A detailed description of the three different methods of generating excess rainfall is given in section 3.3.4. The results obtained using the three different models were compared to the observed hydrographs for 30 storms for Owl Run

watershed in Fauquier County in Virginia.

3.2 Watershed Description

In this study, the predicted hydrographs at the watershed outlet were compared to the observed data obtained from Owl Run Watershed located in Fauquier County, Virginia (Figure 3.1). The 1153 ha watershed is approximately 8 km south of Warrenton, Virginia, and 85 km southwest of Washington D.C.

The data used in this study are part of a 10-year Owl Run Watershed/Water Quality Monitoring project (Mostaghimi et al., 1989). The objective of the monitoring project was to demonstrate the effectiveness of animal waste best management practices (BMPs) in reducing non-point source pollution. Flow rate was monitored at four different locations including the main watershed outlet, while precipitation data were collected at seven different locations over the watershed area. In this study, only the observed flow rate from the watershed outlet was considered. As for the precipitation data, only five out of the seven gages included full data for this study period (1990-1992) and so, only data from these five rain gages were used.

3.2.1 Climate

The climate in Fauquier County, Virginia, is humid continental with hot humid summers, vigorous, but not too severe winters. The average annual rainfall is about 104 cm. Temperatures ranging between 32^{o}C and 35^{o}C are frequent extremes in summer and

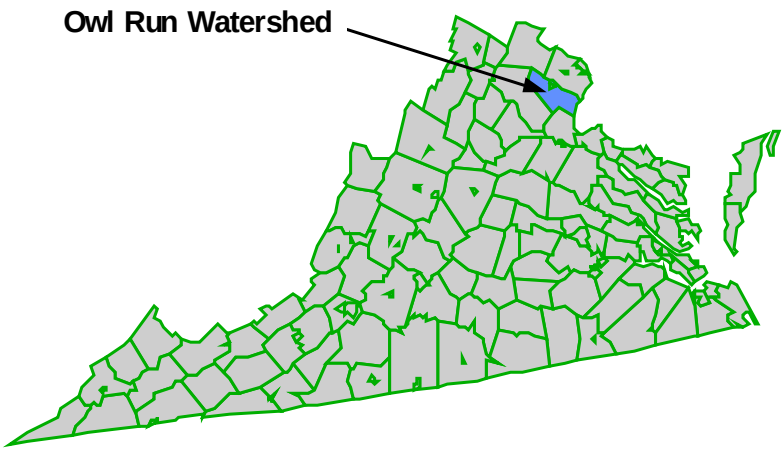

Figure 3.1. Fauquier County, Virginia, with general location of the watershed.

-9^{o}C to -6^{o}C in winter. The average annual rainfall is fairly evenly distributed over the year with the greatest amount occurring during summer and spring (Mostaghimi et al., 1989). In summer, the rains in general are in the form of heavy downpours, showers, and thunderstorms. This causes runoff to be greater during this period. The same rain patterns also occur in late spring and early autumn. Much of the winter rain comes in the form of snow or slowly dizzling rain (Mostaghimi et al., 1989).

3.2.2 Landuse

Over 70% of the watershed area is agricultural land, 20% is forest land, and the rest of the area is used for residential, commercial, and transportation purposes. Table 3.1 shows the percentage of watershed area used for each landuse category (Mostaghimi et al., 1989).

3.2.3 Soils

Soils is Owl Run Watershed are generally shallow (0.3-0.6m deep) silt loam. Over 72% of the watershed area is covered by Penn, Bucks, and Montalto associations soil series. The Penn soils are shallow and excessively drained soils that occur mainly on undulating with slopes ranging from 2%-7% and rolling relief with slopes ranging from 7%-14%. The Penn soils have a medium runoff potential, medium to rapid internal drainage, moderate permeability, and poor water holding capacity. The Buck soil series consist of moderately deep well drained upland soils. They adjoin the Penn soils and occupy moderately large areas on broad undulating ridges. Buck soils have low to medium runoff potential with a medium internal drainage with slopes ranging from 2%-

Table 3.1. Typical landuse activities in the Owl Run watershed (Mostaghimi et al., 1989).

Landuse	Percentage of watershed area
Corn (conventional till)	15
Corn (no-till)	11
Rotational hay	20
Pasture (active)	18
Pasture (idle)	7
Woodland	20
Non-agricultural	9

7%. The Montalto soils are well drained soils with slope ranging from 2%-14%. The runoff potential and internal drainage are medium. In general, Owl Run Watershed soils are relatively fertile because they are moderately well supplied with organic matter and plant nutrients (Mostaghimi et al., 1989).

3.3 Hydrology

3.3.1 Rainfall

A Thiessen weighted average was used to derive a single rainfall value for each rainfall time interval. The average rainfall over the watershed is obtained by weighting each rain gage's rainfall depth in proportion to its area of influence (Thiessen polygon). The initial intention was to generate a distributed rainfall map by interpolating the observed rainfall amounts from the seven rain gages distributed over the entire area of the watershed. However, only five of the seven rain gages had full rainfall data for the study period. These five rain gages (POA, POB, POD, POF, and POH) (Figure 3.2) were not well distributed over the entire area and they were located in the lower portion of the watershed. Interpolating rainfall using only the five available rain gages would have caused values obtained in the northern and south western portions of the watershed to be extrapolated.

3.3.2 Storm Selection

The data used in this study are a part of the 10-year water quantity/quality data collected for Owl Run watershed during the 1986-1996 period (Mostaghimi et al., 1989).

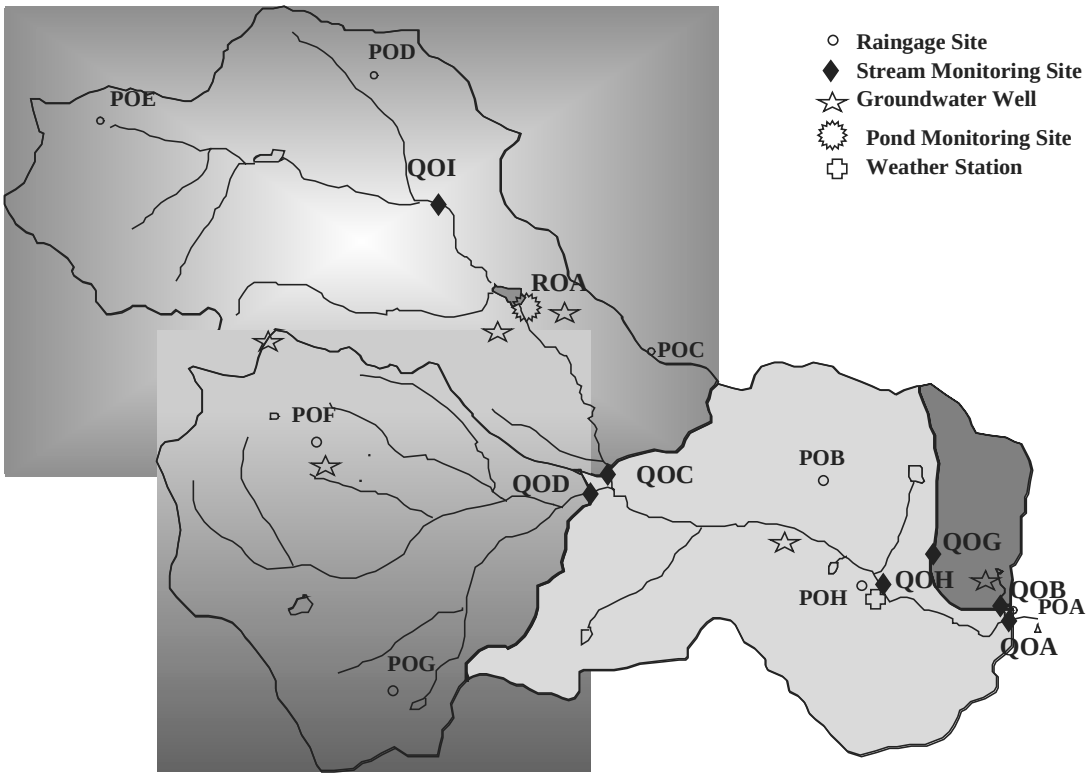

Figure 3.2. Location of monitoring stations within Owl Run watershed.

The Owl Run Watershed monitoring system was designed to provide comprehensive assessment of the surface water quality as influenced by changes in landuse, agronomic, and cultural practices in the watershed over a 10-year study period. The period from 1990 to 1992 was used in this study. Kilgore (1997) selected 40 storms based on the following criteria:

- a minimum of 6.35 mm (0.25 inches) of rainfall;
- a minimum peak flow rate of 0.283 m^3/s (10cfs);
- occur in the period between April and November; and;
- isolated storm events.

Storms occurring in the period from December to March were excluded in this study because the model developed can not account for snowmelt. Storms were considered to be over when there was at least six hour period of no rainfall. Restrictions on the rainfall amount and the peak flow rate for a storm to be modeled were placed to assure sufficiently large storms to produce a noticeable peak flow rate. Ajward (1996) used similar criteria to select storms. However, an additional criterion used by Ajward was to have a recognizable response pattern between the rainfall hyetograph and the streamflow hydrograph. In this study, storms modeled were those falling in the period of 1990 to 1992. While Kilgore (1997) modeled 40 storms in the period between 1990 to 1993, only storms occurring in the period between 1990 to 1992 were modeled in this study. A total of 30 storms were modeled and the additional criterion used by Ajward (1996) was not honored. Table 3.2 gives a summary of the rainfall volumes and peak flow rates for the 30 storms selected.

Table 3.2. Summary of rainfall events.

			Rainfall Volume (mm)	Runoff Volume (mm)	Peak Flow Rate (m^3/s)	Time to Peak (hr)
1	1990	April 1	6.4	0.9	0.50	5
2		April 2	13.4	4.1	3.13	4
3		April 14-15	21.0	3.2	1.34	7
4		May 10	39.0	8.3	4.25	4
5		May 28-29	46.5	23.7	11.02	15
6		July 14	30.0	1.7	1.22	3
7		October 18	42.7	1.1	0.58	5
8		October 22-23	46.4	4.4	1.47	13
9		November 9-10	49.5	6.0	2.75	10
10	1991	June 18	67.3	1.4	1.71	3
11		July 26	48.0	4.5	3.02	6
12		August 9-10	89.0	15.7	12.95	8
13		September 4-5	49.9	2.6	2.57	4
14		September 17-18	46.8	2.8	2.21	6
15		September 24	37.0	2.9	1.93	4
16		October 5-6	31.0	2.3	1.92	3
17	1992	April 21	52.8	13.6	9.00	4
18		May 8	10.0	0.8	0.42	5
19		June 30	27.4	1.0	1.04	2
20		July 3-4	16.8	1.2	0.76	4
21		July 24	25.6	2.1	1.66	3
22		July 27	43.3	15.1	12.35	4
23		July 31	20.4	3.1	3.07	4
24		August 4	17.5	0.6	0.54	3
25		September 2	34.4	0.6	0.46	3
26		September 5-6	18.7	0.7	0.38	3
27		September 10-11	21.4	3.0	1.60	5
28		November 2-3	19.3	1.4	0.83	6
29		November 12	18.4	3.2	1.90	6
30		November 22-23	31.1	16.0	13.2	4

3.3.3 Baseflow Separation

The models proposed in this study are surface runoff models. So the observed hydrographs were separated into two components, surface runoff and baseflow component. Hydrograph separation is the process of separating the time distribution of baseflow from the total runoff hydrograph to produce the direct runoff hydrograph (McCuen, 1989). There is no universal standard for separating baseflow (Brooks et al., 1991). Kilgore (1997) used the constant slope method, a commonly used approach. In this method, the starting point of the separation line is the lowest discharge rate at the start of the rising limb, while the ending point was taken to be the point of inflection on the falling limb of the hydrograph.

3.3.4 Estimation of Excess Rainfall

In order to fairly compare the hydrograph parameters, the excess rainfall used in the models was matched with the observed volume of runoff for a given storm. The observed total runoff volume was found by integrating the direct runoff hydrograph obtained earlier. Three different methods of excess rainfall estimations were used.

3.3.4.1 Excess Rainfall Estimation for the Φ-index Model

The excess rainfall distribution in the Φ-index method is found by “chopping” the hyetograph at a point where the summation of the values above the “chopping” line represents the observed excess rainfall. The summation of the values below the line

represents all different kinds of losses. Figure 3.3 shows a typical hyetograph with the excess rainfall found using the Φ-index method. In this figure, the total depth of rainfall is 46 mm while the total depth of excess rainfall is 4.4 mm.

3.3.4.2 Excess Rainfall Estimation Using the SCS CN Method

3.3.4.2.1 General

Excess rainfall generated in a watershed is known to vary spatially. The variation in excess rainfall follows that of landuse, land cover, and soil type. Typically, the way to account for this variation is to divide the watershed into smaller areas of "uniform" landuse, land cover, and soil type combinations (Ajward, 1996). An average curve number (CN) for the whole watershed determined using the area weighting method is then given by:

$$CN = \frac{CN_i\, A_i + CN_{i+1} A_{i+1} + ... + CN_n A_n}{\sum_{i=1}^{n} A_i} \qquad (3.1)$$

Where:

CN_i is the curve number of the sub-area i (A_i).

n is the total number of sub-areas.

This procedure is the standard procedure used in the SCS rainfall-runoff relationship. It gives an average excess rainfall depth for the entire watershed, P_e, that corresponds to an average rainfall depth, P. This procedure involves a lumping process

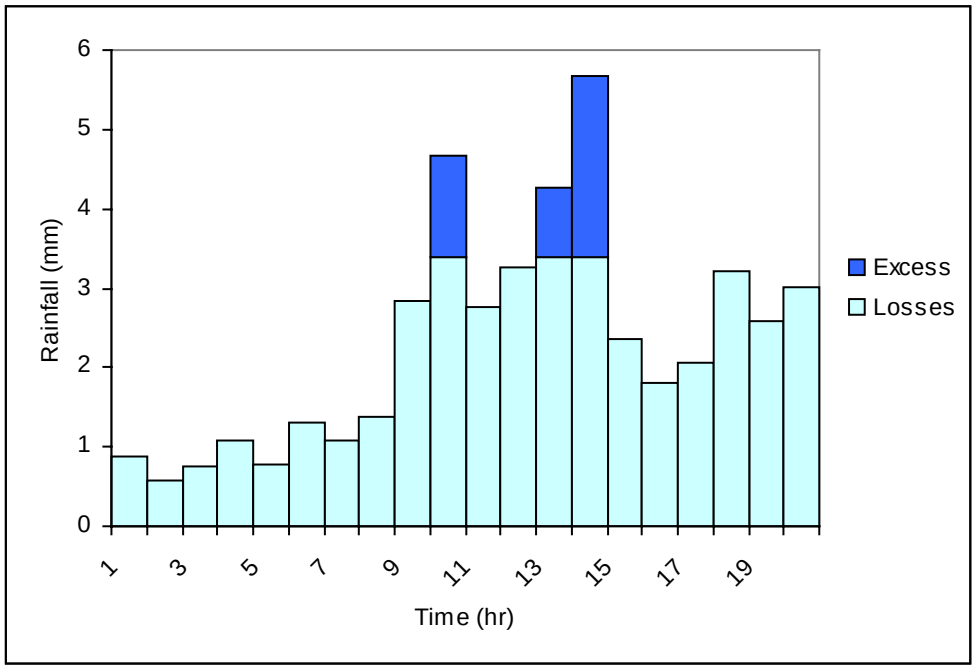

Figure 3.3. Excess rainfall and losses resulting by using the Phi-index method.

that leads to an inaccurate estimate of excess rainfall specially when the variation in the previously mentioned parameters is large.

The rainfall-runoff relationship in this method is derived from the water balance equation and a proportionality relationship between retention and runoff. The SCS rainfall-runoff relationship is given by (Novotny et al., 1994):

$$P_e = \frac{(P - I_a)^2}{(P - I_a) + S} \qquad (3.2)$$

Where:

P is the rainfall depth (mm).

P_e is the depth of excess rainfall (mm).

I_a is the initial abstractions (mm).

S is the volume of total storage (mm).

Storage includes both the initial abstractions and total infiltration. The initial abstraction is a function of landuse, treatment and condition, interception, infiltration, detention storage, and antecedent soil moisture (Novotny et al., 1994). The initial abstraction and the total storage are related in an empirical statistical equation which is given as:

$$I_a = 0.2S \qquad (3.3)$$

Substituting equation 3.3 into equation 3.2 yields:

$$P_e = \frac{(P - 0.2S)^2}{(P + 0.8S)} \qquad (3.4)$$

The storage S (in millimeters) is obtained using the formula:

$$S = \frac{25400}{CN} - 254 \qquad (3.5)$$

Where CN is the curve number that can be obtained from standard tables for different combinations of landuse and land cover, soil hydrologic group, treatment, and condition. A map of different landuses for Owl Run Watershed is shown in Figure 3.4.

The hydrologic soil group reflects a soil's permeability and surface runoff potential. Following is a description of the four different hydrologic soil groups (Novotny et al., 1994):

- Group A are soils with low total surface runoff potential due to their high infiltration rates. They consist mainly of excessively drained sands and gravels.
- Group B are soils with low to moderate surface runoff potential. They have moderate infiltration rates and moderately fine to moderately coarse texture.
- Group C are soils with moderate to high surface runoff potential. They have slow infiltration rates and moderately fine to fine textures.
- Group D are soils with high surface runoff potential. They have very slow infiltration rates and consist chiefly of clay soils.

Owl Run Watershed includes only groups B through D . Figure 3.5 shows the spatial distribution of the three different hydrologic soil groups available in the Owl Run Watershed. Table 3.3 shows different landuses in Owl Run Watershed and their

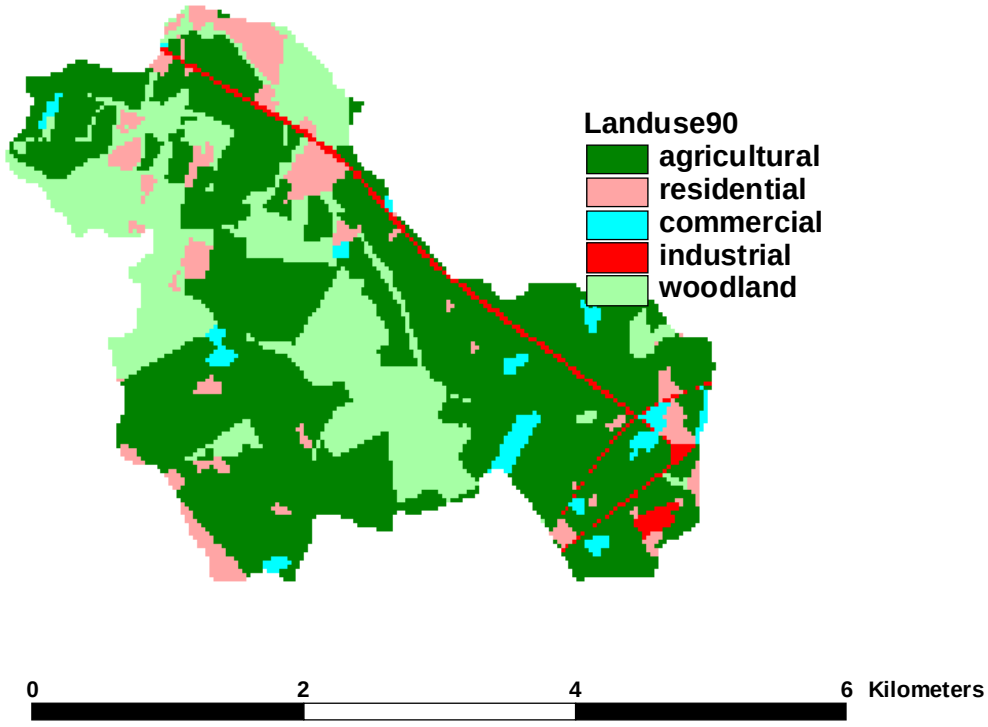

Figure 3.4. Owl Run watershed landuses (1990).

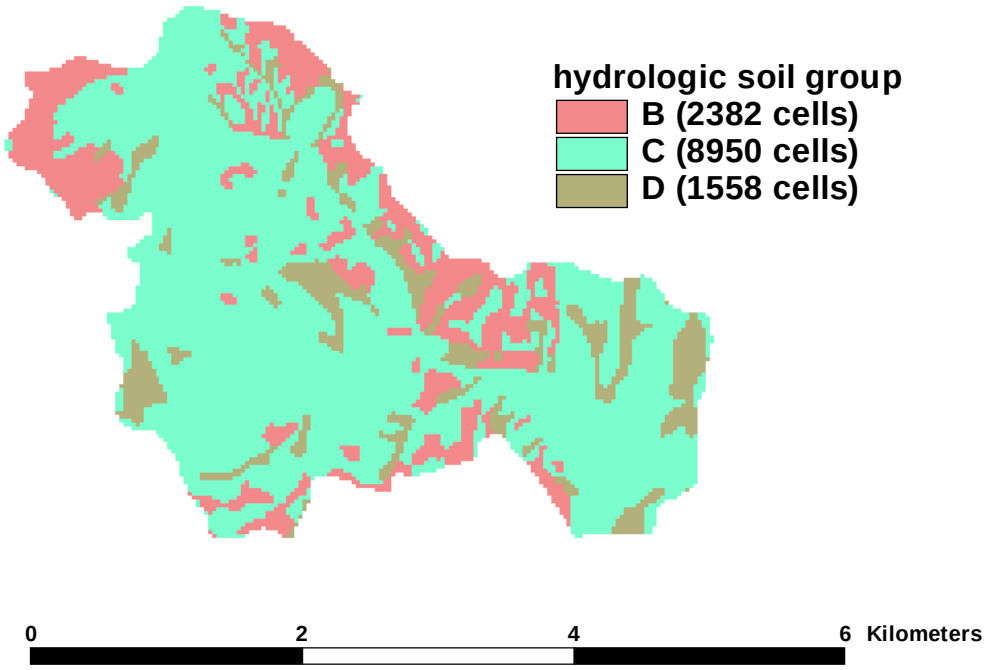

Figure 3.5. The spatial distribution of the hydrologic soil groups in Owl Run watershed.

Table 3.3. Owl Run watershed landuses and their corresponding curve numbers

Landuse	*Code*	*Hydrologic Soil Group*				*Treatment, Hydrologic Condition/source of CN*
		A	*B*	*C*	*D*	
Alfalfa	Alf	58	72	81	85	Straight row, good (3)
Barley	Ba	63	75	83	87	Straight row, good (3)
Church	Ch	46	65	77	82	Residential with 2 acre lot size (2)
Clover	Clo	58	72	81	85	Straight row, good (3)
Commercial	Cm	89	92	94	95	(1)
Commercial 1	cm1	89	92	94	95	(1)
Commercial 2	cm2	89	92	94	95	(1)
Conventional corn	Co	72	81	88	91	(1)
Farmstead	Fa	59	74	82	86	(3)
Full season beans	Fsb	58	72	81	85	Straight row, good (3)
Grass	Gr	30	58	71	78	Meadow-continuous grass (2)
Hay	Ha	65	76	84	88	(4)
Idle	Id	65	76	84	88	(4)
Light industry	Li	81	88	91	93	Average % impervious area 78
Loafing lot	Lo	89	92	94	95	(2)
Minimum till sorghum	Mso	64	75	82	85	Straight row-conservational tillage, good (5)
No-till corn residue	Ncr	74	83	88	90	Crop residue cover, good (2)
No report	Nr	70	73	78	81	
No-till beans	Ntb	58	72	81	85	Straight row, good (2)
no-till corn	Ntc	71	79	86	89	(4)
Oats	Oat	63	75	83	87	Straight row, good (3)
Outside watershed	Out	70	75	80	85	
Pasture	Pa	39	61	74	80	Good (1)
Pond	Po	100	100	100	100	same as waterway
Road/rail road	Rdr	76	85	89	91	gravel surface, (1)
Residential	Res	51	68	79	84	Average lot size 1 acre (1)
Strip conventional corn	Sco	62	71	78	81	Contoured and terraced, good (2)
Small grain	Sg	63	75	83	87	Straight row, good (3)
Sorghum	So	67	78	85	89	Straight row, good (3)
Strip small grain	Ssg	59	70	78	81	Contoured and terraced, good (2)
Wetland	Wet		62	74	85	Herbaceous-mixture of grass, weeds, and low-growing brush, good (2)
Wheat	Wh	63	75	83	87	Straight row, good (3)
Woodland	Wo	30	55	70	77	Good (1)
Waterway	Ww	100	100	100	100	

Sources of CN:

1. SCS (1986)
2. Rawls et. al (1993)
3. SCS (1972)
4. Wang (1991)
5. Novotny et. al (1994)

corresponding CN values. The resulting map of CN values for Owl Run Watershed is shown in Figure 3.6.

3.3.4.2.2 Excess Rainfall Estimation for the DCN Model

In the Distributed Curve Number (DCN) model, each cell is assigned a CN that corresponds to its landuse-land cover and soil hydrologic group. The degree of lumping is limited to the cell size. Since the goal is to maintain the spatial variation in excess rainfall in this model, yet match the total rainfall volume, a technique for adjusting the individual cell CN proportionally until the predicted runoff volume matched the observed volume was developed. The basic approach is based on the assumption that variation in actual runoff from the CNII (base CN) value is due to the antecedent moisture condition (AMC) of the soil. Thus, the relationships between CNIII (AMC = III) and CNI (AMC = I) to CNII (AMC = II) are used to scale the storm CN. The AMC = II represents the average case for annual floods which is an average of the conditions that have preceded the occurrence of the annual flood on numerous watersheds. AMC = I represents dry soils (though not to the wilting point), and AMC = III represents the conditions if heavy rainfall or light rainfall with low temperature occurred during the five days period prior to the given storm and soils in this case are nearly saturated.

Figure 3.7 shows a plot of the three CN conditions versus CNII. Relating this figure to the transformation equations from CNII to both CNI and CNIII, the following may be noticed:

- The transformation equation from CNII to CNI is given by (Novotny et al., 1994):

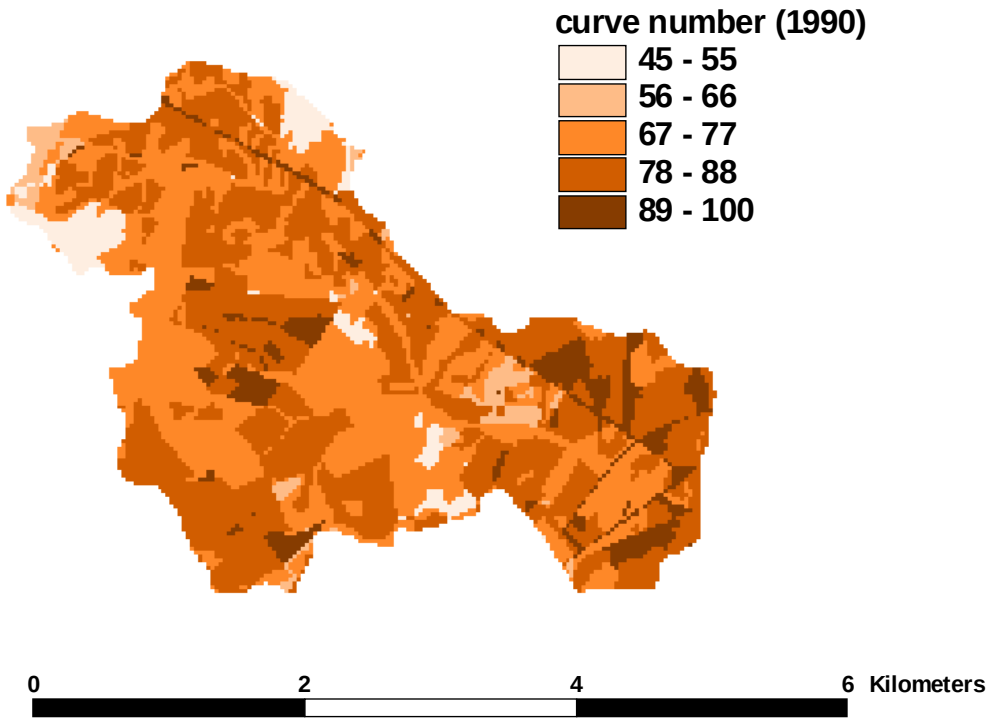

Figure 3.6. Curve numbers of Owl Run watershed (1990).

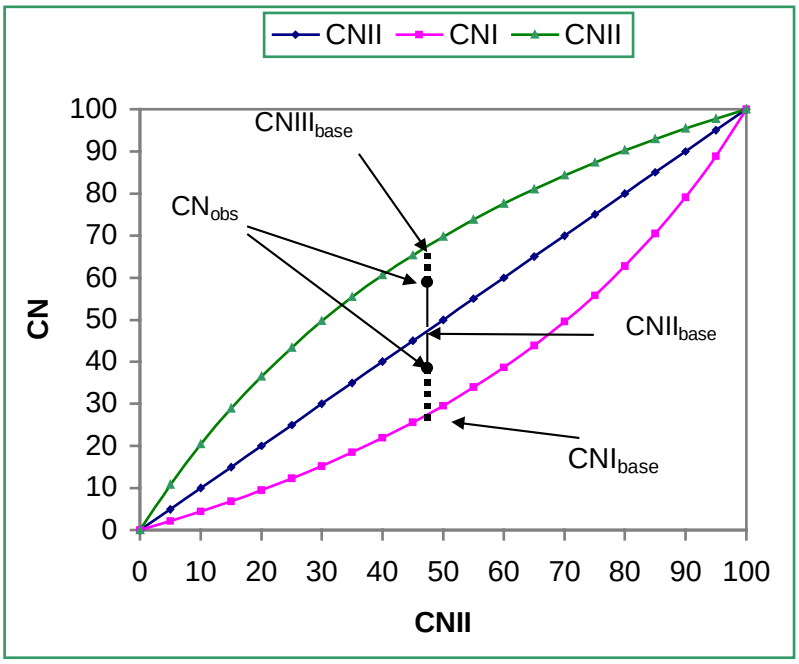

Figure 3.7. Relationships of event CN values to CN for dry (CNI) to wet (CNIII) antecedent moisture conditions.

$$CNI = \frac{4.2CNII}{10 - 0.058CNII} \qquad (3.6)$$

and the amount:

$$[CN\text{II}_{cell} - \frac{4.2 * CN\text{II}_{cell}}{10 - 0.058CN\text{II}_{cell}}]$$

represents the difference between CNII for each cell and the non-linearly transformed CNI for that corresponding cell.

- The transformation equation from CNII to CNIII is given by (Novotny et al., 1994):

$$CNIII = \frac{23\,CN\text{II}}{10 + 0.13\,CN\text{II}} \qquad (3.7)$$

and the amount:

$$[\frac{23 * CN\text{II}_{cell}}{10 + 0.13CN\text{II}_{cell}} - CN\text{II}_{cell}]$$

represents the difference between the non-linearly transformed CNIII for each cell and the CNII for that corresponding cell.

For cases where the observed runoff volume is greater than the base predicted runoff, the CNII needs to be reduced and so, the transformation equations used was a modified form of CNII to CNI equation and is given by equation 3.8.

$$CN_{calibrated} = CNII_{cell} - [CNII_{cell} - \frac{4.2 * CNII_{cell}}{10 - 0.058 CNII_{cell}}][\frac{CNII_{base} - CN_{obs}}{CNII_{base} - CNI_{base}}] \quad (3.8)$$

Where $CNII_{cell}$ is the value of CNII for a given cell

$CNII_{base}$ is the estimated average of CNII as given by the map developed

CNI_{base} is the equivalent CNI value to the $CNII_{base}$

CN_{obs} is the required average CN value to generate the observed runoff volume.

The last term in the equation ($[CNII_{base} - CNobs]/[CNII_{base} - CNI_{base}]$) provides scaling the other part of the equation mentioned earlier linearly. The scalling amount is the proportion of the difference between the base CNI and observed CN (the dashed line in the figure) to the bigger difference (dashed line plus solid line in the figure).

On the other hand, for cases where the observed runoff volume was smaller than the predicted volumes, the CNII needed to be increased. The transformation equation used was:

$$CN_{calibrated} = CNII_{cell} + [\frac{23 * CNII_{cell}}{10 + 0.13 CNII_{cell}} - CNII_{cell}][\frac{CN_{obs} - CNII_{base}}{CNIII_{base} - CNII_{base}}] \quad (3.9)$$

where the $CNIII_{base}$ is the equivalent CNI value to the $CNII_{base}$

The last term in the equation ($[CN_{obs} - CNIII_{base}]/[CNIII_{base} - CNII_{base}]$) provides scaling the other part of the equation mentioned earlier linearly. The scalling amount is the proportion of the difference between the observed CN and the base CNIII (the dashed

line in the figure) to the bigger difference (dashed line plus solid line in the figure).

An iterative procedure was followed until the predicted runoff volume matched the observed one. For each iteration, the predicted excess rainfall was estimated and compared to the observed excess rainfall. If the two amounts were not equal, the older distributed CN map is updated by considering the average distributed CN from the last iteration to be the $CNII_{base}$ for the new iteration. For each iteration, CN_{cell} was taken to be the CN value from the previous iteration.

Once the spatially distributed final CN map is developed, the total storage is obtained using equation 3.5. The excess rainfall equation (equation 3.4) gives the accumulated depth of excess rainfall from the start of the storm to the current time. Therefore, the incremental value of excess rainfall for an interval Δt, $P_e(t)$, is calculated as the difference between the accumulated excess rainfall at the end of that time interval and the accumulated excess rainfall at the beginning of that same interval as follows:

$$P_e(t) = (P_e)_t - (P_e)_{t-1} \qquad (3.10)$$

In the DCN model, all the final CN maps included at least a few cells with the value of CN = 100, therefore, excess rainfall was always generated starting the first rainfall interval.

3.3.4.2.3 Excess Rainfall Estimation for the Uniform Curve Number Model

In the uniform curve number model (UCN), the excess rainfall is generated using the SCS CN approach. However, the CN map used in this model is a single value map

having the value of the average observed CN that would produce the observed total excess rainfall depth given the observed total rainfall depth. Equation 3.5 is solved backwards to get the required value of storage (S). In contrast to the DCN model, equation 3.4 can only be applied when the accumulated rainfall depth is greater than the initial abstraction (0.2S). This means that excess rainfall would only start to be generated after the amount 0.2S is satisfied. The same procedure is followed to find the excess rainfall in each rainfall interval.

3.4 Model Development

3.4.1 General

The GIS software PC-ArcView was used in this study. All calculations were made on raster based themes. Watershed topographic properties needed in this study were derived from a digital elevation model (DEM) with 30-m resolution. The hydrologic model used here utilizes the concept of the spatially distributed unit hydrograph (SDUH). This model is a rainfall-runoff transformation model where the time-area curve method is used for the purpose of generating the output hydrograph at the watershed outlet for a given storm. Spatial variability in the watershed response was accounted for via utilizing a raster based GIS. The temporal variation in excess rainfall pattern was accounted for also.

To apply the time-area method in a grid-based model, the travel time of excess rainfall through each cell is required. Various maps are required to accomplish this task, including both basic maps, and maps derived from the basic maps. The basic maps

required in this study were the elevation map, the landuse-land cover, and the soil type map. Rainfall volume during each time interval is also considered basic theme. The slope, flow direction, flow path, upstream area, and channel network maps are all derived from the elevation map. Soil hydrologic group and landuse-land cover maps were combined to obtain the CN maps for six different seasons for the years 1991 through 1993. Manning's roughness coefficient maps were also obtained by reclassifying the landuse maps.

In all the models used in this study, the excess rainfall generated in each cell was routed to the watershed outlet. The flow characteristics in each cell were either overland or channel flow characteristics depending on the upstream area draining into each cell. Travel time in each cell was obtained by dividing the travel distance in that cell by the travel velocity through the same cell. The cumulative travel time from each cell was obtained by summing the travel times along the path of flow from that cell to the watershed outlet. To generate the time-area curve, the cumulative travel time was reclassified into equal time intervals of one hour, which is the same time period of the hyetograph. The area drained in each time interval was then estimated and therefore the excess rainfall in each time interval. This procedure was then repeated for each excess rainfall interval to account for the temporal variation in the excess rainfall. The final output hydrograph was obtained by convoluting the time-area curves for the whole storm. The flow chart for the two models using the curve number method is shown in Figure 3.8. The flow chart for the Φ-index model would be the same but with a different method of estimating the excess rainfall.

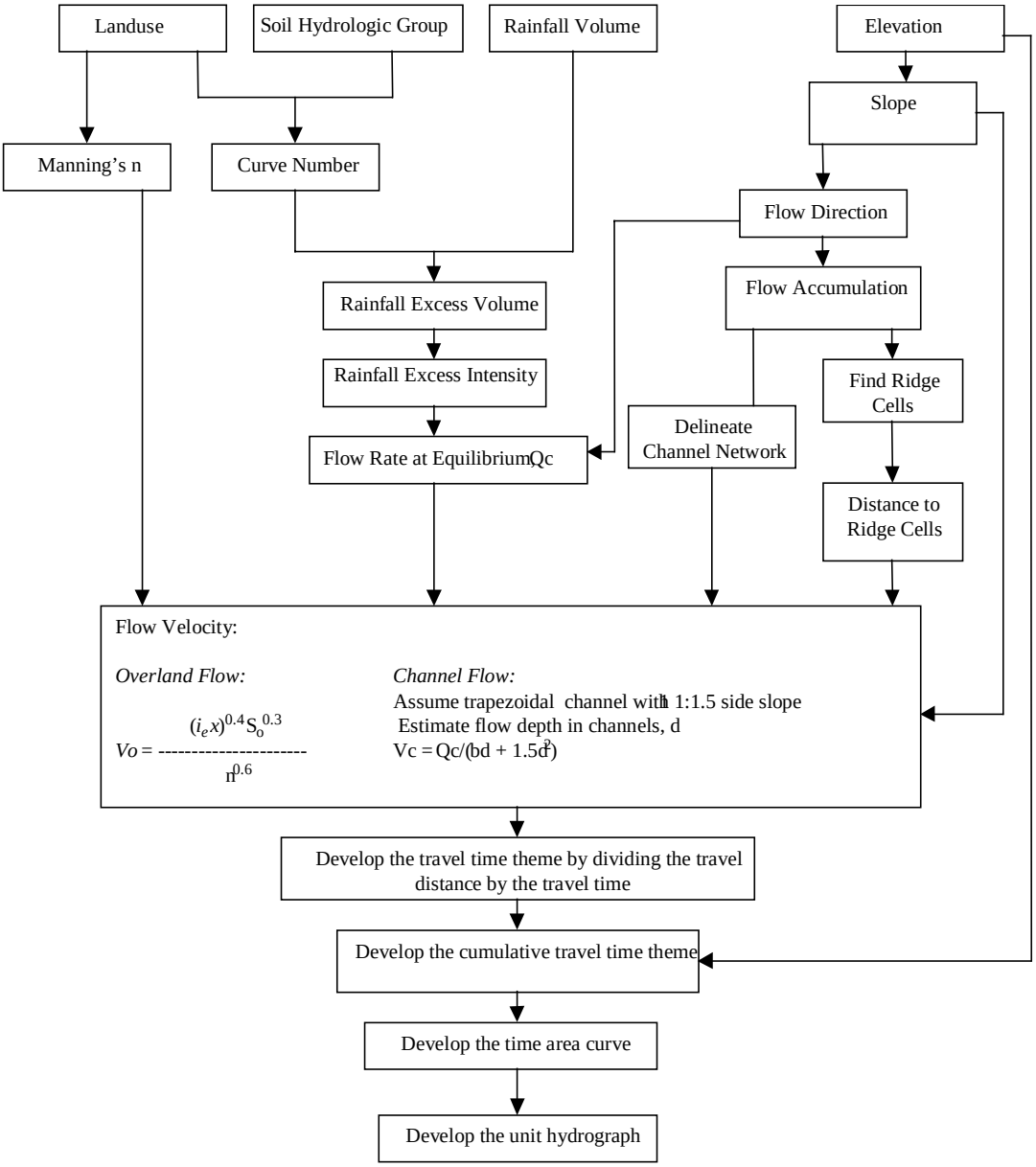

Figure 3.8. Model flow chart for the UCN and the DCN models.

3.4.2 Extracting Watershed Properties from the Digital Elevation Model

The watershed was divided into grid cells of an available digital elevation model (DEM) of 30 m resolution. DEMs comprise the basis for deriving large amounts of information about watershed morphology. They therefore, can be utilized to develop a hydrologic model that relates hydrologic response of the watershed to its morphological characteristics.

3.4.2.1 Slope

Slope represents the maximum rate of change in elevation from each cell to its neighbors. In ArcView, the slope is calculated from a 3x3 neighborhood using the average maximum technique as:

$$Slope\ of\ e = \sqrt{\left(\frac{(a + 2d + g) - (c + 2f + i)}{8 * \text{resolution}}\right)^2 + \left(\frac{(a + 2b + c) - (g + 2h + i)}{8 * \text{resolution}}\right)^2} \qquad (3.11)$$

where a, b, c, d, f, g, h, and i are the elevation values for cells a, b, c, d, f, g, h, and i, respectively (Figure 3.9).

a	b	c
d	e	f
g	h	i

Figure (3.9). Map of cells used to determine the slope of cell e.

3.4.2.2 Flow Direction

Flow direction in ArcView is taken to be the direction of the steepest drop in elevation to one of the surrounding eight cells. This procedure was described by Jenson and Domingue (1988). The output in the flow direction grid is an integer grid whose values range from 1 to 255. The values for each direction from the center are shown in Figure 3.10.

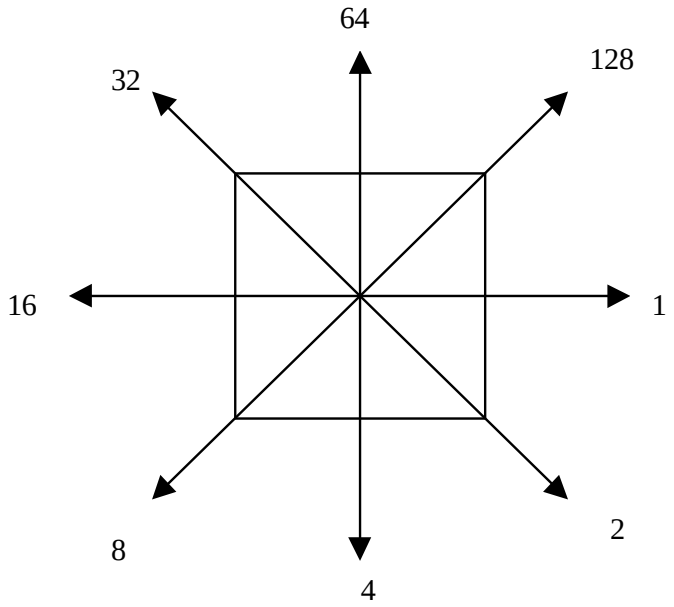

Figure 3.10. Flow direction values.

The direction of flow is taken to be the direction of the biggest drop in elevation from each cell and is calculated as:

$$drop = \frac{change\ in\ elevation}{distance} * 100 \qquad (3.12)$$

Where the distance is the distance between the centers of the two cells undergoing calculations for orthogonal cells, or $\sqrt{2}$ times the distance between the two centers in the case of diagonal cells. If a cell is lower than its eight neighbors, that cell is given the value of its lowest neighbor and flow is defined towards this cell. If multiple neighbors have the lowest value the cell is still given this value, but flow is defined with one of the two methods explained below. This is used to filter out one-cell sinks, which are considered noise.

If a cell has the same change in elevation value in multiple directions and that cell is part of a sink, then the flow direction is undefined. In such cases, the value for that cell in the output flow direction grid will be the sum of those directions. For example, if the change in z value is the same both to the right (flow direction = 1) and down (flow direction = 4), the flow direction for that cell is 1 + 4 = 5. Cells with undefined flow direction can be flagged as sinks using the built-in ArcView request aGrid.Sink. If a cell has the same change in z value in multiple directions and is not part of a sink, the flow direction is assigned with a lookup table defining the most likely direction (Greenlee, 1987).

Flow is only permitted to one of the eight possible directions. So, the output flow direction grid is considered a unidirectional grid of flow direction. This might sound like an unreasonable restriction (because excess rainfall from a grid cell, in reality, can flow into one or more of the adjacent grid cells), but it is necessary for delineating a unique channel network. All AVENUE (the programming language in ArcView) scripts used in this study are presented in Appendix A.

3.4.2.3 Determination of Upstream Area and Channel Delineation

Upstream area and channel network delineation can be obtained by performing a flow accumulation procedure on the flow direction grid. Depending on the flow path, the number of upstream cells flowing into each cell can be accumulated. When a threshold is set, the channel network can be delineated for the watershed. Any cell with a number of cells upstream less than that threshold is considered to be an overland cell and those with a number of cells upstream equal to or greater than the threshold are considered to be channel cells. For Owl Run watershed, a channel flow threshold of 20 cells (1.8 hectares) was chosen. Huggins and Burney (1982) recommended that overland flow can only exist for the first 100 meters along the flow path before the flow starts to concentrate into smaller rills. Assuming that the contributing area can be idealized as a semi-circular area, a 1.8 hectares results in a maximum overland flow distance of 107 meters. Output cells with a flow accumulation of zero are local topographic highs and may be used to identify ridges, where ridges are cells with no upstream cells flowing into them. The resulting channel network is a continuous drainage network for the watershed and is necessary for computing the cumulative time-area curve. Figure 3.11 shows Owl Run Watershed

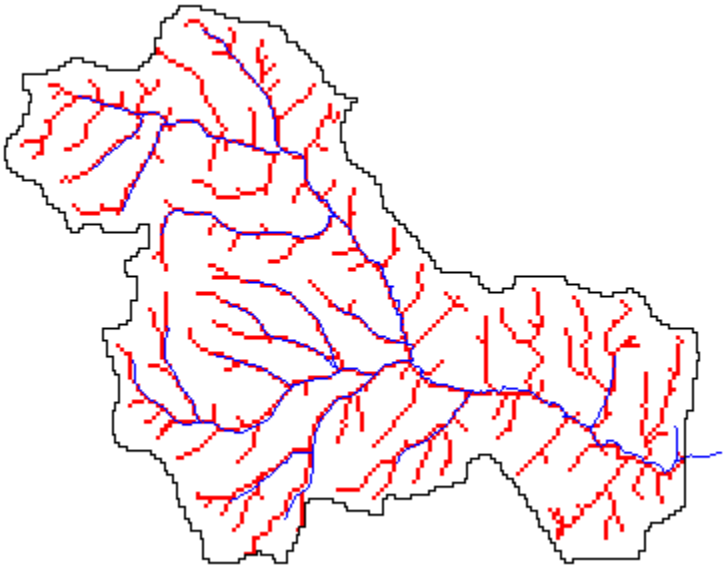

Figure 3.11. Owl Run DEM-based stream network (red) and USGS blue-line stream network (blue).

DEM-based stream network (red) and the USGS blue-line stream network (blue). A good agreement can be noticed between the two. However, the stream network obtained using the GIS shows more streams than the USGS blue line network because many of the GIS streams are ephemeral and intermittent streams. These are small streams that are not represented on the USGS map of streams.

3.4.3 Surface Runoff

Surface runoff is that portion of rainfall which, during and following a rainfall event, eventually appears as flowing water in the drainage network of a watershed (Ajward, 1996). Flow velocity varies both in time and space and the flow is classified as unsteady, non-uniform. Surface runoff can be classified into two categories: overland flow and channel flow. Overland flow is the portion of surface runoff that occurs on the upper end of the slopes in the form of a thin sheet of water. This portion of surface runoff flows on wide areas of the watershed and is not concentrated in channels. It eventually becomes channel flow when entering channels. Channel flow occurs in much narrower streams and has a confined path to flow in. Water flow can be described by the continuity and momentum equations as applied to an incompressible fluid. In this study, the kinematic flow assumptions are made. The dynamic terms in the momentum equation are neglected. As a result, Manning's equation is used to represent uniform flow.

3.4.3.1 Flow Velocity

Flow velocity is estimated for both types of cells, channel and overland. This is a prerequisite for computing travel time and, hence, the cumulative travel time to the

watershed outlet. Maidment (1993b) suggested the use of the SCS relationship of the form given by McCuen (1989):

$$V = k * S_g^{0.5} \tag{3.13}$$

Where:

K is a function of the land cover and landuse information,

S_g is the slope percent, and

V is the velocity.

This approach assumes that the velocity of flow is only a function of the physiographic characteristics of the watershed. It neglects the effect of rainfall intensity and implies that there is only one time-area curve for all storms in a given watershed. However, the procedure used in this study considers the effect of rainfall intensity on the time-area curve. It then can produce time-area curves that are more representative of a given storm.

3.4.3.1.1 Overland Flow Velocity

Overland flow velocity may be estimated by combining a kinematic wave approximation with Manning's equation. The depth of flow at equilibrium is given by (Overton and Meadows, 1976):

$$y = \left(\frac{ni_e x}{S_o^{0.5}} \right)^{0.6} \tag{3.14}$$

Where:

x is the distance along the flow plane (m).

S_o is the decimal slope.

y is the depth of flow at equilibrium (m).

i_e is the excess rainfall intensity (m/s).

n is Manning's roughness coefficient.

By substituting the depth of flow at equilibrium in Manning's equation, the velocity of overland flow can be calculated as:

$$Vo = \frac{(i_e x)^{0.4} S_o^{0.3}}{n^{0.6}} \qquad (3.15)$$

where *Vo* is the overland flow velocity (m/s).

The distance along the flow plane was considered to be the distance between any given cell and the closest ridge cell. This assumption involves simplification. However, it was considered that the error caused by this simplification is not of great importance taking into consideration the more complex procedures that would have been used. For ridge cells, this distance was considered to be half the length of flow inside that cell, i.e. 21 m if the flow is diagonal to the downstream cell and 15 m if the flow is orthogonal through that cell where the grid size used was 30 m.

Kilgore (1997) developed Manning's roughness coefficient maps for the watershed under study. Several assumptions were made to estimate these values since for most of the landuses existing in Owl Run watershed, values of Manning's roughness coefficient were not readily available. Table 3.4 shows these coefficients as well as the assumptions made and the map of these coefficients is shown in Figure 3.12.

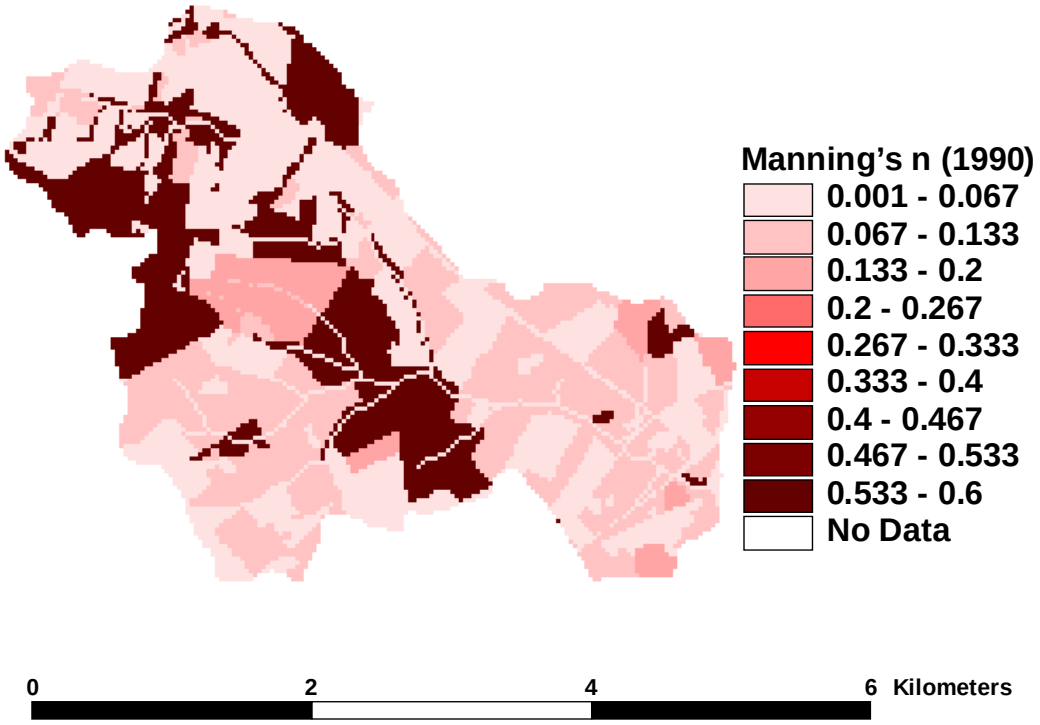

Figure 3.12. Manning's roughness coefficient (1990).

Table 3.4. Summary of Owl Run landuses with their corresponding Manning's roughness coefficients (Kilgore, 1997).

Landuse	*Code*	*Manning's n*	*Notes/Sources**
Alfalfa	Alf	0.04	normal, mature field crop, (1)
Barley	Ba	0.032	small grain (2)
Church	Ch	0.038	¾ good grass (3); ¼ concrete (2)
Clover	Clo	0.16	(2)
Commercial	Cm	0.015	(2)
Commercial 1	cm1	0.015	(2)
Commercial 2	cm2	0.015	(2)
Conventional corn	Co	0.08	(2)
Farmstead	Fa	0.025	½ short grass (2); ½ gravel
full season beans	Fsb	0.04	normal, mature field crop, (1)
Grass	Gr	0.046	(3)
Hay	Ha	0.035	
Idle	Id	0.05	(3)
light industry	Li	0.013	street pavement, (2)
loafing lot	Lo	0.04	lower end of grass/pasture range
Minimum till corn	Mco	0.2	(2) upper end of row crop range
min. till corn residue	Mcr	0.07	(3) cornstalk residue (4 t/ac.)
Minimum till sorghum	Mso	0.2	upper end of row crow range, (2)
no-till corn residue	Ncr	0.2	upper end of row crop range, (2)
no report	Nr	--	
no-till beans	Ntb	0.2	upper end of row crop range, (2)
no-till corn	Ntc	0.2	upper end of row crop range (2)
Oats	Oat	0.032	good, across slope small grain,
outside watershed	Out	--	
Pasture	Pa	0.1	middle of grass/pasture range
Plowed	Plw	0.055	(3)
Pond	Po	0.08	same as waterway
road/rail road	Rdr	0.02	gravel surface, (3)
Residential	Res	0.015	
strip conv. corn	Sco	0.09	½ pasture, ½ corn
small grain	Sg	0.032	(2)
Sorghum	So	0.086	½ good across slope small grain (3); ½ conventional corn (2)
strip small grain	Ssg	0.1	
Wetland	Wet	0.125	sluggish river reach, very weedy, fair condition
Wheat	Wh	0.032	(2)
Woodland	Wo	0.6	(2)
Waterway	Ww	0.08	(4)

*Sources:
1. Gray (1973)
2. Novotny and Olem (1994)
3. Engman (1986)
4. Brater and King (1976)

3.4.3.1.2 Channel Flow Velocity

Rainfall intensity in each cell is transformed into flow rate using:

$$Q = i_e A \tag{3.16}$$

Where:

Q is the equilibrium flow rate (m^3/s).

A is the cell size (900 m^2).

i_e is the rainfall intensity in that individual cell.

Flow is accumulated from each cell to the watershed outlet. The resulting flow accumulation grid is a grid where each cell has the value of the flow entering from all upstream cells. Channels were assumed to be trapezoidal with a side slope of 1:1.5. Manning's equation for flow in channels is found by:

$$Q = \frac{1}{n}\frac{S^{0.5}A^{5/3}}{P^{2/3}} \tag{3.17}$$

where:

Q is the equilibrium flow rate (m^3/s).

S is the channel bed slope (m/m).

n is the Manning's roughness coefficient.

A is the cross sectional area of the channel (m^2).

P is the wetted perimeter (m).

for a trapezoidal channel with a side slope of 1:z, the cross sectional area (A) and the wetted perimeter (P) are given by:

$$A = bd + zd^2 \qquad (3.18)$$

$$P = bd + zd^2 \qquad (3.19)$$

where:

d is the depth of flow at equilibrium (m).

b is the channel base width (m).

By substituting the cross sectional area and the wetted perimeter of the channel in Manning's equation, it can be solved for the depth of flow, d, since it is the only unknown. A FORTRAN program (Appendix A) was written to solve this equation for d using an iterative method. Once the depth of flow at equilibrium is known, the channel area can be calculated and hence, the flow velocity in channels using the following equation:

$$V_{ch} = \frac{Q}{A} \qquad (3.20)$$

where:

V_{ch} is the flow velocity in channels (m/s).

Q is the cumulative flow rate entering the cell (m^3/s).

A is the channel cross sectional area (m^2).

Manning's roughness coefficients were modified for the channel bed with "large" upstream area. For channel cells with upstream area of 18 to 360 ha (4000) cells, a value of Manning's roughness coefficient of 0.06 was assigned while a value of 0.05 was assigned to all cells of upstream area larger than 360 ha. These values were recommended by Brater and King (1976). Figure 3.13 shows these different channel segments and their corresponding Manning's roughness coefficient values. Owl Run watershed has a number of small ponds. A large Manning's roughness coefficient of 0.08 was assigned to cells in those ponds. This large n-value result in low velocities and long flow times to account for the time delay in ponds.

3.4.3.2 Travel Time Estimation

Once the flow velocity of overland and channel cells is determined, the travel time through each cell is estimated as:

$$t = \frac{D}{V} \qquad (3.21)$$

where:

t is the equilibrium travel time through any given cell (s).

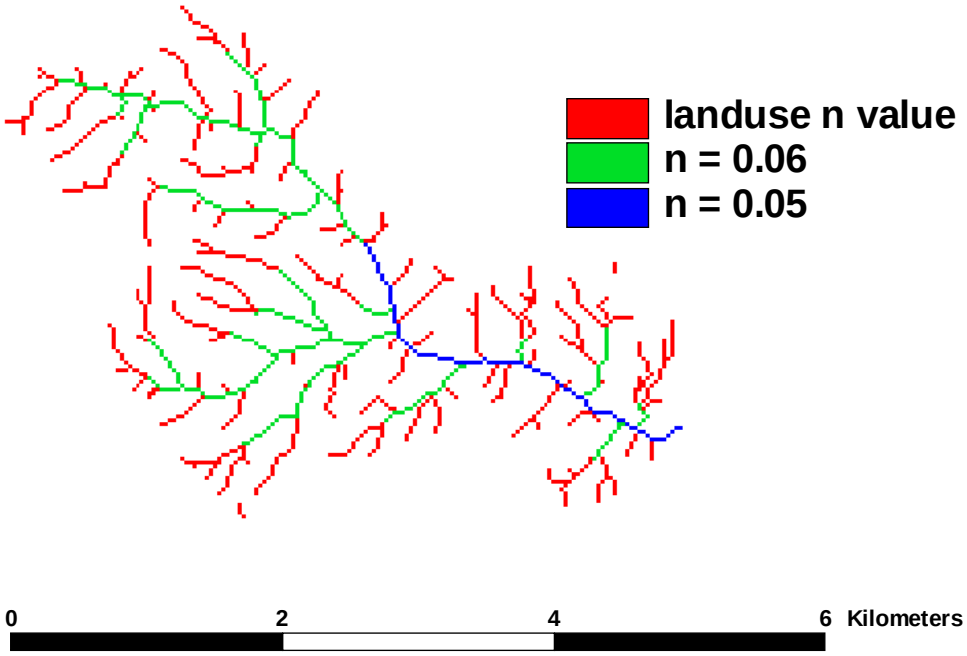

Figure 3.13. Manning's n values used for different stream segments.

D is the distance traveled through that cell (m).

V is the equilibrium flow velocity through the same cell (m/s).

For orthogonal flow, the flow distance is the cell width (30 m), while for diagonal flow, it is the √2 times cell width which yields 42.43 m in this study.

3.4.3.3 Cumulative Travel Time Estimation

At this point of analysis, the travel time through each cell, the flow direction, and the flow path are all known. It follows then that the cumulative travel time grid can be found by summing the travel times along the path of flow. The "Flowlength" request in ArcView was used to create the grid of cumulative flow time from each cell to the outlet cell of the watershed, and the "length" grid being the flow time grid.

3.4.3.4 Time-area Curve and Unit Hydrograph Development

The time-area curve is a representation of the cumulative area of the watershed that drains to the outlet as a function of time. The time-area curve is derived by reclassifying the cumulative time grid into equal time intervals of width Δt. The reclassified grid shows areas of incremental equal travel time. Flow from all cells in one area A_i drain to the watershed outlet during time interval i.

The unit hydrograph of a watershed can be derived from the watershed's time-area curve using a method similar to the S-hydrograph procedure. Maidment (1993b)

described this procedure as presented here in section 2.3.2.2.

3.5 Sensitivity Analysis

Kilgore (1997) investigated the sensitivity of her spatially distributed unit hydrograph (SDUH) to various parameters. The effect of changes in the parameters studied on peak flow rate, time to peak, and the general hydrograph shape was considered. In Kilgore's sensitivity study, the following parameters were investigated:

- Channel flow threshold
- Channel velocity
- Overland flow velocity
- Channel width
- Excess rainfall intensity
- Time step

Variation of the model response to changes in these parameters will be discussed in chapter 4. At the time Kilgore developed her model, only uniform excess rainfall was used since the method of excess rainfall generation used was the Φ-index method. However, using a spatially distributed excess rainfall in this current study introduced new parameters to be taken into consideration. These parameters are explained below.

In the distributed curve number (DCN) model, and in the cases where the whole watershed area is not generating excess rainfall, some cells have zero excess rainfall generated in them but at the same time flow is entering these cells from upstream cells. This causes the "local" travel time in these cells to be infinite since the "local" flow velocity is zero in cells without excess rainfall generated in them. Three options were

studied to assign these cells a travel time to be included in calculating the cumulative travel time for cells which are upstream of these cells: assigning a constant velocity of 0.02m/s, a constant velocity of 0.2m/s, and estimating the travel time based on the amount of inflow excess rainfall from the upstream cells.

Another factor tested was the effect of distributing the excess rainfall spatially over the watershed area versus considering a uniform excess rainfall. This effect was studied in two different ways. First, the spatially distributed excess rainfall from a single interval storm was found and tested against the equivalent uniform excess rainfall. Using single excess rainfall interval ensures isolating the temporal effect of the excess rainfall distribution on the output hydrograph shape and parameters, and hence, only the effect of the spatial distribution would be investigated.

Second, three hypothetical storms with excess rainfall amounts of 2, 10, and 20mm were studied. For each storm, the watershed area was divided into 3, 6, and 9 sub-areas based on travel time from the outlet. Figure 3.14 shows how the watershed area was divided when 3 sub-areas were used. The sub-areas were defined to be of approximately equal area. Two scenarios were compared. While keeping the average excess rainfall constant for all three classes of sub-areas, the excess rainfall was distributed spatially with the smaller excess rainfall being close to the streams in one case, and far from the streams in the other case. Table 3.5 shows the excess rainfall amounts (mm) for different numbers of sub-areas when excess rainfall of 2 mm was used. For the other two excess rainfall amounts, the values in Table 3.5 were multiplied by a constant. Hydrographs were also obtained using the same average excess rainfall but distributed uniformly.

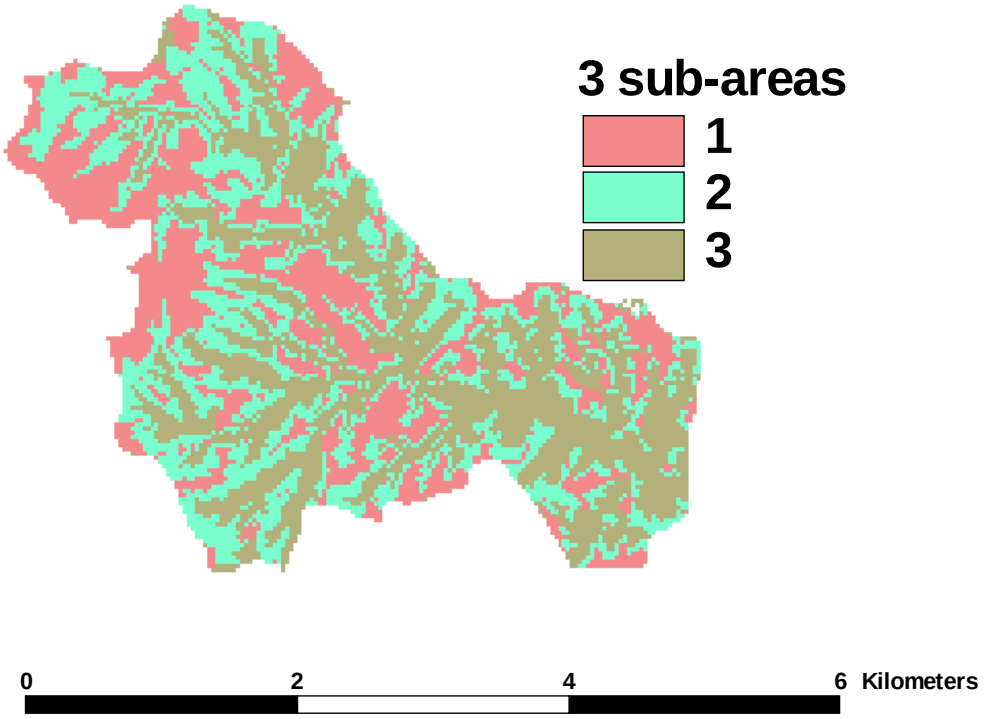

Figure 3.14. The three sub-areas of the watershed divided according to the flow time to the outlet.

Table 3.5. Amounts of excess rainfall in each sub-area in mm (average = 2 mm).

	Excess rainfall using 3 sub-areas	Excess rainfall using 6 sub-areas	Excess rainfall using 9 sub-areas
sub-area 1	0	0.0	0.0
sub-area 2	2	0.8	0.5
sub-area 3	4	1.6	1.0
sub-area 4		2.4	1.5
sub-area 5		3.2	2.0
sub-area 6		4.0	2.5
sub-area 7			3.0
sub-area 8			3.5
sub-area 9			4.0
Average	***2***	***2***	***2***

3.6 Evaluation

The resulting hydrographs using the three different models were compared among models as well as to the observed hydrograph. Several statistics were used along with the visual evaluation. Parameters evaluated were the peak flow rate, the time to peak, and the shape of the hydrograph. The following statistics were used.

- The relative error in the peak flow rate was calculated by:

$$rel.error = \frac{q_{ps} - q_{po}}{q_{po}} \qquad (3.22)$$

where: q_{ps} = simulated peak flow rate.

q_{po} = observed peak flow rate.

- In order to compare the three models' predictive capabilities, the mean arithmetic relative error (MARE) was calculated by:

$$MARE = \frac{\sum_{i=1}^{n} |rel.error|}{n} \qquad (3.23)$$

where n = number of events.

The MARE emphasizes outliers and good prediction results in MARE values that are close to zero

- The logarithmic mean arithmetic relative error LMARE. The LMARE was calculated by:

$$LMARE = \frac{\sum_{i=1}^{n} \log_{10} |rel.error|}{n} \qquad (3.24)$$

The LMARE statistic places less importance on the extreme values and good predictions result in LMARE values that are negative.

- Model efficiency (R^2) is a dimensionless coefficient that was first proposed by Nash and Sutcliffe (1970). This coefficient is widely accepted (Green and Stephenson, 1986). It ranges from zero to one. While an R^2 value of zero may be interpreted as that the model prediction is as accurate as using an average of the observed data, an R^2 value of one means that the simulated and observed hydrographs perfectly fit each other. The model efficiency was calculated for each storm event by:

$$R^2 = \frac{F_o^2 - F^2}{F_o^2} \qquad (3.25)$$

where:

$$F_o^2 = \sum_{i=1}^{n} [q_o(t) - \bar{q}_o]_i^2$$

$$F^2 = \sum_{i=1}^{n} [q_o(t) - q_s(t)]_i^2$$

$q_o(t)$ = observed flow rate at time t.

$q_s(t)$ = simulated flow rate at time t.

$\bar{q}_o$ = average observed flow rate for each time t.

n = number of pairs of ordinates compared in a single event.

- The sum of absolute residuals (SAR) was calculated by:

$$SAR = \sum_{i=1}^{n} \left| q_o(t) - q_s(t) \right|_i \qquad (3.26)$$

- and the total sum of absolute residuals (TSAR) was calculated by:

$$TSAR = \sum_{j=1}^{m} SAR_j \qquad (3.27)$$

where:

m = number of storm events.

- The sum of squared residuals (SSR) was calculated by:

$$SSR = \sum_{i=1}^{n} \left(q_o(t) - q_s(t) \right)_i^2 \qquad (3.28)$$

The SSR is one of the most common statistics used to evaluate hydrograph shapes (Green and Stephenson, 1986).

- The total sum of squared residuals (TSSR) was calculated by:

$$TSSR = \sum_{j=1}^{m} SSR_j \qquad (3.29)$$

- A test statistic was performed to test the hypothesis that the slope of the line

connecting the observed and predicted values for both the time to peak flow rate and the peak flow rate obtained from each model has a value of one. This test along with the correlation coefficients was used to statistically judge the closeness of predicted to observed data.

The results obtained using the three models were compared based on these statistics. The results of these comparisons may be found in Section 4.1.

4 Results and Discussion

The three different models (DCN, UCN, and Phi-index) were used to predict the output hydrograph for thirty storms. Results obtained using these three models were compared to the observed flow data for each corresponding storm. The relative error in peak flow rate, percent error in the time to peak flow rate, sum of squared residuals, sum of absolute residuals, and model efficiency were estimated for each event. In addition, test statistics was performed to assess the significance of closeness of predicted and observed hydrograph parameters.

For shape statistics such as sum of squared residuals, sum of absolute residuals, and model efficiency, Green and Stephenson (1986) suggested that the predicted hydrograph be shifted on the time axes to best visually fit the observed hydrograph. Their argument is that it is not fair to penalize a predicted output hydrograph that has a shape close to the observed hydrograph simply because there is a time lag between the two. For shape statistics in this study, predicted hydrographs were shifted so that the best visual fit was obtained with the observed hydrograph for each storm.

4.1 Model Output Analysis

4.1.1 Visual Comparison

The ASCE Task Committee on Definition of Criteria for Evaluation of Watershed Models of the Watershed Management Committee, Irrigation and Drainage Committee (1993) recommended that both visual and statistical comparison between model predicted and observed flows be made whenever data are presented. The visual comparison is considered a necessary first step in the evaluation process. It takes the form of graphic plots of predicted and observed flows. This step provides an overall view of the model performance and feeling for the model capabilities. Following is a description of three sample storms representing different ranges of storm size and seasons. Graphs for all 30 storms may be found in Appendix B.

Storm # 5: May28-29, 1990:

Storm # 5 is one of the larger storms with a total rainfall of 46.5 mm. It had an excess rainfall amount of 23.7 mm. This proportion of excess rainfall is considered high with regard to the total amount of rainfall. In the DCN model, the excess rainfall always starts with the first rainfall interval since there are a few cells in the watershed with a CN value of 100. For the other two models, excess rainfall was also generated at a very early time interval in the storm (first interval for the Phi model and in the second interval for the UCN model) because of the large proportion of runoff. All three models predicted the

time to peak in the same interval (Figure 4.1). The Phi model gave the closest prediction of peak flow rate to the observed peak flow, while both the DCN and the UCN models over-predicted the peak flow rate. Both the DCN and the UCN models predicted the hydrograph shape well. The Phi model predicted an additional smaller earlier peak because it had the largest excess rainfall generated at early stages of the storm following the pattern existing in the rainfall hyetograph. Overall, a clear relationship can be noticed between the temporal distribution of the excess rainfall generated by the different models and the predicted shape of the simulated hydrographs.

Storm # 27: September 10-11, 1992:

Storm # 27 was a 21.4 mm rainfall storm (Figure 4.2) with a 3 mm excess rainfall. The distribution of the rainfall was such that about half the total rainfall volume occurred in the first rainfall interval. The Phi model did a poor job predicting the time to peak, the peak flow rate, and the overall hydrograph shape. Looking at the excess rainfall predicted by the Phi model, it can be seen that the total amount of the 3 mm excess rainfall was predicted to occur in the first interval. This happened because the difference between the rainfall amount in that interval and the next highest amount of rainfall in any other interval was larger than the total excess rainfall value. Therefore, the first interval could, by itself, support all the excess rainfall. For the other two models, it can be noticed that the excess rainfall starts to be a smaller portion of the rainfall in earlier intervals because the total storage is not yet satisfied and then starts to become a larger portion of the rainfall in the following intervals. It can also be seen that the excess rainfall is larger in

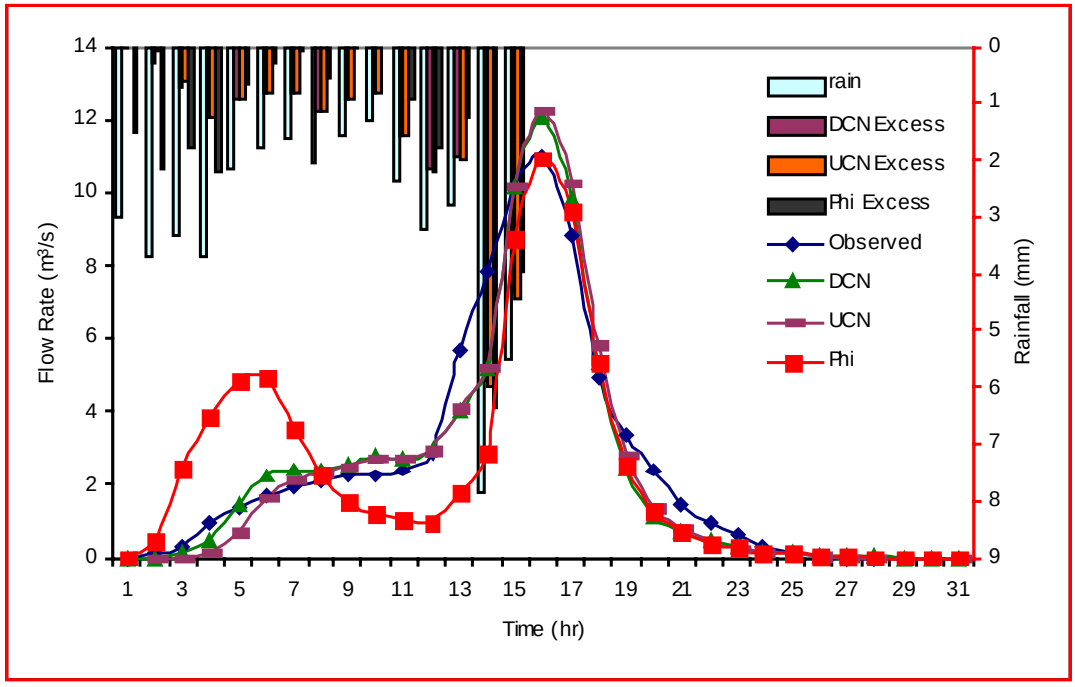

Figure 4.1. Observed and predicted hydrographs and different excess rainfall temporal distribution for storm # 5 (May 28-29, 1990).

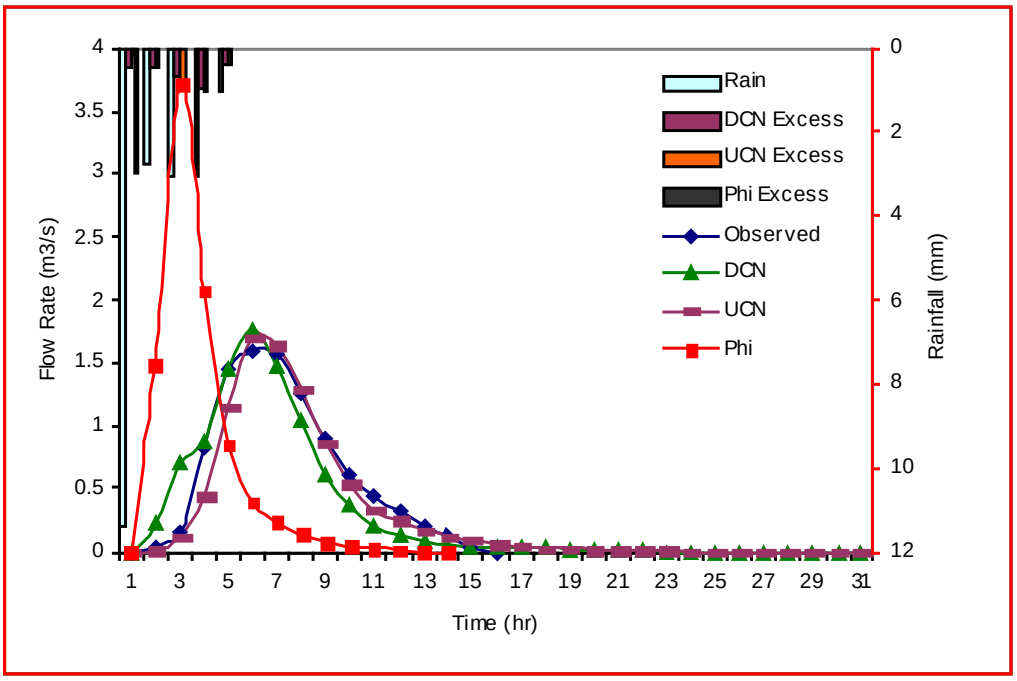

Figure 4.2. Observed and predicted hydrographs and different excess rainfall temporal distribution for storm # 27 (September 10-11, 1992).

earlier rainfall intervals using the DCN model than using the UCN model. The opposite happens in later intervals towards the end of the rainfall temporal distribution. Both the DCN and the UCN models predicted the right time to peak flow rate. The DCN model did a slightly better job predicting the peak flow rate and the overall hydrograph shape.

Storm # 9: November 9-10, 1990

Storm # 9 was a 49.5 mm rainfall storm with a 6 mm total excess rainfall (Figure 4.3). All three models under-predicted the time to peak flow rate and over-predicted the peak flow rate value. The Phi model under-predicted the time to peak flow rate by four hours. The starting points of the predicted hydrographs are not the same. For this study, the starting point of a given predicted hydrograph was taken to be the first interval that the corresponding model predicts excess rainfall. While this interval is always the first rainfall interval in the case of the DCN model (there are always at least few cells with a CN value of 100), it is different for the other two models. The UCN model starts generating excess rainfall after the total storage (0.2 S) is satisfied. This happened in the seventh interval for storm # 9. The excess rainfall continues to be generated in all the consecutive rainfall intervals for the UCN model. As for the Phi model, "chopping" the hyetograph resulted in excess rainfall generated in three non-consecutive rainfall intervals (6^{th}, 8^{th}, and 12^{th}).

The Phi model hydrograph started later than the DCN hydrograph but peaked earlier because it had a sharp rising limb. This happened because as much as 50% of the excess rainfall predicted by the Phi model occurred in the first interval of excess rainfall.

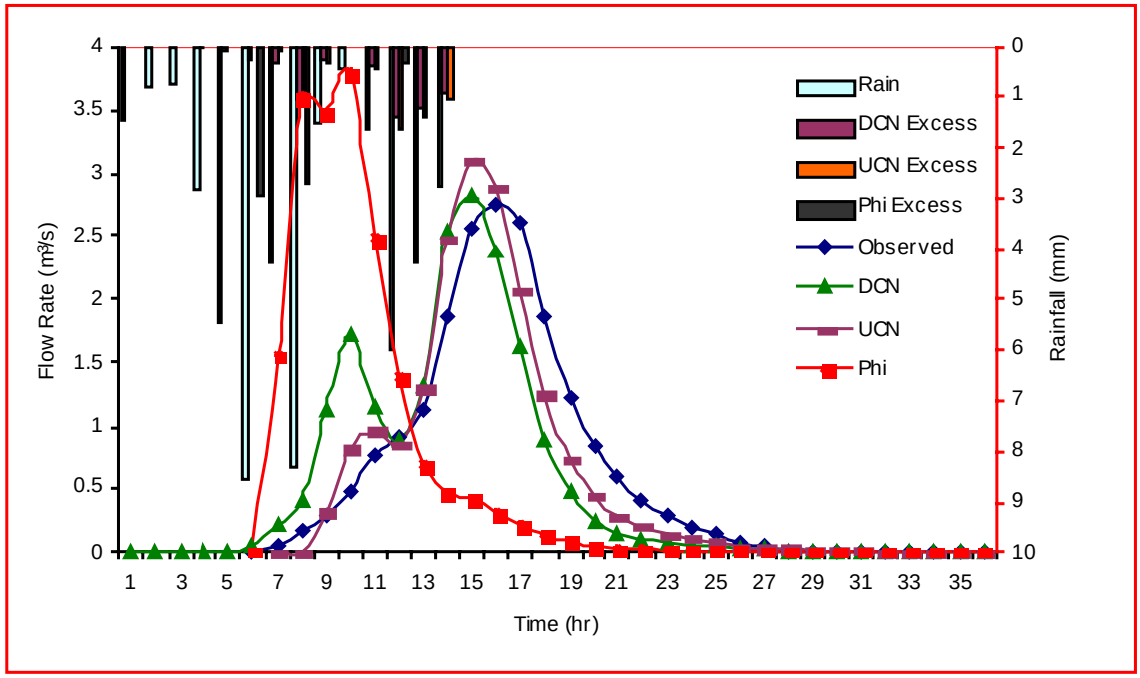

Figure 4.3. Observed and predicted hydrographs and different excess rainfall temporal distribution for storm # 9 (November 9-10, 1990).

Looking at the temporal distribution of the rainfall, one would predict that the resulting storm hydrograph should have two peaks. However, the response of the watershed was not as one would expect. The observed hydrograph had only one peak with a very mild neck seven hours after the starting point of the observed hydrograph. Such a storm is not showing the expected cause (input) and effect (output) phenomenon. There should be a recognizable pattern connecting the hyetograph and the resulting storm hydrograph. The lack of this cause and effect phenomenon in the observed data makes it quite hard for any model to predict a close hydrograph in parameters and shape to the observed one. Since the UCN model only started generating excess rainfall after the bulk of the first rainfall group was over, the UCN model predicted the closest shape and time to peak among the three models.

Overall, the following may be noticed from a visual inspection of the observed and predicted data for the 30 storms (Appendix B):

- There is a distinct relationship between the shape of the resulting hydrograph (using any model) and the temporal distribution of excess rainfall.
- Both the DCN and the UCN models predicted the hydrograph shape and parameters better than the Phi model.
- The DCN model hydrograph, in general, peaked before the UCN model hydrograph and had a higher peak flow rate. This could be attributed to the fact that for smaller storms, only portion of the watershed contributes to runoff and, hence, the excess rainfall intensity is higher. Higher excess rainfall intensities lead to higher flow velocities and shorter flow times. For larger

storms, and on the average, excess rainfall intensities resulting from the DCN model are higher (up to five times those obtained using the UCN model) for more than half the watershed area. This leads to higher flow velocities and shorter flow times.

- While the excess rainfall obtained using the DCN model always started at the first rainfall interval, the excess obtained using the other two models started at either the first rainfall interval or in later intervals.
- The UCN response to temporal changes in excess rainfall was smoother than that for the DCN model (Figure 4.3).
- For storms which have small excess rainfall but are distributed over multiple excess rainfall periods (see storms # 19, 20, 26, in Appendix B), the resulted UCN model hydrograph tended to have large attenuation.
- There was an exact match between the hydrograph obtained using the UCN and Phi models in one case where the excess rainfall was exactly the same for both models (storm # 24 in Appendix B).
- The hydrograph shape and parameters obtained using the UCN and the DCN models were closer to each other as the storm size increased. This resulted because for larger storms, the effect of spatial distribution of excess rainfall becomes less important since all cells generate large excess rainfall intensities.

4.1.2 Peak Flow Rate Analysis

Table 4.1 summarizes the observed peak flow rates along with the predicted peak flow rates using the DCN, the UCN, and the Phi models. Relative error in peak flow rate

Table 4.1. Observed and predicted peak flow rates (m^3/s).

	Peak flow rate (m^3/s)			
Storm	**Observed**	**DCN**	**UCN**	**Phi**
1	0.50	0.68	0.61	0.51
2	3.13	3.49	3.64	5.29
3	1.34	1.72	1.82	2.97
4	4.25	4.72	3.89	8.34
5	11.02	12.03	12.28	10.96
6	1.22	1.73	1.39	1.75
7	0.58	1.13	0.63	0.93
8	1.47	1.68	1.95	3.17
9	2.75	2.95	3.09	3.79
10	1.71	1.80	1.35	1.69
11	3.02	3.91	3.68	5.51
12	12.95	13.56	14.11	11.09
13	2.57	2.73	2.16	3.21
14	2.21	2.42	2.32	3.51
15	1.93	2.56	2.05	3.65
16	1.92	2.54	1.92	2.87
17	8.96	8.81	8.74	10.73
18	0.42	0.57	0.47	0.57
19	1.04	1.02	0.47	0.80
20	0.76	0.68	0.50	1.04
21	1.66	2.65	1.98	2.32
22	12.35	13.02	16.51	18.60
23	3.07	3.12	2.82	3.86
24	0.54	0.66	0.42	0.42
25	0.46	0.48	0.35	0.42
26	0.43	0.42	0.22	0.39
27	1.60	1.77	1.71	3.71
28	0.83	0.78	0.77	1.39
29	1.90	2.27	1.86	2.94
30	13.20	18.20	17.92	21.38

estimation, mean arithmetic relative error (MARE) (equation 3.23), and logarithmic mean arithmetic relative error (LMARE) (equation 3.24) values are summarized in Table 4.2.

The UCN model had the lowest MARE value followed by the DCN model and finally the Phi model. While the MARE values for DCN and UCN models were close to each other (0.198 and 0.184, respectively), the value of MARE for the Phi model was more than double these amounts (0.485). Since the lower the MARE the more accurate the prediction, it can be said that both the DCN and the UCN models did a better job predicting the peak flow rate value than the Phi model, with a slight preference of the DCN model over the UCN model. According to the LMARE statistics (which places less importance on the extreme values), and since the more negative the LMARE value the better, the DCN did the best job predicting the peak flow rate values followed by the UCN model and then the Phi model.

For the DCN model, 63% of the predicted hydrographs had relative error values in peak flow rates lower than 0.2. This percent was 60 for the UCN model and only 23 for the Phi model. However the maximum relative error in peak flow rate was the lowest for the UCN model (0.55) followed by the DCN model (0.95) and a large value of 1.32 for the Phi model. While the UCN model over-predicted the peak flow rate value for 60% of the storms modeled, the Phi model over-predicted that parameter for 76% of the storms followed by the DCN model (83%). Figure 4.4 shows a graphical comparison between the observed and the predicted values of the peak flow rate. It can be seen that there is a general trend of over-prediction especially for the Phi and the DCN models.

The hypothesis that a straight line with a slope of one (predicted data are not different from observed data) best fits the observed versus predicted peak flow rates for

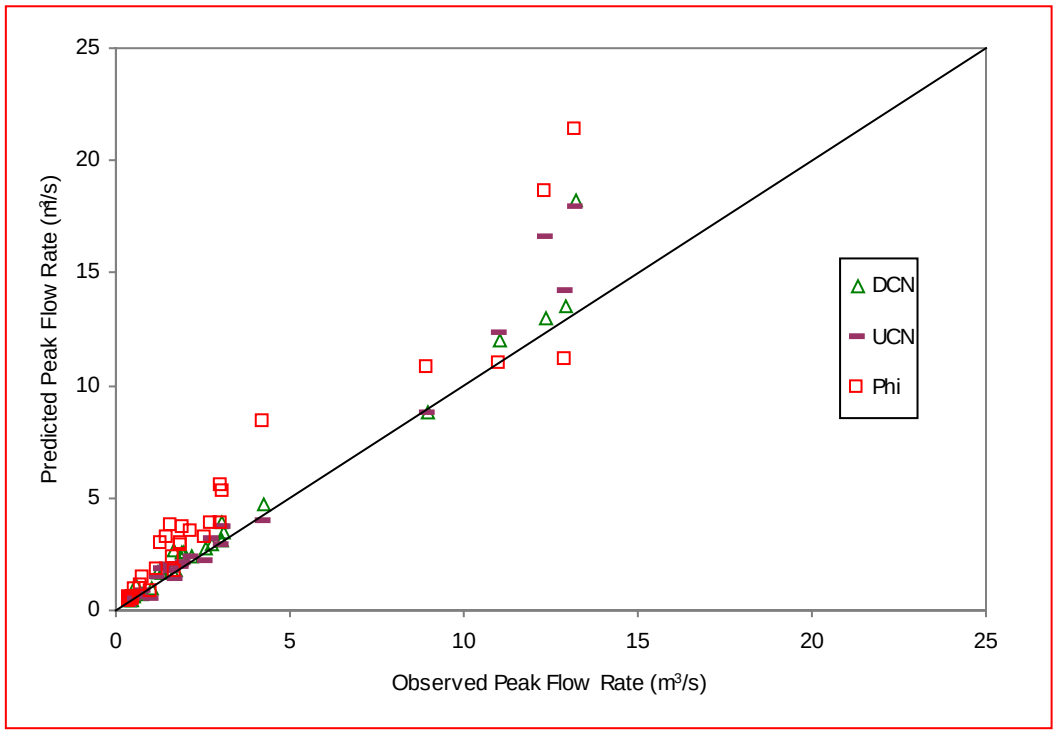

Figure 4.4. Predicted versus observed peak flow rate plot for the three models.

Table 4.2. Relative error in peak flow rate for the three models.

Storm	DCN	UCN	Phi
1	0.360	0.220	0.020
2	0.115	0.163	0.690
3	0.284	0.358	1.216
4	0.111	-0.085	0.962
5	0.092	0.114	-0.005
6	0.418	0.139	0.434
7	0.948	0.086	0.603
8	0.143	0.327	1.156
9	0.073	0.124	0.378
10	0.053	-0.211	-0.012
11	0.295	0.219	0.825
12	0.047	0.090	-0.144
13	0.062	-0.160	0.249
14	0.095	0.050	0.588
15	0.326	0.062	0.891
16	0.323	0.000	0.495
17	-0.017	-0.025	0.198
18	0.357	0.119	0.357
19	-0.019	-0.548	-0.231
20	-0.105	-0.342	0.368
21	0.596	0.193	0.398
22	0.054	0.337	0.506
23	0.016	-0.081	0.257
24	0.222	-0.222	-0.222
25	0.043	-0.239	-0.087
26	-0.023	-0.488	-0.093
27	0.106	0.069	1.319
28	-0.060	-0.072	0.675
29	0.195	-0.021	0.547
30	0.379	0.358	0.620
MARE	***0.198***	***0.184***	***0.485***
LMARE	***-0.927***	***-0.815***	***-0.527***

each model was statistically tested. This hypothesis was rejected for all models at a level of significance (p-value) less than 0.01. Level of significance represents the probability of observing a sample outcome more contradicting to the null hypothesis and the smaller the p-value, the more evidence there is to reject the null hypothesis (Ott, 1993). Typically, a p-value of 0.05 is considered as a threshold value where lower values cause the null hypothesis to be rejected. The correlation coefficients between the observed and predicted peak flow rates were 0.972, 0.976, and 0.891 for the DCN, UCN, and Phi models, respectively. These relatively high correlation coefficients indicate that the data points were closely scattered around the best fit line. The results of this test statistics show that, statistically, peak flow rate predictions from all models were different from the observed peak flow rate data.

4.1.3 Time to Peak Flow Rate

Table 4.3 summarizes the observed time to peak flow rate values along with the corresponding predicted time to peak flow rate value using each model. The relative error in time to peak prediction is given in Table 4.4. The logarithmic mean arithmetic relative error (LMARE) was not calculated for the time to peak because for few cases, the predicted value matched exactly the observed value which caused the relative error to be zero for these cases. The logarithm of zero is undefined and hence the LMARE was not calculated. The mean arithmetic relative error (MARE) was calculated for each model. The UCN model had the lowest MARE value followed by the DCN model and finally the Phi model.

Table 4.3. Observed and predicted time to peak flow rate values using the three models (hr).

	Time to peak (hr)			
Storm	Observed	DCN	UCN	Phi
1	5	3	4	3
2	6	4	4	4
3	8	7	7	5
4	11	10	10	9
5	16	16	16	16
6	7	6	6	6
7	9	6	8	6
8	23	22	22	17
9	16	15	15	10
10	5	3	4	4
11	8	6	6	4
12	11	9	10	8
13	7	7	8	7
14	7	6	7	4
15	7	5	7	6
16	4	3	4	3
17	15	14	14	14
18	6	4	5	5
19	3	3	6	3
20	5	4	6	4
21	4	3	3	3
22	6	4	4	3
23	4	4	4	3
24	5	5	5	4
25	8	8	9	5
26	9	8	8	7
27	6	6	6	3
28	11	9	11	9
29	10	7	8	5
30	6	4	4	4

Table 4.4. Relative error in time peak flow rate for the three models.

Storm	DCN	UCN	Phi
1	-0.400	-0.200	-0.400
10	-0.400	-0.200	-0.200
2	-0.333	-0.333	-0.333
7	-0.333	-0.111	-0.333
18	-0.333	-0.167	-0.167
22	-0.333	-0.333	-0.500
30	-0.333	-0.333	-0.333
29	-0.300	-0.200	-0.500
15	-0.286	0.000	-0.143
11	-0.250	-0.250	-0.500
16	-0.250	0.000	-0.250
21	-0.250	-0.250	-0.250
20	-0.200	0.200	-0.200
12	-0.182	-0.091	-0.273
28	-0.182	0.000	-0.182
6	-0.143	-0.143	-0.143
14	-0.143	0.000	-0.429
3	-0.125	-0.125	-0.375
26	-0.111	-0.111	-0.222
4	-0.091	-0.091	-0.182
17	-0.067	-0.067	-0.067
9	-0.063	-0.063	-0.375
8	-0.043	-0.043	-0.261
5	0.000	0.000	0.000
13	0.000	0.143	0.000
19	0.000	1.000	0.000
23	0.000	0.000	-0.250
24	0.000	0.000	-0.200
25	0.000	0.125	-0.375
27	0.000	0.000	-0.500
MARE	***0.172***	***0.153***	***0.265***

The predicted time matched the observed time exactly for 27% of the modeled storms using the UCN model, 23% for the DCN model, and only 10% for the Phi model. The UCN model showed closer overall prediction. Using this model, 80% of the storms had relative error lower or equal to 0.2. For the DCN model, the percent of storms with relative error lower or equal to 0.2 was 50. Again, this percent was lower for the Phi model (30).

Figure 4.5 shows a comparison between the time to peak obtained using the three different methods versus the observed time to peak for each storm. It can be seen that there is a general trend of under-predicting the time to peak flow rate. The UCN model was the most moderate model in this regard where 60% of the times were under-predicted. The DCN model under-predicted the time to peak for 77% of the storms while 90% of the time to peak flow rates were under-predicted using the Phi model. The maximum value of the relative error in time to peak prediction resulted in the case of the UCN model (1.0). The maximum value was 0.55 for the DCN model and 0.5 for the Phi model. Even though the UCN model produced the maximum relative error in predicting the time to peak among all three models, the next highest value of the relative error in the UCN model was 0.33 compared to many values more than this value (0.33) using the other two models.

The hypothesis that a straight line with a slope of one best fits the observed versus predicted time to peak flow rates for each model was statistically tested. This hypothesis was accepted at a p-values of 0.337, 0.8822, and 0.271 for the DCN, UCN, and Phi models, respectively. The correlation coefficients between the observed and predicted peak flow rates were 0.960, 0.938, and 0.876 for the DCN, UCN, and Phi models,

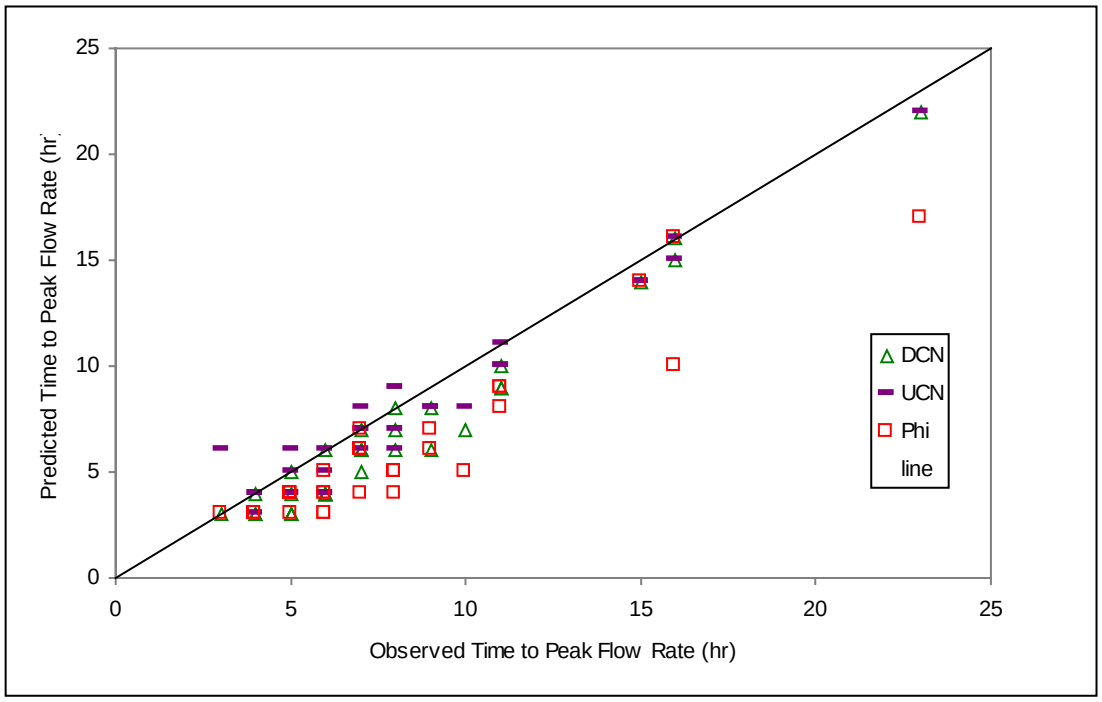

Figure 4.5. Predicted versus observed time to peak flow rate plot for the three models.

respectively. The results of this test statistics indicate that, statistically, the predicted times to peak flow rate obtained using all models were not different from the observed times.

4.1.4 Shape Statistics and Goodness of Fit

The shapes of the hydrographs obtained using the three different models were compared to the observed hydrograph shape for each corresponding storm. Statistics used for this comparison were the Nash-Sutcliffe (model efficiency, R^2) coefficient, sum of squared residuals (SSR), and sum of absolute residuals (SAR). The ASCE Task Committee (1993) recommended that the number of goodness-of-fit criteria be kept to a minimum.

4.1.4.1 Model Efficiency

The model efficiency (R^2) is a goodness-of-fit criterion and is defined by equation (3.23). Table 4.5 summarizes the R^2 values for all storms using the DCN, UCN, and the Phi model. Overall, the DCN model had the highest average R^2 followed closely by the UCN model and then came the Phi model with an average value of about half that of the other two models. Of the 30 storms analyzed in this study, the UCN model had the highest R^2 value for 14 storms followed by the DCN (12 storms) and the Phi model (4 storms). The UCN model also had the least number of storms with the lowest R^2 value followed by the DCN model and then the Phi model. These results are summarized in Table 4.5.

Table 4.5. R^2 values, number of storms each model had the lowest and the highest R^2 value, and number of storms where each model had R^2 values greater or equal to 0.90 and 0.95 (out of 30 storms).

	Storm	DCN	UCN	Phi
	1	0.992	0.995	0.998
	2	0.778	0.869	-0.914
	3	0.867	0.891	0.301
	4	0.853	0.869	-1.789
	5	0.955	0.952	0.758
	6	0.899	0.987	0.947
	7	0.963	0.995	0.969
	8	0.935	0.943	0.720
	9	0.806	0.962	0.713
	10	0.972	0.896	0.915
	11	0.693	-0.228	-1.578
	12	0.838	0.933	0.727
	13	0.764	-0.104	0.733
	14	0.885	0.547	-1.756
	15	0.868	0.914	-0.063
	16	0.725	0.955	0.797
	17	0.924	0.910	0.821
	18	0.996	0.996	0.993
	19	0.989	0.957	0.978
	20	0.989	0.984	0.977
	21	0.797	0.928	0.884
	22	0.914	0.786	0.450
	23	0.949	0.807	0.745
	24	0.997	0.997	0.997
	25	0.995	0.997	0.999
	26	0.995	0.988	0.999
	27	0.847	0.909	-0.860
	28	0.976	0.990	0.937
	29	0.917	0.935	0.719
	30	0.719	0.736	0.573
	Average	***0.893***	***0.843***	***0.423***
Number of storms with:	***Highest R^2***	***12***	***14***	***4***
	Lowest R^2	***6***	***4***	***20***
	$R^2 \geq 0.90$	***16***	***20***	***11***
	$R^2 \geq 0.95$	***11***	***13***	***8***

For 20 of the 30 storms modeled, the hydrographs obtained using the UCN model had an R^2 of 0.9 or more while this number was 16 and 11 out of 30 for the DCN model and the Phi model, respectively. The same trend existed for values of R^2 greater or equal to 0.95. The UCN model had the largest number of storms falling into that category followed by the DCN model and then the Phi model. These results are summarized in Table 4.5.

4.1.4.2 Sum of Squared Residuals (SSR) and Total Sum of Squared Residuals (TSSR)

Table 4.6 summarizes the SSR values for all storms using the three models. According to the TSSR, the DCN model did the best job predicting the hydrograph shapes. The TSSR value for the UCN model followed very closely that for the DCN model with the Phi model falling behind with a TSSR value of more than twice that for the other two models. For half the storms, the UCN model predicted the hydrograph shape better than the other two models while the DCN model was the best for 12 out of 30 storms. For the remaining 3 storms, the Phi model did the best job predicting the hydrograph shape. Table 4.6 summarizes the number of storms each model had the lowest and the highest SSR value.

4.1.4.3 Sum of Absolute Residuals (SAR) and Total Sum of Absolute Residuals (TSAR)

The SAR values for all storms are given in table 4.7. According to the TSAR, the UCN model did the best overall job predicting the hydrograph shape followed closely by the DCN model and then the Phi model. The TSAR values are also given in table 4.7.

Table 4.6. Sum of squared residuals for each storm using the three models, and the number of storms each model had the lowest and the highest SSR value (out of 30 storms).

	Storm	DCN	UCN	Phi
	1	0.129	0.081	0.037
	2	1.020	0.602	8.811
	3	1.100	0.898	5.759
	4	2.600	2.320	49.347
	5	16.672	17.944	90.643
	6	0.855	0.108	0.448
	7	0.467	0.065	0.390
	8	1.112	0.985	4.815
	9	4.479	0.879	6.624
	10	0.239	0.902	0.734
	11	3.021	12.093	25.378
	12	60.995	25.107	102.853
	13	1.621	7.581	1.831
	14	0.546	2.144	13.054
	15	0.723	0.473	5.831
	16	1.903	0.311	1.409
	17	10.502	12.564	24.944
	18	0.065	0.067	0.106
	19	0.153	0.584	0.298
	20	0.140	0.193	0.283
	21	1.361	0.480	0.775
	22	22.515	55.759	143.481
	23	0.357	1.340	1.777
	24	0.041	0.048	0.048
	25	0.079	0.044	0.017
	26	0.086	0.224	0.011
	27	0.511	0.303	6.200
	28	0.226	0.100	0.600
	29	0.604	0.474	2.046
	30	90.351	84.851	137.188
	TSSR	***224.470***	***229.523***	***635.739***
Number of storms with:	***Highest SSR***	***4***	***4***	***22***
	Lowest SSR	***12***	***15***	***3***

Table 4.7. Sum of absolute residuals for each storm using the three models, and the number of storms each model had the lowest and the highest SAR value (out of 30 storms).

	Storm	DCN	UCN	Phi
	1	1.109	0.939	0.701
	2	3.086	1.829	6.904
	3	3.976	3.487	7.309
	4	5.172	5.279	21.193
	5	14.191	14.855	34.240
	6	2.556	0.999	1.574
	7	1.746	0.756	1.724
	8	4.515	4.229	7.604
	9	6.348	3.320	8.343
	10	1.232	2.289	1.824
	11	5.756	10.105	12.265
	12	19.087	11.151	27.381
	13	2.909	7.279	3.383
	14	2.160	3.752	8.348
	15	2.325	2.007	5.923
	16	3.185	1.387	2.688
	17	11.798	10.148	15.445
	18	0.724	0.760	1.036
	19	0.814	1.901	1.054
	20	1.143	1.335	1.535
	21	2.845	1.731	2.069
	22	12.609	15.815	24.737
	23	1.598	2.826	2.957
	24	0.535	0.607	0.607
	25	0.835	0.563	0.377
	26	1.077	1.808	0.286
	27	2.070	1.601	5.839
	28	1.367	1.143	1.945
	29	2.508	1.916	4.035
	30	20.044	17.572	22.946
	TSAR	***139.319***	***133.392***	***236.272***
Number of storms with:	***Highest SAR***	***6***	***4***	***20***
	Lowest SAR	***12***	***15***	***3***

Similar to the SSR statistics, the UCN model had the lowest SAR for half the storms while the DCN model had the lowest value for 12 storms out of the 30 modeled storms. The Phi model had the lowest SAR value for only 3 storms. Table 4.7 summarizes the number of storms each model had the lowest and the highest SAR value.

4.1.5 Analysis Based on Season

The effect of seasonal effects on the hydrograph prediction accuracy was investigated. Each year was divided into three seasons. "Spring" was considered to be the period from April first until June 15th. "Summer" was considered to be the period from June 16th until September 15th. "Fall" is the remaining period from September 16th through November. Seven storms fell in the spring period, 14 storms in summer, and 9 storms in the fall period.

Looking first at the peak flow rate, the models' accuracy varied from season to season. There was also the variation among all models for a given season. Table 4.8 summarizes these results. According to both the MARE and the LMARE, both the DCN model and the UCN model did a better job predicting the peak flow rate value than the Phi model. For summer season, the DCN did a better job than the UCN model according to both the MARE and the LMARE statistics. The DCN model had a value of MARE of about 60% of that for the UCN model. On the other hand (according to both the MARE and the LMARE), for both spring and fall, the UCN model seemed to produce better results than the DCN model. The difference in the MARE and the LMARE values was more obvious in favor of the UCN model in fall rather than spring season. In comparing the performance of each model for different seasons, the DCN model did the best job

Table 4.8. Seasonal effect on peak flow rate prediction.

	Spring (n = 7)		*Summer (n = 14)*		*Fall (n = 9)*	
	MARE	***LMARE***	***MARE***	***LMARE***	***MARE***	***LMARE***
DCN	0.191	-0.878	0.147	-1.094	0.282	-0.706
UCN	0.155	-0.920	0.238	-0.699	0.122	-0.915
Phi	0.493	-0.744	0.367	-0.629	0.662	-0.201

Table 4.9. Seasonal effect on time to peak flow rate prediction (MARE).

	Spring (n = 7)	*Summer (n = 14)*	*Fall (n = 9)*
DCN	0.193	0.123	0.215
UCN	0.140	0.203	0.083
Phi	0.218	0.258	0.312

Table 4.10. Seasonal effect on average model efficiency.

	Spring (n = 7)	*Summer (n = 14)*	*Fall (n = 9)*
DCN	0.909	0.903	0.866
UCN	0.926	0.774	0.886
Phi	0.167	0.565	0.401

predicting the peak flow rate in summer followed by spring and lastly fall season. As for the UCN model, it did the best job in fall followed by spring and then summer. The Phi model predicted the peak flow rate best in spring followed then by summer and finally fall season.

For the time to peak prediction and its relation to seasonal variation, a similar trend was noticed as for the peak flow rate prediction accuracy. Table 4.9 gives the average MARE values for each combination of model and season. Both the DCN model and the UCN model predicted the time to peak more accurately than the Phi model. The DCN model had the best time to peak prediction accuracy for the summer season. On the other hand, the UCN model best predicted the time to peak in both spring and fall seasons. As for each model and its prediction accuracy variation from season to season, the DCN model showed best prediction accuracy in summer followed by fall and then spring. The UCN model did its best job in fall with a low MARE value followed by that in spring and finally in summer. The Phi model showed its best prediction accuracy in spring followed by summer and finally fall season.

As for the hydrograph shapes and according to the average R^2 value, again, the DCN model showed the best results for summer season. The DCN did the best job predicting the hydrograph shape in both spring and fall. Both the DCN model and the UCN model showed greater accuracy in the time to peak prediction than the Phi model in all seasons. Average R^2 for different seasons are given in Table 4.10 for each model.

As discussed earlier in section 4.1.1, hydrographs obtained using the DCN model, in general, peaked earlier and had higher peak flow rates than hydrographs obtained using the UCN model. Summer rains in Owl Run watershed cause more runoff since they are,

in general, in the form of heavy downpours, showers, and thunderstorms. This caused the hydrographs predicted using the DCN model to better match the observed hydrographs than those predicted using the UCN model in summer.

4.1.6 Analysis Based on Storm Size

The prediction accuracy of the three models was evaluated as a function of the storm size. Both the DCN and the UCN models did a better job predicting the peak flow rate value than the Phi model for all storm size classes. For both the DCN model and the UCN model, there was a distinct trend of better prediction as the storm size increased (Table 4.11). According to both the MARE and LMARE statistics, the DCN model did a much better job predicting the peak flow rate value for larger storms than the UCN model. For both smaller and mid-size storms, the UCN model seemed to give better predictions for the peak flow rate values. The Phi model gave better predictions for both smaller and larger storms than for mid-size storms.

The same trend was observed for the time to peak flow rate predictions. The accuracy of prediction increased for both the DCN model and the UCN model as the storm size increased (Table 4.12). The UCN model gave better predictions regarding the time to peak flow rate for small and large storm size classes than the DCN model. Prediction accuracy for the two models were close for mid-size storms. The Phi model predicted the time to peak flow rate better for smaller and larger storms than for mid-size storms.

Due to the limited sample size in classes of storm size, strong conclusions may not be derived at this moment and further investigation of the prediction accuracy as a

Table 4.11. Storm size effect on peak flow rate prediction.

	R.V. ≤ 18mm (n = 5)		*18mm < R.V. ≤ 49mm (n = 20)*		*49mm < R.V. (n = 5)*	
	MARE	***LMARE***	***MARE***	***LMARE***	***MARE***	***LMARE***
DCN	0.232	-0.692	0.226	-0.882	0.050	-1.345
UCN	0.213	-0.698	0.192	-0.797	0.122	-1.008
Phi	0.332	-0.679	0.595	-0.396	0.196	-0.901

Table 4.12. Storm size effect on time to peak flow rate prediction (MARE).

	R.V. ≤ 18mm (n = 5)	*18mm < R.V. ≤ 49mm (n = 20)*	*49mm < R.V. (n = 5)*
DCN	0.253	0.152	0.142
UCN	0.180	0.156	0.113
Phi	0.260	0.286	0.183

Table 4.13. Storm size effect on average model efficiency (R^2).

	R.V. ≤ 18mm (n = 5)	*18mm < R.V. ≤ 49mm (n = 20)*	*49mm < R.V. (n = 5)*
DCN	0.950	0.887	0.861
UCN	0.968	0.843	0.719
Phi	0.610	0.287	0.782

function of storm size is required. However, one possible explanation for the improved prediction accuracy with larger storms is the effect of storage time in channels which is not accounted for in all models discussed in this study. Neglecting storage time is believed to have more impact on prediction accuracy with smaller storms in which flow is slower in reality.

According to the R^2 values, and for both the DCN model and the UCN models, there was a trend of better predictions for the hydrograph shape as the storm size decreased (Table 4.13). The Phi model predicted the hydrograph shape worst for mid-size storms.

4.2 Sensitivity Analysis

Kilgore (1997) conducted a series of sensitivity analyses to investigate the effect of changing model parameters on the output hydrograph. Following is a description of the parameters investigated in that study.

The effect of the *channel flow threshold* (CFT) was significant. The CFT represents the number of upstream cells after which the flow is considered to have the characteristics of channel flow. The larger the CFT the more attenuation and the lower the peak flow rate value. This is attributed to the fact that higher CFT values mean larger number of overland flow cells and, hence, larger values for the cumulative travel time since the travel time is higher in overland flow cells than in channel flow cells.

The second factor investigated was the *channel velocity*. It appeared that changes in channel velocity affected the time to peak to a much greater extent than the peak flow rate. The higher the channel velocity, the lower the cumulative travel time and eventually

the lower the time to peak. On the other hand, changes in the *overland flow velocity* had more impact on the peak flow rate than on the time to peak. Increasing the *channel bottom width* slightly increased the time to peak flow rate, but had very little impact on the peak flow rate and the overall hydrograph shape.

Excess rainfall intensity was found to have a big impact on both the time to peak flow rate and the peak flow rate. Increasing the excess rainfall intensity caused an earlier and larger peak flow rate. Sensitivity analysis was also performed on the *time step* used in that study. There was very little change in the peak flow rate value and the general hydrograph shape due to changes in the time step used. According to Kilgore (1997) the time step did not seem to be a significant parameter in the spatial distributed unit hydrograph model she developed.

In Kilgore's study, only spatially uniform excess rainfall was used. However, in this current study, both spatially distributed and spatially uniform excess rainfall were used. The use of spatially distributed excess rainfall introduced new parameters that did not exist in Kilgore's study. Following are the results from a sensitivity analysis study for these new parameters and their effect on the output hydrograph shape and parameters.

4.2.1 Spatially Varied versus Distributed Excess Rainfall

To differing extents, the models used in this study account for the temporal variation in excess rainfall. Temporal variation, in combination with spatial variation in the DCN model, affects the shape and parameters of the resulting hydrograph. The effect of the spatial distribution of excess rainfall was studied in two ways. Firstly, to study the effect of the spatial distribution of excess rainfall in isolation of its temporal variation,

two hypothetical storms with excess rainfall in a single interval were used. The two storms differed in the rainfall volume; a smaller storm with total rainfall of 15 mm and a larger storm with total rainfall of 43 mm. For each storm, the total volume of the spatially varied excess rainfall was calculated. This total volume of excess rainfall was then uniformly distributed over the entire area of the watershed. The two scenarios were then modeled using the DCN model for the spatially distributed excess rainfall and the UCN model for the spatially uniform excess rainfall. Resulting hydrographs are shown in Figures 4.6 and 4.7.

For the same excess rainfall volume, the DCN model produces a higher peak flow rate than the UCN model. The proportional difference between the peak flow rates is larger in the case in which the total rainfall volume was lower. This can be attributed to the fact that for smaller storms, and using the DCN model to estimate the excess rainfall, only a portion of the total watershed area contribute to generating excess rainfall. This requires that a smaller area produces excess rainfall equal in amount to that produced using the UCN model with a contributing area equal to the total watershed area. Therefore, the excess rainfall intensity is, on the average, higher in the case of using the DCN model. Higher excess rainfall intensities produce higher peak flow rates and earlier time to peak flow rate.

Secondly, three hypothetical storms with excess rainfall of 2, 10, and 20 mm in a single 1-hr interval were studied. For each storm, the excess rainfall was distributed over

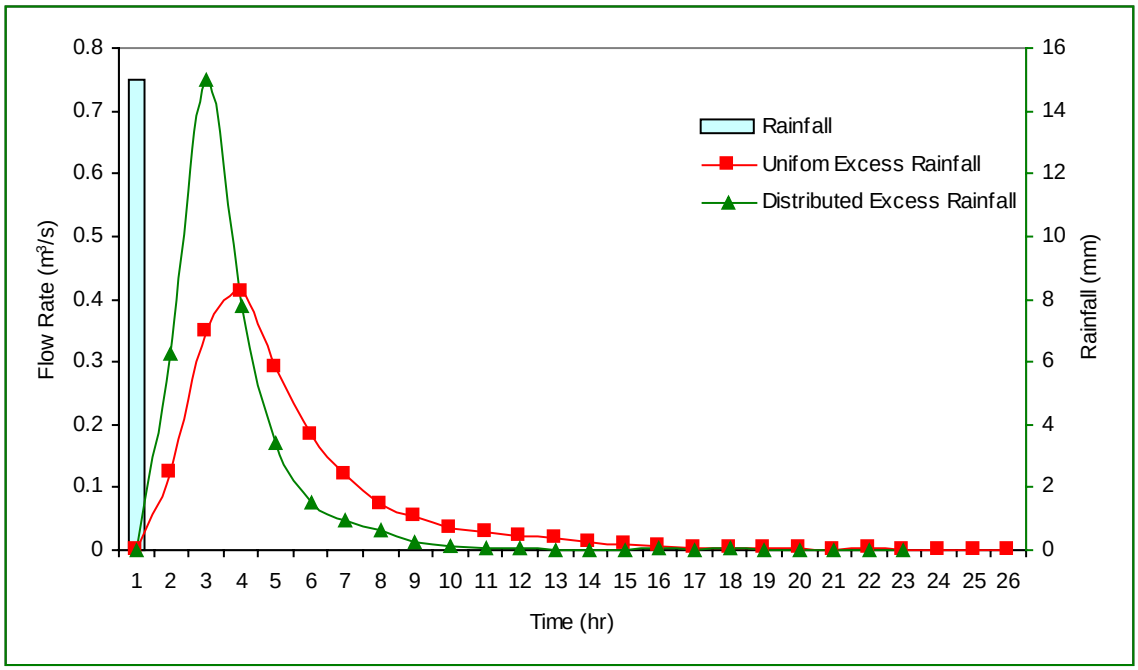

Figure 4.6. Comparison of distributed versus uniform excess rainfall (Rainfall volume = 15mm).

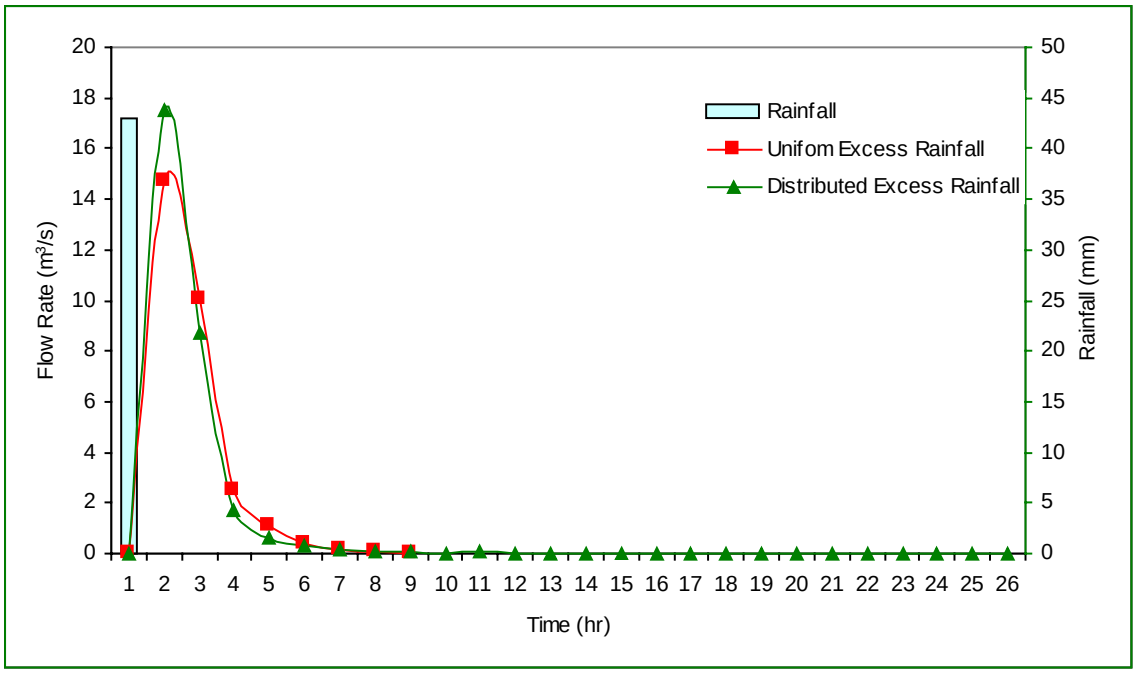

Figure 4.7. Comparison of distributed versus uniform excess rainfall (Rainfall volume = 43mm).

3, 6, and 9 sub-areas with the smaller excess rainfall being closer to the streams in one scenario and farther from the streams in the other scenario. For all storm sizes (2, 10, or 20mm excess rainfall), the excess rainfall amount was kept constant with using different numbers of sub-areas. For each storm size, the hydrograph was also obtained using a spatially uniform excess rainfall. The resulting hydrographs are shown in Figures 4.8 through 4.10.

Visually, it can be seen that the peak flow rate obtained with the larger excess rainfall being closer to the streams, was larger than that obtained with larger excess rainfall being farther from the streams (roughly, twice as much). This kind of behaviour is expected since the time required for excess rainfall to reach the watershed outlet is a function of (among other factors) the excess rainfall intensity. When the higher excess rainfall is closer to the channel system, it is expected to reach the watershed outlet in a shorter time than being farther from the channel system. The time to peak flow rate was earlier with the larger excess rainfall being closer to the streams in the case of 2 and 10 mm excess rainfall but not in the case of 20 mm excess rainfall.

In general, and in the case of having the larger excess rainfall closer to the streams, the peak flow rate was higher as the number of sub-areas decreased. No distinct trend is observed in the case of having the larger excess rainfall farther from the streams. It can also be noticed that there is more attenuation in the hydrograph shape when the larger excess rainfall is farther from the streams. The hydrographs obtained using the uniform excess rainfall for the larger two storms (10 and 20mm excess rainfall) fell somewhere between those obtained using larger excess closer to the streams versus farther from the streams. For the smaller storm, the “uniform” hydrograph had too much

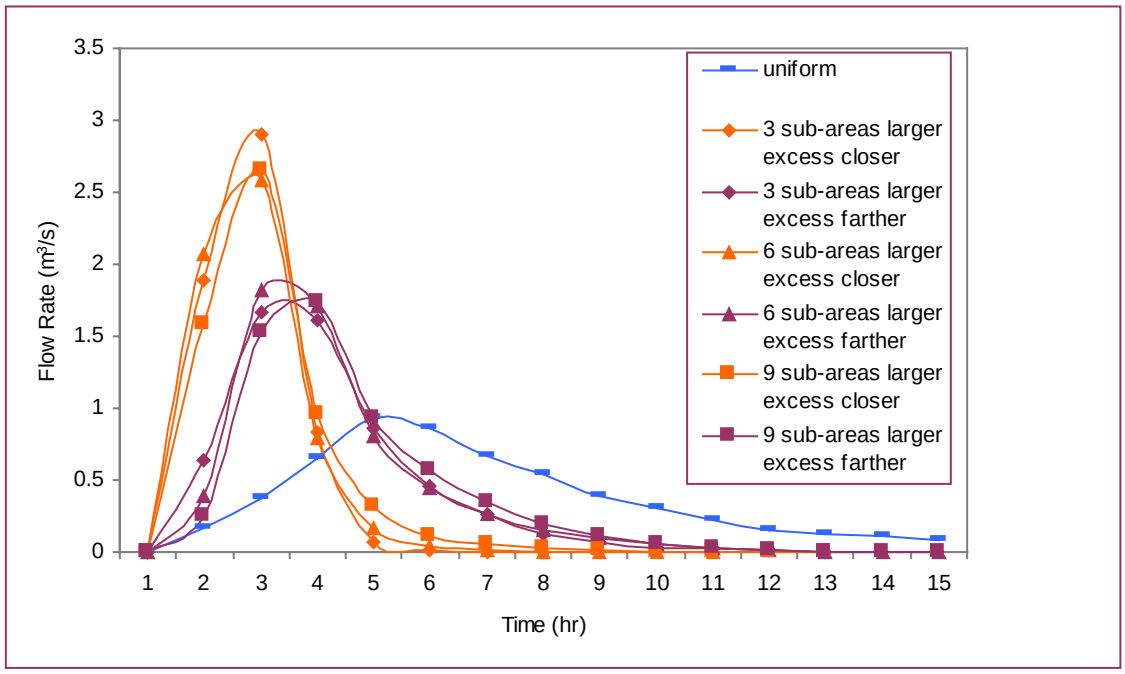

Figure 4.8. DCN model's predicted hydrographs using 3, 6, and 9 sub-areas for excess rainfall distribution (total excess rainfall = 2 mm).

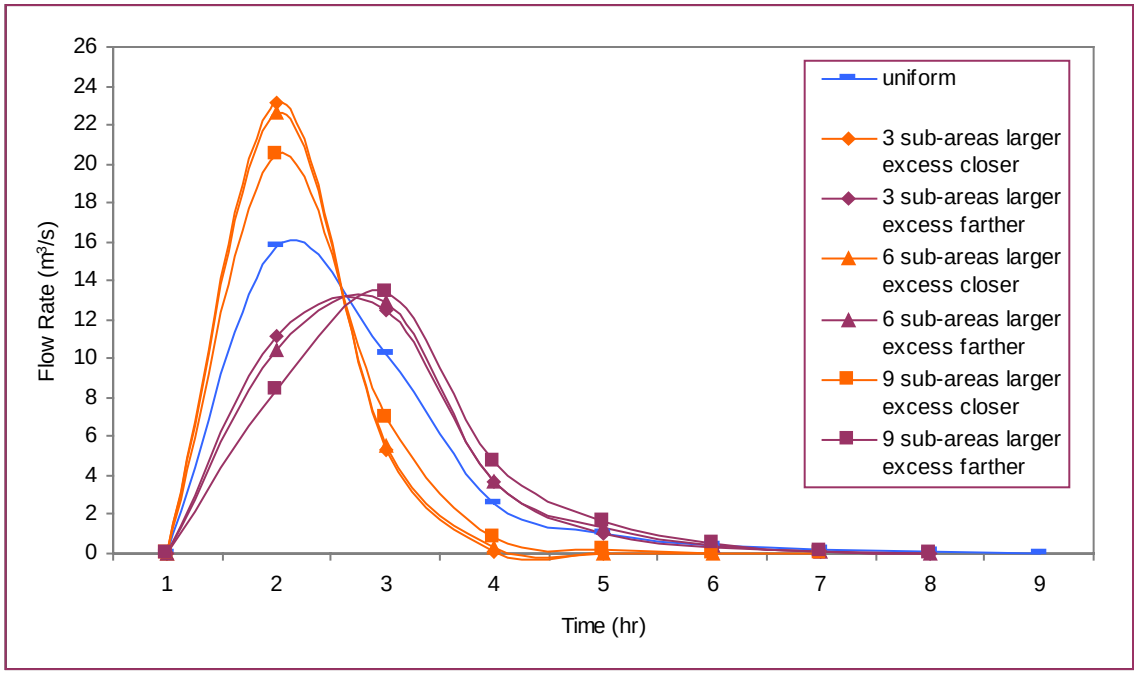

Figure 4.9. DCN model's predicted hydrographs using 3, 6, and 9 sub-areas for excess rainfall distribution. (total excess rainfall = 10 mm).

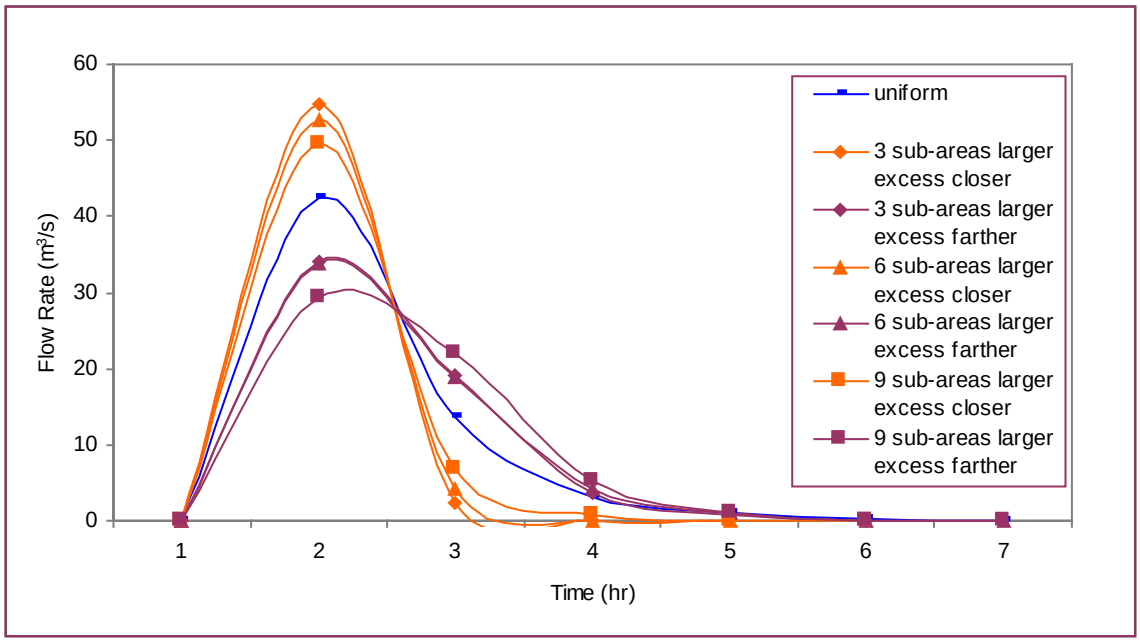

Figure 4.10. DCN model's predicted hydrographs using 3, 6, and 9 sub-areas for excess rainfall distribution. (total excess rainfall = 20 mm).

attenuation compared to those obtained using the two scenarios of spatially distributed excess rainfall.

In summary, it can be said that the distribution of the excess rainfall over the watershed area has an impact on the resulting output hydrograph. The trend of distributing the excess rainfall over the watershed area (higher excess rainfall either closer to or farther from streams) shows more impact on the resulting hydrograph than the degree the excess rainfall was partitioned.

4.2.2 Velocity Estimation in Cells with Zero Excess Rainfall and Non-zero Inflow

In the spatially distributed excess rainfall model (DCN), and for cases where the whole watershed area is not contributing to excess rainfall generation, there will be cells with no "local" excess rainfall generated in them but at the same time, have inflow from upstream cells. This leads to infinite value for the cell travel time. Knowing that there is flow entering these cells, there should then be a cell travel time value for them to be included in estimating the cumulative travel time for cells that are upstream of the zero excess rainfall cells.

To overcome this problem, three different scenarios for "assigning" cell velocity were studied. [Two fixed flow velocities (0.2m/s or 0.02m/s), and one scenario of varied flow velocity by cell where the flow velocity value is a function of the incoming flow and the cell characteristics.] In the latest scenario, equation 3.15 was used to estimate overland flow velocity with i_e considered to be the cumulative i_eA from all upstreams cells. Results of these three scenarios are shown in Figure 4.11 It can be seen that there

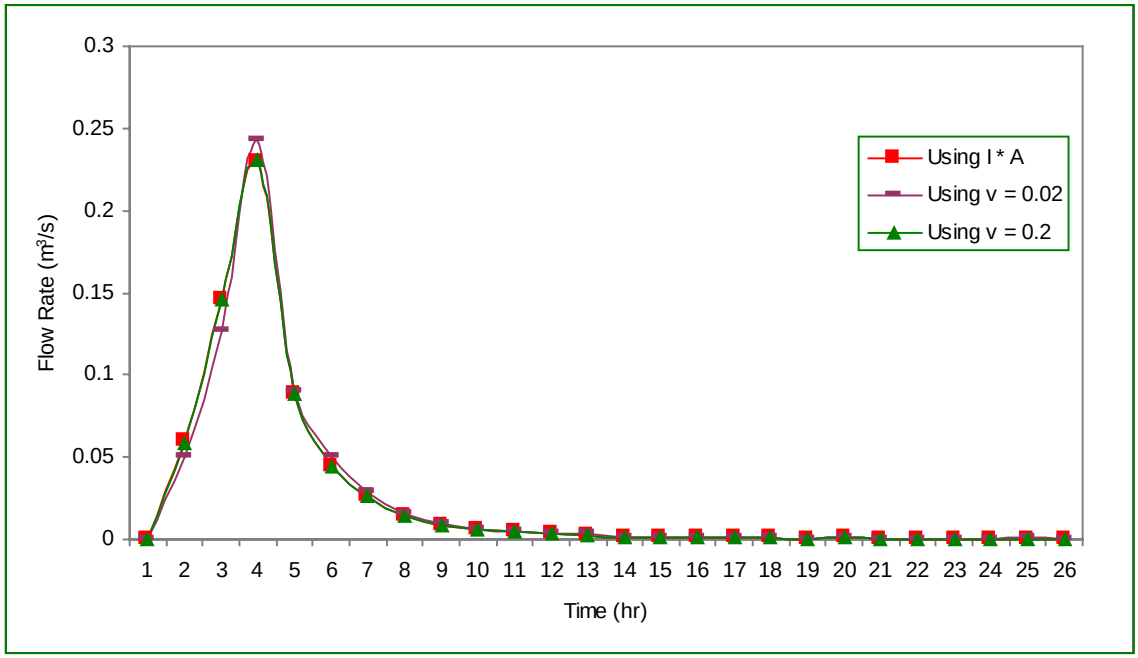

Figure 4.11. Comparison of different alternatives for estimating flow velocity in cells with zero excess rainfall and non-zero inflow into them.

was no significant difference between the peak flow rate values for the three scenarios. The time to peak flow rate was the same for the three cases. The third option was used in all DCN simulations reported here since it is related to the cell characteristics and the inflow values estimated using the model.

5 Summary and Conclusions

5.1 Summary

A GIS-based hydrologic model was developed to simulate the output hydrograph from a watershed. Three methods of generating the excess rainfall were studied and the model's accuracy of predicting the hydrograph shape and parameters was tested against observed flow data for 30 storms.

The models used in this study utilize the concept of the time-area diagram where cumulative time of travel from each cell to the watershed outlet is required. The hydrologic models were applied to a 1153-ha agricultural watershed in the Piedmont region of Virginia. The excess rainfall was generated using three methods:

1) The Distributed Curve Number (DCN) model uses a CN for each cell, generating spatially distributed excess rainfall using the SCS CN method.
2) The Uniform Curve Number (UCN) model uses a single "average" CN for the whole watershed, thus generating a uniform excess rainfall.
3) The Phi index (Φ) model uses the Φ-index method to generate uniform excess rainfall.

A 30-m resolution USGS DEM was used to derive the slope, flow direction, and flow density, and to delineate the stream channel network. The stream channel network delineation process involves setting a threshold on the upstream area of each cell after

which the flow in that cell is considered to have the characteristics of channel flow. Cells with upstream area of 1.8 ha or more were considered channel cells. Flow in the rest of the cells was considered overland flow. In overland flow cells, the flow velocity was estimated using a kinematic wave approximation. Manning's equation was used with the equilibrium flow rate to estimate the velocity in channel cells. The cumulative travel time was found for each cell by summing the travel time of all downstream cells along the flow path.

The results showed that the DCN model and the UCN models, both predicted the hydrograph shape and parameters better than the Phi model. Visual comparison showed that both the DCN and the UCN models had the ability to predict the shape of the hydrograph since they both account for the temporal variation of the rainfall patterns. According to different statistics, both the DCN and the UCN models predicted the peak flow rate better than the Phi model. However, the two models alternated on how well they predicted the peak flow rate. All three models tended to over-predict the peak flow rate. The hypothesis that there is no difference between the observed and the predicted values for the peak flow rate was accepted for the time to peak flow rate and rejected for the peak flow rate for all models. Therefore, statistically, all models predicted time to peak more accurately than peak flow rate. For the time to peak flow rate predictions, the UCN model seemed to give the best results followed by the DCN model and finally the Phi model. The UCN model had the highest number of storms in which the predicted time to peak exactly matched the observed one. It also had the largest number of storms in which the relative error in time to peak prediction was lower or equal to 0.2. All three models tended to under-predict the time to peak. However, the UCN model was the most

moderate model in this regard since it under-predicted the time to peak for 18 out of the 30 storms versus 23 and 27 for the DCN and the Phi model, respectively. Shape statistics showed that both the DCN model and the UCN model predicted the hydrograph shape better than the Phi model with a slight preference of the UCN model over the DCN model.

In examining seasonal effect, the DCN model predicted both the peak flow rate and the time to peak best in summer, the UCN model predicted these two factors better in both spring and fall seasons. Looking at the results on the basis of storm size showed improved prediction accuracy by the UCN and the DCN models for both peak flow rate and time to peak flow rate as the storm size increased. The UCN model predicted the time to peak most accurately for all storm size classes. According to the R^2 values, the DCN and the UCN models did not match hydrograph shape as well as the storm size increased. This could be attributed to the fact that with larger storms, the shape of the hydrograph is, in general, more complex and therefore, harder to simulate accurately. The Phi model did not show a distinct trend of better accuracy in predicting the hydrograph parameters with changes in storm size.

In the DCN model, the effect of incorporating the excess rainfall as a spatially distributed parameter was tested against using a uniform excess rainfall. For the same excess rainfall volume, a higher peak flow rate resulted when the excess rainfall was spatially distributed. The difference between the two peak flow rates was larger when a smaller storm was modeled. The sensitivity of the DCN model to several methods of estimating the flow velocity in cells with no excess rainfall was shown to have no significant impact on the hydrograph shape or peak flow rate.

A sensitivity analysis also showed that with the larger amount of excess rainfall closer to the streams, the resulting hydrograph had higher and earlier peak flow rates with less attenuation than the case of the larger excess rainfall being far from the streams.

5.2 Conclusions

1. The prediction accuracy of the model improved greatly when the temporal variation of excess rainfall was accounted for. While both the DCN and the UCN models have the ability to account for the temporal variation in excess rainfall patterns, the Phi model, in general, lacks that ability.
2. For the watershed under study, incorporating the excess rainfall as a spatially varied input to the model did not seem to improve the prediction accuracy of the model. However, a sensitivity analysis of the effect of the spatial variation of excess rainfall indicated that the spatial variation of excess rainfall can have a significant impact on the output hydrograph.
3. The DCN model and the UCN model predicted the hydrograph shape better than the Phi model. While different statistics favored both the DCN model and the UCN model over the Phi model, neither of the two models was clearly superior to the other. Overall, the UCN model is favored over the DCN model since it is simpler and gave comparable prediction accuracy to the DCN model. Therefore, the UCN model is recommended to be used for Owl Run watershed.
4. Among the three models, the DCN model gave better results in summer, the UCN model showed better predictions in both spring and fall seasons.

5. Both the DCN model and the UCN model predicted the peak flow rate and the time to peak more accurately as the storm size increased. The opposite happened in predicting the hydrograph shape.

5.3 Recommendations

The following areas need further research and development:

- Add a component to the model to account for the channel storage effect.
- Apply the model to different watersheds with different topography, landuses, and drainage characteristics. The model should also be applied to watersheds in different climatic regions with different rainfall patterns.
- Evaluate the effect of cell size on prediction accuracy.
- Obtain more extensive data about the channel cross section and roughness coefficient so that the assumptions made about these factors could be replaced by observed data.

6 References

ASCE Task Committee of the Watershed Management Committee. 1993. Criteria for evaluation of watershed models. *J. Irrig. Drainage Eng.* 119(3):429-443.

Ajward, M. H. 1996. A spatially distributed unit hydrograph model using a geographical information system. Ph.D. diss. Civil Engineering Dept., University of Calgary, Calgary.

Beasley, D. B. and L. F. Huggins. 1981. ANSWERS Users Manual, EPA 905/9-82-001. U. S. Environmental Protection Agency, Chicago, IL.

Bedient, P. B. and W. C. Huber. 1992. *Hydrology and Floodplain Analysis*. 2nd edition. New York: Addison-Wesley Publishing Company.

Berry, J. K. and J. K. Sailor. 1987. Use of geographic information systems for storm runoff prediction from small urban watershed. *Environmental Management* 11(1):21-27.

Bhaskar, N. R., W. P. James and R. S. Devulapalli. 1992. Hydrologic parameter estimation using geographic information system. *J. Water Resources Planning and Management* 118(5):492-512.

Bondelid, T. R., R. H. McCuen, and T. J. Jackson. 1982. Sensitivity of SCS models to curve number variation. *Water Resources Bulletin* 18(1):111-116.

Brater, E. F. and H. W. King. 1976. *Handbook of Hydraulics for the Solution of Hydraulic Engineering Problems.* New York: McGraw-Hill Book Company.

Brooks, K. N., P. F. Ffolliott, H. M. Gregersen, and J. L. Thames. 1991. *Hydrology and Management of Watersheds.* Ames, Iowa: Iowa State University Press.

Chieng, S. and J. Luo. 1993. Application of GIS to peak flow estimation. In *Applications of Advanced Information Technologies: Effective Management of Natural Resources*. ed. C. D. Heatwole. 279-289. St. Joseph, Mich.: ASAE.

Chow, V. T., D. R. Maidment, and L. W. Mays. 1988. *Applied Hydrology*. New York: McGraw-Hill Book Company.

Clark, C. O. 1945. Storage and the unit hydrograph. *Trans. ASCE* 110:1419-1446.

Cunge, K. A. 1969. On the subject of flood propagation method (Muskingum method). *Journal of Hydraulic Research* 7(2):205-230.

DeBarry, P. A. and Carrington, J. T. 1990. Computer watershed. *ASCE Civil Engineering Magazine* July:68-70.

Dooge, J. C. I. 1959. A general theory of the unit hydrograph. *Journal of Geophysical Research* 64(2):241-256.

Environmental Systems Research Institute, Inc. 1992. ArcView GIS version 3.0a online help. Redlands, CA.

Gray, D. M. 1961. Synthetic unit hydrographs for small watersheds. *Journal of the Hydraulics Division, ASCE* 87(HY4):33-54.

Green, I. R. A. and D. Stephenson. 1986. Criteria for comparison of single event models. *Hydrological Sci. J.* 31(3):395-411.

Hill, J. M., V. P. Singh and H. Aminian. 1987. A computerized data base for flood prediction modeling. *Water Resources Bull*. 23(1):21-27.

James, W. P., P. W. Winsor, and J. R. Williams. 1987. Synthetic unit hydrograph. *Journal of Water Resources Planning and Management* 113(1):70-81.

Jenson, S. K. and J. O. Domingue. 1988. Extracting topographic structure from digital elevation data for geographic information system analysis. *Photogrammetric Engineering and Remote Sensing* 54(11):1593-1600.

Johnson, D. L. and A. C. Miller. 1997. A spatially distributed hydrologic model utilizing raster data structures. *Computers and Geosciences* 23(3):267-272.

Kilgore, J. L. 1997. *Development and evaluation of a GIS-based spatially distributed unit hydrograph model*. M. S. thesis, Biological Systems Engineering Dept., Virginia Tech, Blacksburg.

Lee, M. T. 1985. Applications of geographic information systems for hydrologic investigation. In Hydraulics and Hydrology.

Lee, M. T. 1991. Integration of GIS databases and water quality modeling for agricultural and urban watersheds. In *Computing in Civil Engineering, Proceedings of the National Conference on Computing in Civil Engineering*, 469-478. New York, NY: ASCE.

Linsley, R. K., M. A. Kohler, and J. L. H. Paulhus. 1982. *Hydrology for Engineers*. New York: McGraw-Hill Book Company.

Maidment, D. R. 1993a. GIS and hydrologic modeling. In *Environmental Modeling with GIS*. eds. M. F. Goodchild, B. O. Parks, L. Steyaert, New York: Oxford University Press.

Maidment, D. R. 1993b. Developing a spatially distributed unit hydrograph by using GIS. In *HydroGIS 93: Application of Geographic Information Systems in Hydrology and Water Resources, Proceedings of the Vienna Conference*, eds. K. Dovar and H. P. Natchnebel, 181 - 192. Vienna: Int. Assoc. of Hydrological Sci.

McCuen, R. H. 1989. *Hydrologic Analysis and Design*. Englewood Cliffs, N.J.: Prentice-Hall.

McCuen, R. H., W. J. Rawls and S. L. Wong. 1984. SCS urban peak flow methods. *J. Hydraulic Eng.* 110(3):290-299.

Moeller, R. A. 1991. Application of geographic information systems to hydrologic modeling using HEC-1. In *Civil Engineering Applications Remote Sensing and Geographic Information Systems*. ed. D. B. Stafford. 269-277. New York, NY: ASCE.

Mostaghimi, S., P. W. McClellan, U. S. Tim, J. C. Carr, R. K. Byler, T. A. Dillaha, V. O. Shanholtz, and J. R. Pratt. 1989. Watershed/water quality monitoring for evaluating animal waste BMP effectiveness: Owl Run watershed. Pre-BMP evaluation final report. Report No. 0-P1-8906. Agricultural Engineering Department. Virginia Polytechnic Institute and State University, Blacksburg, VA.

Muzik, I. 1988. Applications of GIS to SCS procedure for design flood hydrographs. In *Modeling Agricultural, Forest and Rangeland Hydrology*, 494 - 499. Chicago, Ill., 12-13 Dec.

Muzik, I. and Chang, C. 1993. A microcomputer-based geographic information system for hydrologic modeling. *Microcomputers in Civil Engineerin.*8:355-365.

Muzik, I. 1995. GIS derived distributed unit hydrograph, a new tool for flood modeling. In *Developments in Computer Aided Design and Modeling for Civil Engineering*, ed. B. H. V. Topping, 243-247. Edinburgh, UK: Civil-Comp Press.

Muzik, I. 1996. Flood modeling with GIS-derived distributed unit hydrograph. *Hydrological processes.* 10:1401-1409.

Nash, J. E. and J. V. Sutcliffe. 1970. River flow forecasting through conceptual models. Part I - A discussion of principles. *J. Hydrol.* 10(3):282-290.

Novotny, V. and H. Olem. 1994. *Water Quality: Prevention, Identification, and Management of Diffuse Pollution*. New York: Van Nostrand Reinhold.

Overton, D. E. and M. E. Meadows. 1976. *Stormwater Modeling*. New York: Academic Press.

Ponce, V. M. 1989. *Engineering Hydrology: Principles and Practices.* Englewood Cliffs, N.J.: Prentice Hall.

Rawls, W. J., L. R. Ahuja, D. L. Brakensiek, and A. Shirmohammadi. 1993. Infiltration and soil water movement. In *Handbook of Hydrology*. ed. Maidment, D. R. 5.1-5.51. McGraw-Hill, inc. New York, NY.

Rewerts, C. C. and B. A. Engel. 1991. ANSWERS on GRASS: integrating a watershed simulation with a GIS. ASAE paper 91 - 2621. St. Joseph, Mich.: ASAE.

Rodriguez-Iturbe, I. and J. B. Valdes. 1979. The geomorphological structure of hydrologic response. *Water Resources Research* 15(6):1409-1420.

Sherman, L. K. 1932. Streamflow from rainfall by the unit-graph method. *Eng. News Record* 108:501-505.

Singh, V. P. 1988. *Hydrologic Systems: Rainfall-Runoff Modeling*. vol. 1. Englewood Cliffs, N.J.: Prentice Hall.

Singh, V. P. and H. Aminian. 1985. The watershed hydrology simulation model. In *Proceedings of the International Workshop on Operational Applications of Mathematical Models (Surface Water) in Developing Countries*. New Delhi.

Snyder, F. F. 1938. Synthetic unit-graphs. *Transactions, American Geophysics Union* 19:447-454.

SCS. 1986. Urban Hydrology for Small Watersheds (TR-55). Washington, D. C.: USDA.

SCS. 1972. Hydrology: National Engineering Handbook, section 4. Washington, D. C.: USDA.

Solomon, S. I., J. P. Denouvilliez, E. J. Chart, and J. A. Woolley. 1968. The use of a square grid system for computer estimation of precipitation, temperature, and runoff. *Water Resources Research* 4(5):919-929.

Stuebe, M. M. and Johnston, D. M. 1990. Runoff volume estimation using GIS techniques. *Water Resources Bulletin* 26(4):611-620.

Terstriep, M. L. and Lee, M. T. 1989. Regional stormwater modeling: Q-ILLUDAS and ARC/INFO. In *Computing in Civil Engineering, Proceedings of the National Conference on Computing in Civil Engineering,* 338-345. New York, NY: ASCE.

Wang, Yang. 1991. Application of a nonpoint source pollution model to a small watershed in Virginia. M.S. thesis. Blacksburg: Virginia Polytechnic Institute and State University.

Watt, W. E. and K. C. A. Chow. 1985. A general expression for basin lag time. *Canadian Journal of Civil Engineerin.*12(2):294-300.

Wilson, E. M. 1983. *Engineering Hydrology.* MacMillan Publishers, London, United Kingdom.

Wolfe, M. L. and C. M. U. Neale. 1988. Input data development for a distributed parameter hydrologic model (FESHM). In *Proceedings of the International Symposium on Modeling in Agricultural, Forest, and Rangeland Hydrology*. 462-469. Chicago, Mich. ASAE.

Woolhiser, D. A. and J. A. Liggett. 1967. Unsteady, one-dimensional flow over a plane-the rising hydrograph. *Water Resources Research* 3(3):753-771.

Wood, E. F. and P. E. O'Connell. 1985. Real-time forecasting. In *Hydrological Forecasting.* eds. M. G. Anderson and T. P. Burt. 505-558. New York: John Wiley and Sons.

Young, R. A., C. A. Onstad, D. D. Bosch and W. P. Anderson. 1985. Agricultural nonpoint surface pollution models (AGNPS) I and II, model documentation. St. Paul: Minn. Pollution Control Agency and Washington, D. C.: USDA-ARS.

Zollweg, J. A., W. J. Gburek and T. S. Steenhuis. 1996. SMoRMod- a GIS-integrated rainfall-runoff model. *Trans. ASAE* 39(4):1299-1307.

Appendix A: Programs and Codes

Table A.1: FORTRAN program used to find the equilibrium flow depth in a trapezoidal channel with a 1.5:1 side slope.

INPUT	***FILE NAME***
All of the input files used in this program are ASCII ArcView grids.	
Channel width	width.txt
Slope	slope.txt
Manning's roughness coefficient	mannings.txt
Equilibrium flow rate	flowRate.txt

OUTPUT	***FILE NAME***
Equilibrium flow depth	depth.out

```
      DIMENSION WIDTH(221,200),SLOPE(221,200)
      DIMENSION TRUEFLOW(221,200)
      REAL MANNING(221,200)

      OPEN (UNIT=2, FILE='width.txt', STATUS='OLD')
      OPEN (UNIT=4, FILE='slope.txt', STATUS='OLD')
      OPEN (UNIT=15, FILE='mannings.txt', STATUS='OLD')
      OPEN (UNIT=3, FILE='flowRate.txt',STATUS='OLD')

      OPEN (UNIT=16, FILE='depth.out',STATUS='unknown')



      DX=0.005
      NROWS    = 221
      NCOLUMNS = 200
      NCELLS   = 44200
      Z        = 1.5


      DO 787 I = 1, NROWS
787         READ(2,*) (WIDTH(I,J),J=1, NCOLUMNS)
      DO 788 I = 1, NROWS
788         READ(3,*) (TRUEFLOW(I,J),J=1, NCOLUMNS)
      DO 789 I = 1, NROWS
789         READ(4,*) (SLOPE(I,J),J=1, NCOLUMNS)
      DO 790 I = 1, NROWS
790         READ(15,*) (MANNING(I,J),J=1, NCOLUMNS)
```

```
      DO 13 I = 1,221
        DO 14 J = 1,200
        DEPTH = 0.0
        IF (TRUEFLOW(I,J).GT.0.0.AND.SLOPE(I,J).NE.0.0) THEN
              IF (MANNING(I,J).GT.0.0.AND.WIDTH(I,J).GT.0.0)THEN

7               DEP       = DEPTH+DX
                A         = DEPTH*(WIDTH(I,J)+1.75*DEPTH**2)
                P         = WIDTH(I,J)+2.0*DEPTH*SQRT(1.0+Z**2)
                R         = A/P
                Q         = (A*SLOPE(I,J)**.5*R**(2./3.))/MANNING(I,J)

                    IF (Q.GT.TRUEFLOW(I,J)) THEN
                    GOTO 33
                    ELSE IF (Q.LE.TRUEFLOW(I,J)) THEN
                    GOTO 7
                    ENDIF
              ENDIF
        ENDIF
33      WRITE(16,*)DEPTH
14      CONTINUE
13    CONTINUE

      END
```

Table A.2: AVENUE code for deriving the flow direction.

INPUT	***NAME***
Elevation	elevation

OUTPUT	***NAME***
Flow direction	direction

```
theView   = av.GetActiveDoc
theTheme  = theview.GetActiveThemes.Get(0)
theGrid   = theView.FindTheme("elevation").GetGrid
direction = theGrid.FlowDirection(TRUE)
theGTheme=Gtheme.Make(direction)
      if(direction.HasError)then
      return(NIL)
      end

theView.addTheme(theGtheme)
```

Table A.3: AVENUE code for deriving the flow density and channel network grids.

INPUT	***NAME***
Flow direction	direction

OUTPUT	***NAME***
Flow density	density
Channel network	streams

```
theView=av.GetActiveDoc
theTheme=theview.GetActiveThemes.Get(0)
theGrid=theView.FindTheme("direction").GetGrid
density=theGrid.FlowAccumulation(NIL)
streams=(density>=20.AsGrid).SetNull(1.AsGrid)

theGTheme=Gtheme.Make(density)
      if(density.HasError)then
      return(NIL)
      end
theView.addTheme(theGtheme)

theGTheme=Gtheme.Make(streams)
      if(streams.HasError)then
      return(NIL)
      end
theView.addTheme(theGtheme)
```

Table A.4: AVENUE code for estimating the excess rainfall.

INPUT	***NAME (CONDITION " ")***
Cumulative rainfall	"active theme"
Storage	S

OUTPUT	***NAME***
Excess rainfall	Pe

```
theView   = av.GetActiveDoc
thegTheme = theView.getactivethemes.get(0)
agrid     = thegtheme.getgrid
theGrid   = theView.FindTheme("S").GetGrid
pe        = (((((agrid)-(0.2.asgrid*thegrid))>0.asgrid)*((agrid)-
(0.2.asgrid*thegrid))).pow(2)/((agrid)+(0.8.asgrid*thegrid))/1000.asgri
d)

theGTheme = Gtheme.Make(pe)
      if(pe.HasError)then
      return(NIL)
      end
theView.addTheme(theGtheme)
```

Table A.5: AVENUE code for adjusting the curve number grid when the predicted excess rainfall (using curve number condition II) is more than the observed excess rainfall.

INPUT	***NAME***
Curve number	"active theme"

OUTPUT	***NAME***
Adjusted curve number	CN

```
theView   = av.GetActiveDoc
thegTheme = theView.getactivethemes.get(0)
agrid     = thegtheme.getgrid
cn        = agrid - ((agrid - ((4.2.asgrid*agrid)/(10.asgrid -
(0.058.asgrid*agrid))))*0.3.asgrid)

theGTheme = Gtheme.Make(cn)
      if(cn.HasError)then
      return(NIL)
      end
theView.addTheme(theGtheme)
```

Table A.6: AVENUE code for adjusting the curve number grid when the predicted excess rainfall (using curve number condition II) is more than the observed excess rainfall.

INPUT	***NAME***
Curve number	"active theme"

OUTPUT	***NAME***
Adjusted curve number	CN

```
theView   = av.GetActiveDoc
thegTheme = theView.getactivethemes.get(0)
agrid     = thegtheme.getgrid


cn        =
agrid+((((23.asgrid*agrid)/(10.asgrid+(0.13.asgrid*agrid)))-
agrid)*0.843.asgrid)

theGTheme = Gtheme.Make(cn)
     if(cn.HasError)then
      return(NIL)
      end
theView.addTheme(theGtheme)
```

Table A.7: AVENUE code for deriving the cumulative inflow into each cell.

INPUT	***NAME***
Flow direction	direction
Excess rainfall intensity	“active theme”

OUTPUT	***NAME***
Cumulative flow	

```
theView   = av.GetActiveDoc
thegTheme = theView.getactivethemes.get(0)
agrid     = thegtheme.getgrid
theGrid   = theView.FindTheme("direction").GetGrid
thePrj    = theView.GetProjection
’ calculate flow accumulation
itimes900  = agrid * 900.asgrid
flowAccGrid = thegrid.FlowAccumulation(itimes900)
theGTheme = Gtheme.Make(flowaccgrid)
    if(flowaccgrid.HasError)then
      return(NIL)
      end

theView.addTheme(theGtheme)
```

Table A.8: AVENUE code to find the flow velocity in channels, flow velocity in overland flow cells, cell flow time, cumulative flow time, reclassify the cumulative flow time into one hour intervals, finds the summation of excess rainfall in each time interval, and produces a summary table for all the zones. This code works for the DCN model.

INPUT	***NAME***
Excess rainfall	Pe
Excess rainfall intensity	i
Equilibrium flow rate	q
Equilibrium flow depth	depth
Slope	slope
Mannings's roughness coefficient	Mannings
Distance to ridge cells	`distancetoridg`
Channel width	width
Channel network	streams
Reclass of channel network	reclass of streams

OUTPUT	***NAME***
`Summary table`	`User given name`

```
theView            = av.GetActiveDoc
pe                 = theview.findtheme("pe").getgrid
i                  = theview.findtheme("i").getgrid
manning            = theView.FindTheme("manning").GetGrid
slope              = theview.findtheme("slope").getgrid
distancetoridg     = theview.findtheme("distancetoridg").getgrid
thePrj             = theView.GetProjection
ov                 =i*distancetoridg).pow(0.4)*slope.pow(0.3)
                    /manning.pow(0.6)

depth              = theview.findtheme("ddepth").getgrid
width              = theView.FindTheme("width").GetGrid
q                  = theView.FindTheme("q").GetGrid
cv                 = q/((width*depth)+(1.5.asgrid*depth.pow(2)))

thesrc = cv.getsrcname
'theSRC = SRCName.Make(cv.asstring)
theTheme = Theme.Make(theSRC)
theView.AddTheme(theTheme)
theTheme.SetActive(true)


'*****************************************
' RECLASSIFINGY THE CHANNEL VELOCITY

theView = av.GetActiveDoc
' reclassify first active GTheme
```

```
theTheme = theview.getactivethemes.get(0)
’ obtain grid from theme
theGrid = theTheme.getGrid
’ obtain reclassification parameters
theParameters = ReclassEditor.Show(theTheme)
’ check for Cancel from dialog
if (theParameters = NIL) then
  return NIL
end
fieldName = theParameters.Get(0)
classList = theParameters.Get(1)
’ run operation
reclassofCV = theGrid.ReclassByClassList(fieldName, classList, FALSE)

’ create a theme
theGTheme = GTheme.Make(reclassOfCV)
’ check if output is ok
if (reclassOfCV.HasError) then
  return NIL
end
’*****************************************

’make no theme active’make no themes active
for each t in theview.getthemes
   t.setactive(false)
end


streams            = theView.FindTheme("streams").GetGrid
reclassofstreams   = theView.FindTheme("reclass of streams").GetGrid

velocityInCellsWithZeronExcess =
((q>0.asgrid)and(pe=0.asgrid)and(streams=0.asgrid))*((q*distancetoridg)
.pow(0.4)*slope.pow(0.3)/manning.pow(0.6))

totalOV            = ov+ velocityInCellsWithZeronExcess
totalVelocity      = (totalOV * reclassofstreams) + (reclassOfCV *
streams)
time               = (1.asgrid/totalvelocity)
theGrid            = theView.FindTheme("direction").GetGrid
cumulativetime     = theGrid.flowLength(time,false)
adjustedCumulativeTimeAfterZeros = cumulativetime * (pe>0)


thesrc = adjustedCumulativeTimeAfterZeros.getsrcname
’theSRC = SRCName.Make(adjustedCumulativeTimeAfterZeros.asstring)
theTheme = Theme.Make(theSRC)
theView.AddTheme(theTheme)
theTheme.SetActive(true)



’ RECLASSIFYING THE CUMULATIVE TIME ***************************

theView = av.GetActiveDoc
’ reclassify first active GTheme
```

```
theTheme = theview.getactivethemes.get(0)
’ obtain grid from theme
theGrid = theTheme.getGrid
’ obtain reclassification parameters
theParameters = ReclassEditor.Show(theTheme)
’ check for Cancel from dialog
if (theParameters = NIL) then
  return NIL
end
fieldName = theParameters.Get(0)
classList = theParameters.Get(1)
’ run operation
reclassofumulativeTime = theGrid.ReclassByClassList(fieldName,
classList, FALSE)

’ create a theme
theGTheme = GTheme.Make(reclassofumulativeTime)
’ check if output is ok
if (reclassofumulativeTime.HasError) then
  return NIL
end
’*****************************************************************
’ add theme to the view
theView.AddTheme(thegtheme)

’make no theme active’make no themes active
for each t in theview.getthemes
   t.setactive(false)
end


thesrc = reclassofumulativeTime.getsrcname
’theSRC = SRCName.Make(reclassofumulativeTime.asstring)
theTheme = Theme.Make(theSRC)
theView.AddTheme(theTheme)
theTheme.SetActive(true)


’SUMMARIEZE ZONES

theView = av.GetActiveDoc


’ obtain zone Theme and set object and VTab
zoneTheme = theView.GetActiveThemes.Get(0)
if (zoneTheme.Is(FTHEME)) then
  zoneObj = zoneTheme.GetFTab
  theVTab = zoneObj
elseif (zoneTheme.Is(GTHEME)) then
  zoneObj = zoneTheme.GetGrid
  theVTab = zoneObj.GetVTab
else
  return NIL
end

’get zone Field from zoneObj
if (zoneObj.Is(FTab)) then
```

```
  fl = {}
  for each f in theVTab.GetFields
    if (f.IsVisible and
        (f.IsTypeShape.Not and
        ((f.GetType <> #FIELD_DECIMAL) and
         (f.GetType <> #FIELD_DOUBLE) and
         (f.GetType <> #FIELD_FLOAT) and
         (f.GetType <> #FIELD_MONEY) and
         (f.GetType <> #FIELD_ISODATETIME) and
         (f.GetType <> #FIELD_ISOTIME)) or
         ((f.GetType = #FIELD_DECIMAL) and (f.GetPrecision = 0)))) then
      fl.Add(f)
    end
  end
  zoneField = MsgBox.List(fl, "Pick field that defines zones:",
"Summarize Zones")
  if (zoneField = NIL) then return NIL end
else
  zoneField = theVTab.FindField("Value")
end

’ make list of value themes from available themes
valueList = List.Make
for each t in theView.GetThemes
  if (t.Is(GTHEME)) then
    valueList.Add(t)
  end
end

’ remove zone theme from list
valueList.RemoveObj(zoneTheme)

’ get value theme
valueTheme = MsgBox.List(valueList, "Pick theme containing variable to
summarize:", "Summarize Zones")
if (valueTheme = NIL) then return NIL end

’ make sure themes overlay
zoneExtent = zoneTheme.ReturnExtent
valueExtent = valueTheme.ReturnExtent
if (zoneExtent.Intersects(valueExtent).Not) then
  MsgBox.Error("Input themes do not overlay","Summarize Zones")
  return NIL
end

’ obtain Grid for value theme and create VTab
theMaskGTheme = theView.GetExtension(AnalysisEnvironment).GetMask
if (theMaskGTheme = NIL) then
  g = valueTheme.GetGrid
else
  g = valueTheme.GetGrid.ExtractByMask(theMaskGTheme.GetGrid)
end
aPrj = theView.GetProjection
aFN = av.GetProject.GetWorkDir.MakeTmp("zstat","dbf")
zt = g.ZonalStatsTable(zoneObj, aPrj, zoneField, FALSE, aFN)
if (zt.HasError) then return NIL end
zoneTable = Table.Make(zt)
```

```
zoneTable.SetName("Stats of " + valueTheme.GetName + " Within Zones of
" + zoneTheme.GetName)
zoneTable.GetWin.Activate

’ check value to make sure it is ok to chart
if (zt.GetNumRecords > 25) then
  MsgBox.Warning("Number of unique zones is more than 25.  A chart will
not be created", "Summarize Zones")
  return NIL
end

’ obtain variable to chart
choiceList = zt.GetFields
statList = {}
statStringList = {}
pickList = choiceList.Clone
for each stat in pickList
  if (stat.GetAlias.Count > 0) then
    statStringList.Add(stat.GetAlias)
  else
    statStringList.Add(stat.GetName)
  end
end
for each statString in statStringList
  if ((statString <> "Count") and (statString <> zoneField.GetName) and
(statString <> "Zone-code")) then
    tokenList = statString.AsTokens("-")
    statString2 = tokenList.Get(tokenList.Count - 1)
    tokenList2 = statString2.AsTokens("_")
    statList.Add((tokenList2.Get(tokenList2.Count - 1)).Proper)
  end
end
pickStat = MsgBox.ListAsString(statList, "Select statistic to chart:",
"Summarize Zones")
if (pickStat = NIL) then return NIL end
for each statString in statStringList
  if (statString.Contains(pickStat.LCase)) then
    fieldName = statString
    break
  end
end
pickStatField = zt.FindField(fieldName)

’ create chart with colors matching zoneObj legend
fieldList = {pickStatField}
theChart = Chart.Make(zt, fieldList)
theChart.SetRecordLabelField(zt.FindField(zoneField.GetName))
theChart.SetName(pickStat.Proper ++ "of" ++ valueTheme.GetName ++
"Within Zones of" ++ zoneTheme.GetName)
theLegend = zoneTheme.GetLegend
if (theLegend.GetLegendType <> #LEGEND_TYPE_CHART) then
  theSymbols = theLegend.GetSymbols
  if (theLegend.GetLegendType = #LEGEND_TYPE_SIMPLE) then
    theChartDisplay = theChart.GetChartDisplay
    for each rec in zt
      theChartDisplay.SetSeriesColor(rec, theSymbols.Get(0).GetColor)
    end
```

```
  else
    labelDictionary = Dictionary.Make(zt.GetNumRecords)
    symbolDictionary = Dictionary.Make(theSymbols.Count)
    legendFieldList = theLegend.ReturnFieldNames
    theCount = 0
    for each rec in theVTab
      indexList = {}
      for each fieldString in legendFieldList

indexList.Add(theVTab.ReturnValue(theVTab.FindField(fieldString), rec))
      end
      theIndex = theLegend.GetIndex(indexList)
      classInfoList = theLegend.ReturnClassInfo(theIndex)
      labelString = classInfoList.Get(0)
      labelDictionary.Add(theVTab.ReturnValue(zoneField,
rec),labelString)
      if (symbolDictionary.Get(labelString) = NIL) then
        symbolDictionary.Add(labelString,classInfoList.Get(2).GetColor)
      end
      theCount = theCount + 1
    end
    zt.SetEditable(TRUE)
    aField = Field.Make("Label", #FIELD_CHAR, 40, 0)
    tempFieldList = {aField}
    zt.AddFields(tempFieldList)
    addField = zt.FindField(zoneField.GetName)
    for each rec in zt
      zt.SetValue(aField, rec,
labelDictionary.Get(zt.ReturnValue(addField, rec)))
    end
    if (theLegend.GetLegendType <> #LEGEND_TYPE_DOT) then
      theChart.SetRecordLabelField(aField)
    end
    theChartDisplay = theChart.GetChartDisplay
    for each rec2 in zt
      theChartDisplay.SetSeriesColor(rec2,
symbolDictionary.Get(zt.ReturnValueString(aField, rec2)))
    end
    zt.SetEditable(FALSE)
  end
end
theTitle = theChart.GetTitle
theYAxis = theChart.GetYAxis
theTitle.SetName("Values of " + valueTheme.GetName + " Summarized
Within the Zones of " + zoneTheme.GetName)
theYAxis.SetName(pickStat ++ "of" ++ valueTheme.GetName)
theYAxis.SetLabelVisible(TRUE)
theXAxis = theChart.GetXAxis
theXAxis.SetName("Zones")
theXAxis.SetLabelVisible(TRUE)
theXAxis.SetAxisVisible(FALSE)
theXAxis.SetTickLabelsVisible(FALSE)
theChart.GetWin.Activate
```

Table A.9: AVENUE code to find the flow velocity in channels, flow velocity in overland flow cells, cell flow time, cumulative flow time, reclassify the cumulative flow time into one hour intervals, finds the summation of excess rainfall in each time interval, and produces a summary table for all the zones. This code works for the UCN model and the Phi model.

INPUT	***NAME***
Excess rainfall	Pe
Excess rainfall intensity	i
Equilibrium flow rate	q
Equilibrium flow depth	depth
Slope	slope
Mannings's roughness coefficient	Mannings
Distance to ridge cells	`distancetoridg`
Channel width	width
Channel network	streams
Reclass of channel network	reclass of streams

OUTPUT	***NAME***
Summary table	User given name

```
theView            = av.GetActiveDoc
i                  = theview.findtheme("i").getgrid
manning            = theView.FindTheme("manning").GetGrid
slope              = theview.findtheme("slope").getgrid
distancetoridg     = theview.findtheme("distancetoridg").getgrid
ov                 =
(i*distancetoridg).pow(0.4)*slope.pow(0.3)/manning.pow(0.6)

depth              = theview.findtheme("depth").getgrid
width              = theView.FindTheme("width").GetGrid
q                  = theView.FindTheme("q").GetGrid
thePrj             = theView.GetProjection
cv                 = q/((width*depth)+(1.5.asgrid*depth.pow(2)))

thesrc = cv.getsrcname
'theSRC = SRCName.Make(cv.asstring)
theTheme = Theme.Make(theSRC)
theView.AddTheme(theTheme)
theTheme.SetActive(true)



' RECLASSIFINGY THE CHANNEL VELOCITY ***************************

theView = av.GetActiveDoc
' reclassify first active GTheme
theTheme = theview.getactivethemes.get(0)
```

```
’ obtain grid from theme
theGrid = theTheme.getGrid
’ obtain reclassification parameters
theParameters = ReclassEditor.Show(theTheme)
’ check for Cancel from dialog
if (theParameters = NIL) then
  return NIL
end
fieldName = theParameters.Get(0)
classList = theParameters.Get(1)
’ run operation
reclassofCV = theGrid.ReclassByClassList(fieldName, classList, FALSE)

’ create a theme
theGTheme = GTheme.Make(reclassOfCV)
’ check if output is ok
if (reclassOfCV.HasError) then
  return NIL
end
’*****************************************************************

’make no theme active’make no themes active
for each t in theview.getthemes
   t.setactive(false)
end


streams            = theView.FindTheme("streams").GetGrid
reclassofstreams   = theView.FindTheme("reclass of streams").GetGrid
totalVelocity      = (OV * reclassofstreams) + (reclassOfCV * streams)
time               = (1.asgrid/totalvelocity)
theGrid            = theView.FindTheme("direction").GetGrid
cumulativetime     = theGrid.flowLength(time,false)


thesrc = CumulativeTime.getsrcname
’theSRC = SRCName.Make(cumulativeTime.asstring)
theTheme = Theme.Make(theSRC)
theView.AddTheme(theTheme)
theTheme.SetActive(true)



’************************************************
' RECLASSIFYING THE CUMULATIVE TIME

theView = av.GetActiveDoc
' reclassify first active GTheme
theTheme = theview.getactivethemes.get(0)
' obtain grid from theme
theGrid = theTheme.getGrid
' obtain reclassification parameters
theParameters = ReclassEditor.Show(theTheme)
' check for Cancel from dialog
if (theParameters = NIL) then
  return NIL
end
```

```
fieldName = theParameters.Get(0)
classList = theParameters.Get(1)
’ run operation
reclassofumulativeTime = theGrid.ReclassByClassList(fieldName,
classList, FALSE)

’ create a theme
theGTheme = GTheme.Make(reclassofumulativeTime)
’ check if output is ok
if (reclassofumulativeTime.HasError) then
  return NIL
end
’*****************************************************************
’ add theme to the view
theView.AddTheme(thegtheme)

’make no theme active’make no themes active
for each t in theview.getthemes
   t.setactive(false)
end


thesrc = reclassofumulativeTime.getsrcname
’theSRC = SRCName.Make(reclassofumulativeTime.asstring)
theTheme = Theme.Make(theSRC)
theView.AddTheme(theTheme)
theTheme.SetActive(true)


’SUMMARIEZE ZONES

theView = av.GetActiveDoc


’ obtain zone Theme and set object and VTab
zoneTheme = theView.GetActiveThemes.Get(0)
if (zoneTheme.Is(FTHEME)) then
  zoneObj = zoneTheme.GetFTab
  theVTab = zoneObj
elseif (zoneTheme.Is(GTHEME)) then
  zoneObj = zoneTheme.GetGrid
  theVTab = zoneObj.GetVTab
else
  return NIL
end

’get zone Field from zoneObj
if (zoneObj.Is(FTab)) then
  fl = {}
  for each f in theVTab.GetFields
    if (f.IsVisible and
        (f.IsTypeShape.Not and
        ((f.GetType <> #FIELD_DECIMAL) and
         (f.GetType <> #FIELD_DOUBLE) and
         (f.GetType <> #FIELD_FLOAT) and
         (f.GetType <> #FIELD_MONEY) and
         (f.GetType <> #FIELD_ISODATETIME) and
```

```
          (f.GetType <> #FIELD_ISOTIME)) or
          ((f.GetType = #FIELD_DECIMAL) and (f.GetPrecision = 0)))) then
        fl.Add(f)
      end
    end
    zoneField = MsgBox.List(fl, "Pick field that defines zones:",
"Summarize Zones")
    if (zoneField = NIL) then return NIL end
else
    zoneField = theVTab.FindField("Value")
end

' make list of value themes from available themes
valueList = List.Make
for each t in theView.GetThemes
    if (t.Is(GTHEME)) then
      valueList.Add(t)
    end
end

' remove zone theme from list
valueList.RemoveObj(zoneTheme)

' get value theme
valueTheme = MsgBox.List(valueList, "Pick theme containing variable to
summarize:", "Summarize Zones")
if (valueTheme = NIL) then return NIL end

' make sure themes overlay
zoneExtent = zoneTheme.ReturnExtent
valueExtent = valueTheme.ReturnExtent
if (zoneExtent.Intersects(valueExtent).Not) then
    MsgBox.Error("Input themes do not overlay","Summarize Zones")
    return NIL
end

' obtain Grid for value theme and create VTab
theMaskGTheme = theView.GetExtension(AnalysisEnvironment).GetMask
if (theMaskGTheme = NIL) then
    g = valueTheme.GetGrid
else
    g = valueTheme.GetGrid.ExtractByMask(theMaskGTheme.GetGrid)
end
aPrj = theView.GetProjection
aFN = av.GetProject.GetWorkDir.MakeTmp("zstat","dbf")
zt = g.ZonalStatsTable(zoneObj, aPrj, zoneField, FALSE, aFN)
if (zt.HasError) then return NIL end
zoneTable = Table.Make(zt)
zoneTable.SetName("Stats of " + valueTheme.GetName + " Within Zones of
" + zoneTheme.GetName)
zoneTable.GetWin.Activate

' check value to make sure it is ok to chart
if (zt.GetNumRecords > 25) then
    MsgBox.Warning("Number of unique zones is more than 25.  A chart will
not be created", "Summarize Zones")
    return NIL
```

```
end

’ obtain variable to chart
choiceList = zt.GetFields
statList = {}
statStringList = {}
pickList = choiceList.Clone
for each stat in pickList
  if (stat.GetAlias.Count > 0) then
    statStringList.Add(stat.GetAlias)
  else
    statStringList.Add(stat.GetName)
  end
end
for each statString in statStringList
  if ((statString <> "Count") and (statString <> zoneField.GetName) and
(statString <> "Zone-code")) then
    tokenList = statString.AsTokens("-")
    statString2 = tokenList.Get(tokenList.Count - 1)
    tokenList2 = statString2.AsTokens("_")
    statList.Add((tokenList2.Get(tokenList2.Count - 1)).Proper)
  end
end
pickStat = MsgBox.ListAsString(statList, "Select statistic to chart:",
"Summarize Zones")
if (pickStat = NIL) then return NIL end
for each statString in statStringList
  if (statString.Contains(pickStat.LCase)) then
    fieldName = statString
    break
  end
end
pickStatField = zt.FindField(fieldName)

’ create chart with colors matching zoneObj legend
fieldList = {pickStatField}
theChart = Chart.Make(zt, fieldList)
theChart.SetRecordLabelField(zt.FindField(zoneField.GetName))
theChart.SetName(pickStat.Proper ++ "of" ++ valueTheme.GetName ++
"Within Zones of" ++ zoneTheme.GetName)
theLegend = zoneTheme.GetLegend
if (theLegend.GetLegendType <> #LEGEND_TYPE_CHART) then
  theSymbols = theLegend.GetSymbols
  if (theLegend.GetLegendType = #LEGEND_TYPE_SIMPLE) then
    theChartDisplay = theChart.GetChartDisplay
    for each rec in zt
      theChartDisplay.SetSeriesColor(rec, theSymbols.Get(0).GetColor)
    end
  else
    labelDictionary = Dictionary.Make(zt.GetNumRecords)
    symbolDictionary = Dictionary.Make(theSymbols.Count)
    legendFieldList = theLegend.ReturnFieldNames
    theCount = 0
    for each rec in theVTab
      indexList = {}
      for each fieldString in legendFieldList
```

```
indexList.Add(theVTab.ReturnValue(theVTab.FindField(fieldString), rec))
      end
      theIndex = theLegend.GetIndex(indexList)
      classInfoList = theLegend.ReturnClassInfo(theIndex)
      labelString = classInfoList.Get(0)
      labelDictionary.Add(theVTab.ReturnValue(zoneField,
rec),labelString)
      if (symbolDictionary.Get(labelString) = NIL) then
        symbolDictionary.Add(labelString,classInfoList.Get(2).GetColor)
      end
      theCount = theCount + 1
    end
    zt.SetEditable(TRUE)
    aField = Field.Make("Label", #FIELD_CHAR, 40, 0)
    tempFieldList = {aField}
    zt.AddFields(tempFieldList)
    addField = zt.FindField(zoneField.GetName)
    for each rec in zt
      zt.SetValue(aField, rec,
labelDictionary.Get(zt.ReturnValue(addField, rec)))
    end
    if (theLegend.GetLegendType <> #LEGEND_TYPE_DOT) then
      theChart.SetRecordLabelField(aField)
    end
    theChartDisplay = theChart.GetChartDisplay
    for each rec2 in zt
      theChartDisplay.SetSeriesColor(rec2,
symbolDictionary.Get(zt.ReturnValueString(aField, rec2)))
    end
    zt.SetEditable(FALSE)
  end
end
theTitle = theChart.GetTitle
theYAxis = theChart.GetYAxis
theTitle.SetName("Values of " + valueTheme.GetName + " Summarized
Within the Zones of " + zoneTheme.GetName)
theYAxis.SetName(pickStat ++ "of" ++ valueTheme.GetName)
theYAxis.SetLabelVisible(TRUE)
theXAxis = theChart.GetXAxis
theXAxis.SetName("Zones")
theXAxis.SetLabelVisible(TRUE)
theXAxis.SetAxisVisible(FALSE)
theXAxis.SetTickLabelsVisible(FALSE)
theChart.GetWin.Activate
```

Appendix B: Graphical Comparison of the Different Models

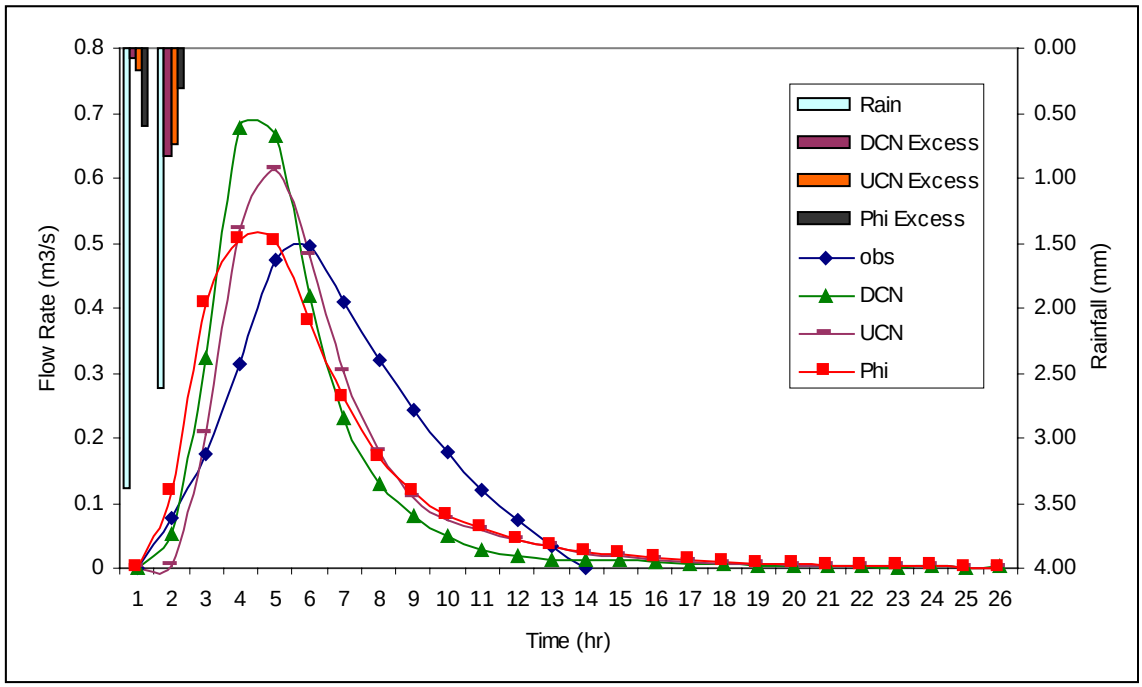

Figure B.1. Storm #1 (April 1, 1990)

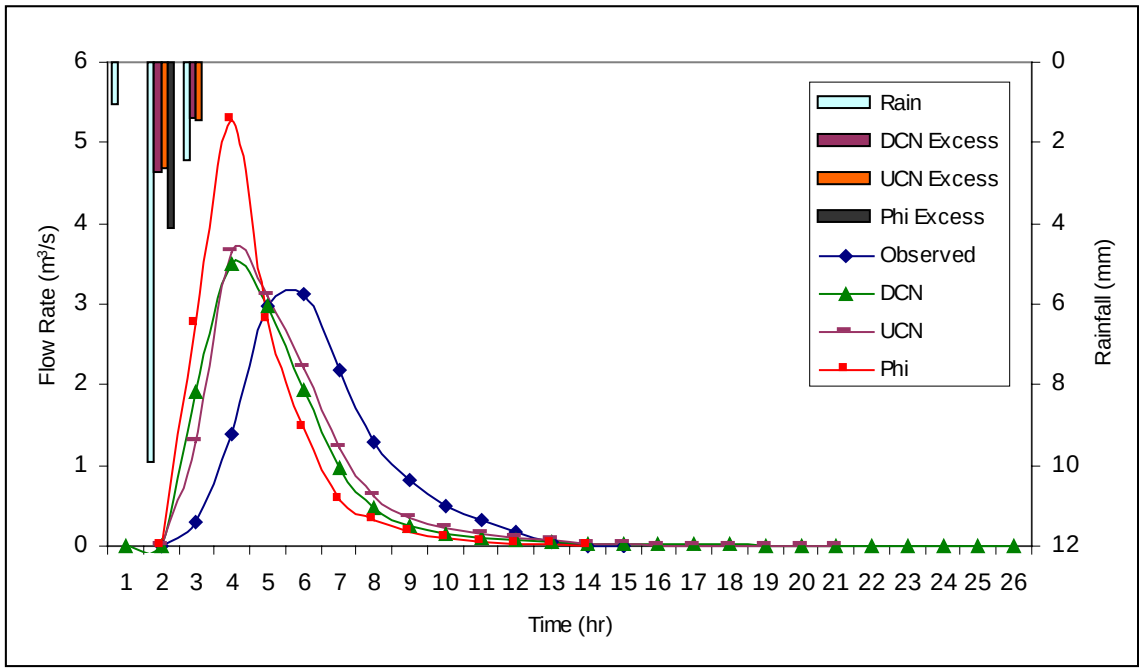

Figure B.2. Storm #2 (April 2, 1990)

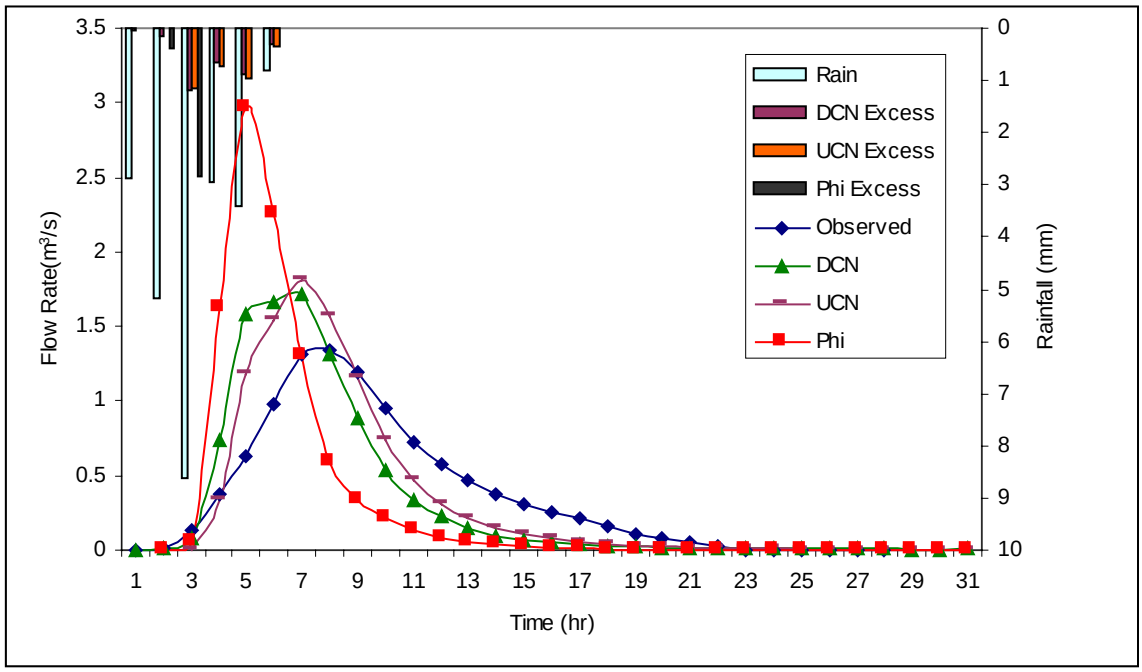

Figure B.3. Storm #3 (April 14-15, 1990)

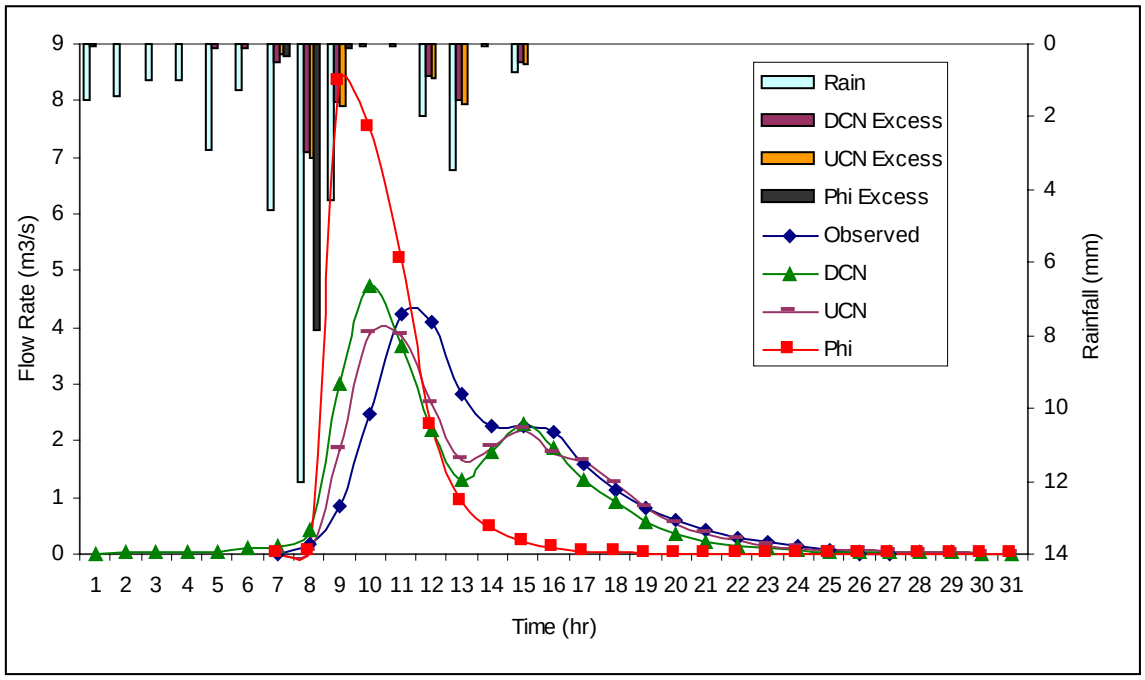

Figure B.4. Storm #4 (May 10, 1990)

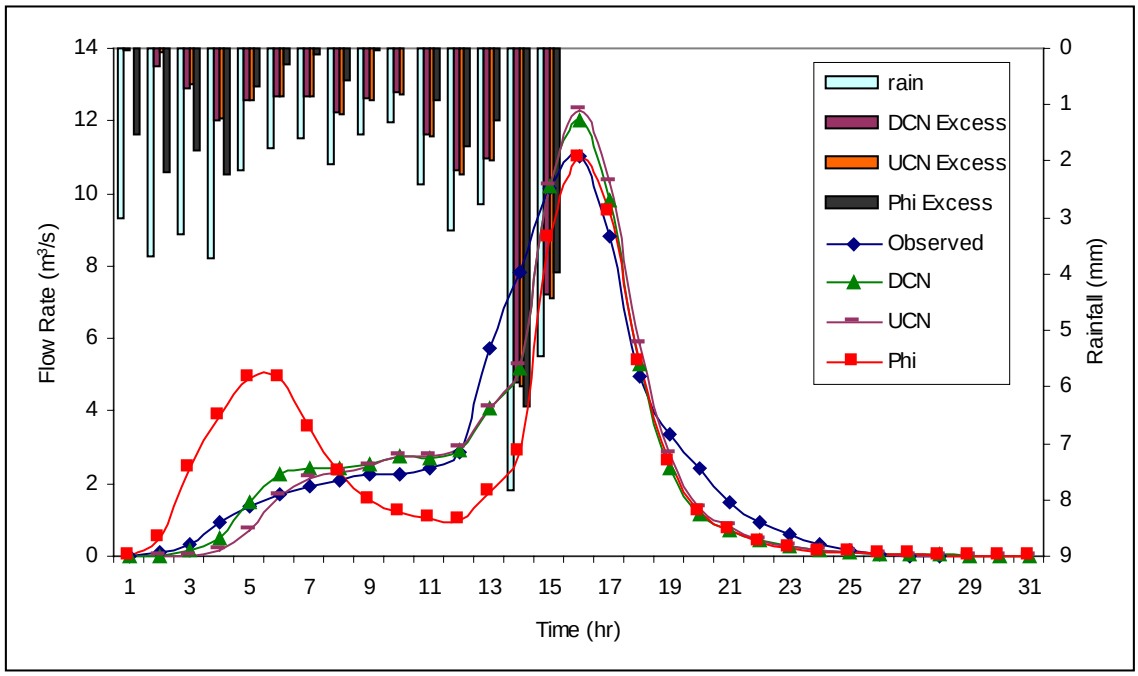

Figure B.5. Storm #5 (May 28-29, 1990)

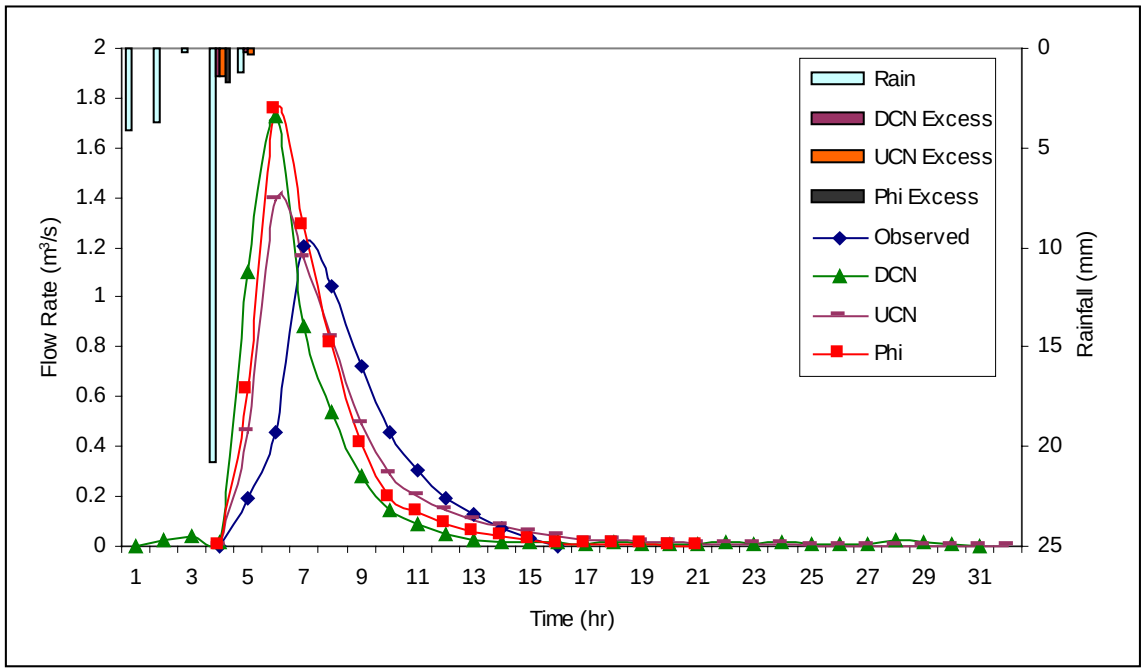

Figure B.6. Storm #6 (July 13-14, 1990)

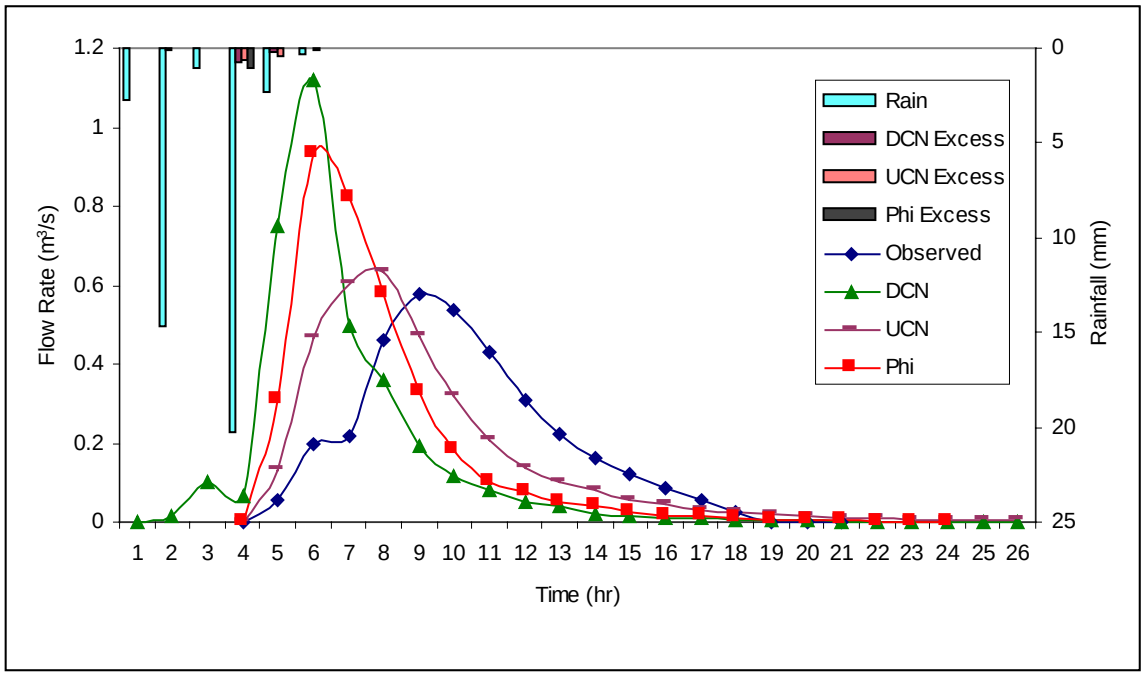

Figure B.7. Storm #7 (October 18, 1990)

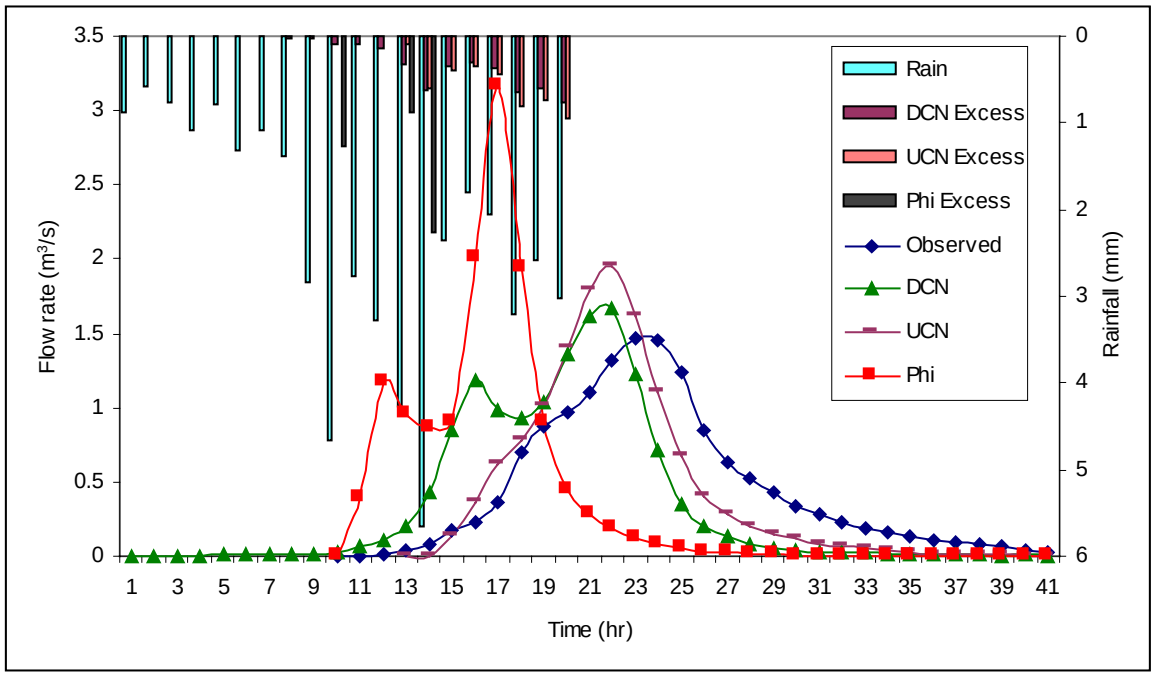

Figure B.8. Storm #8 (October 22-23, 1990)

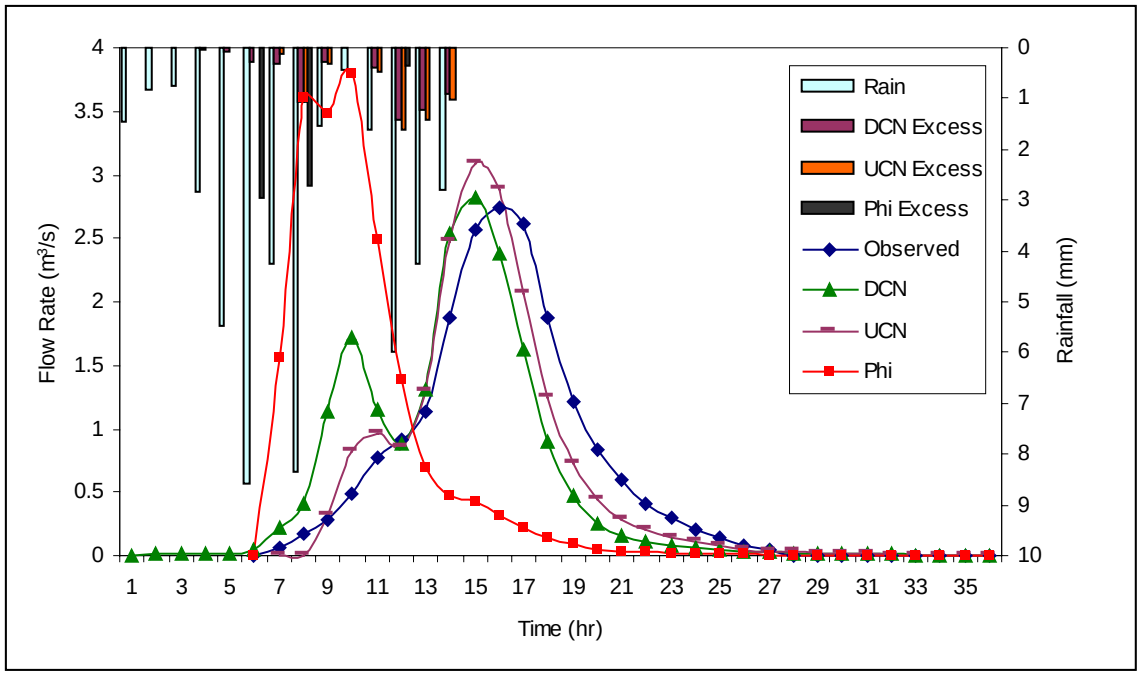

Figure B.9. Storm #9 (November 9-10, 1990)

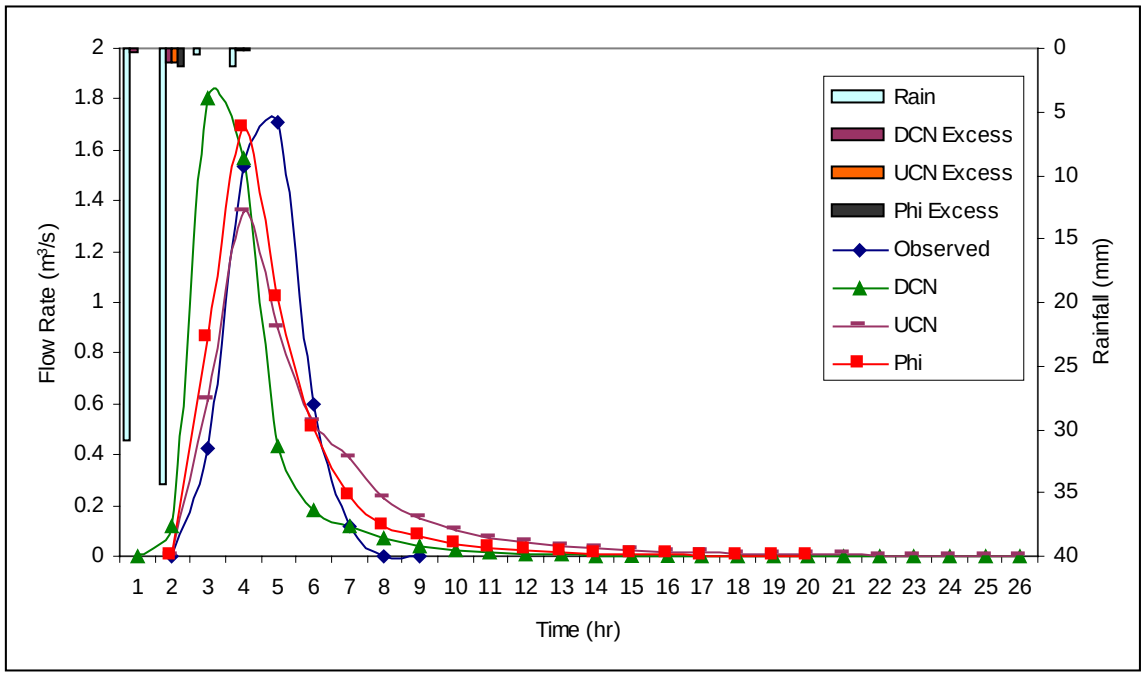

Figure B.10. Storm #10 (June 18, 1991)

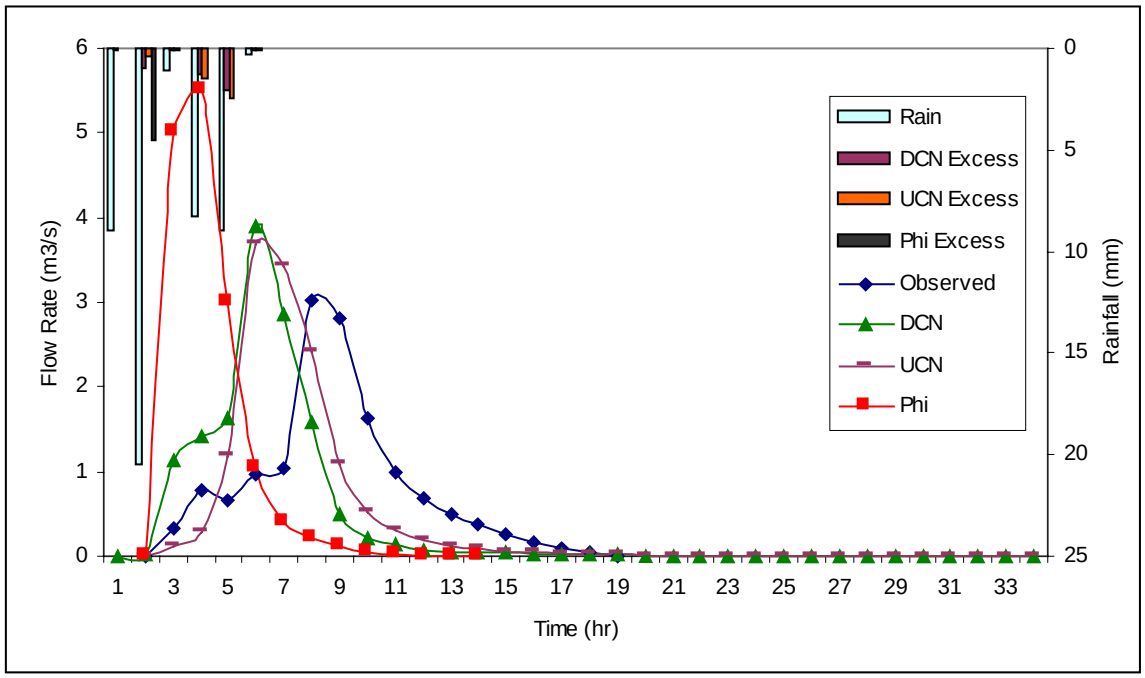

Figure B.11. Storm #11 (July 25-26, 1991)

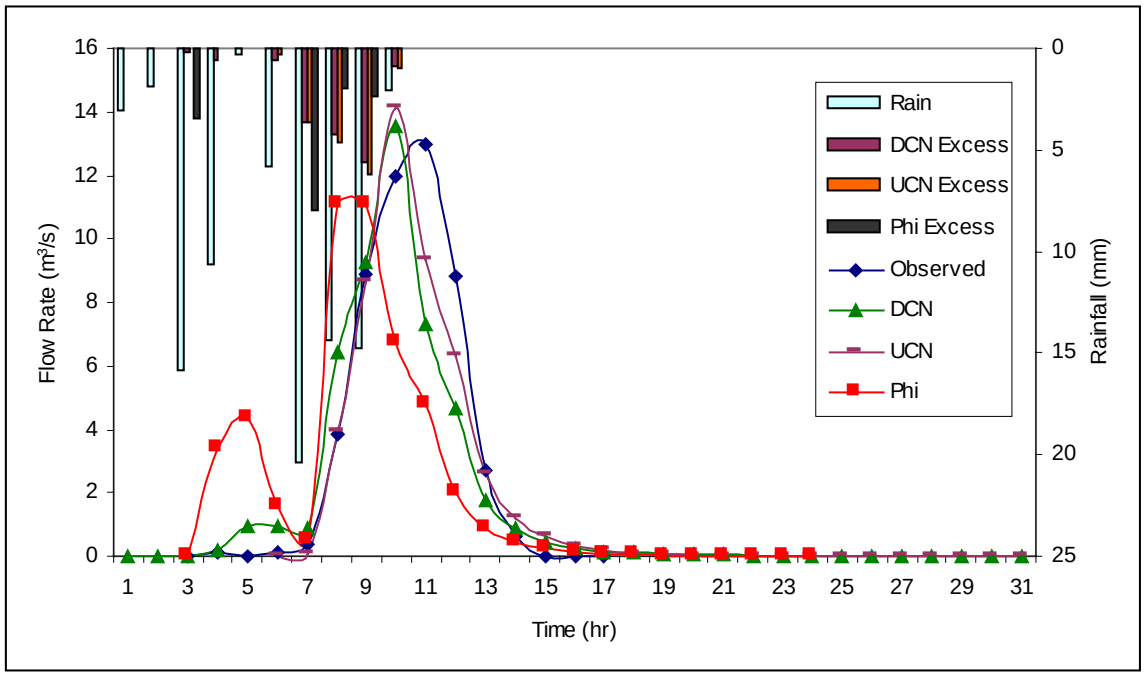

Figure B.12. Storm #12 (August 9-10, 1991)

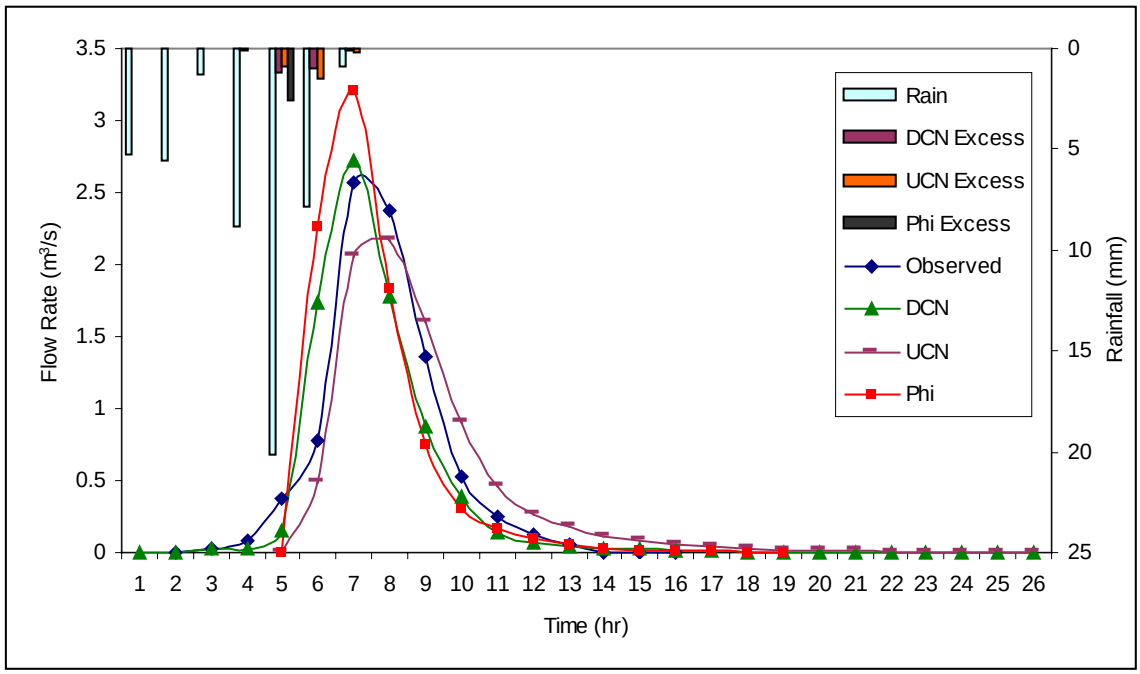

Figure B.13. Storm #13 (September 4-5, 1991)

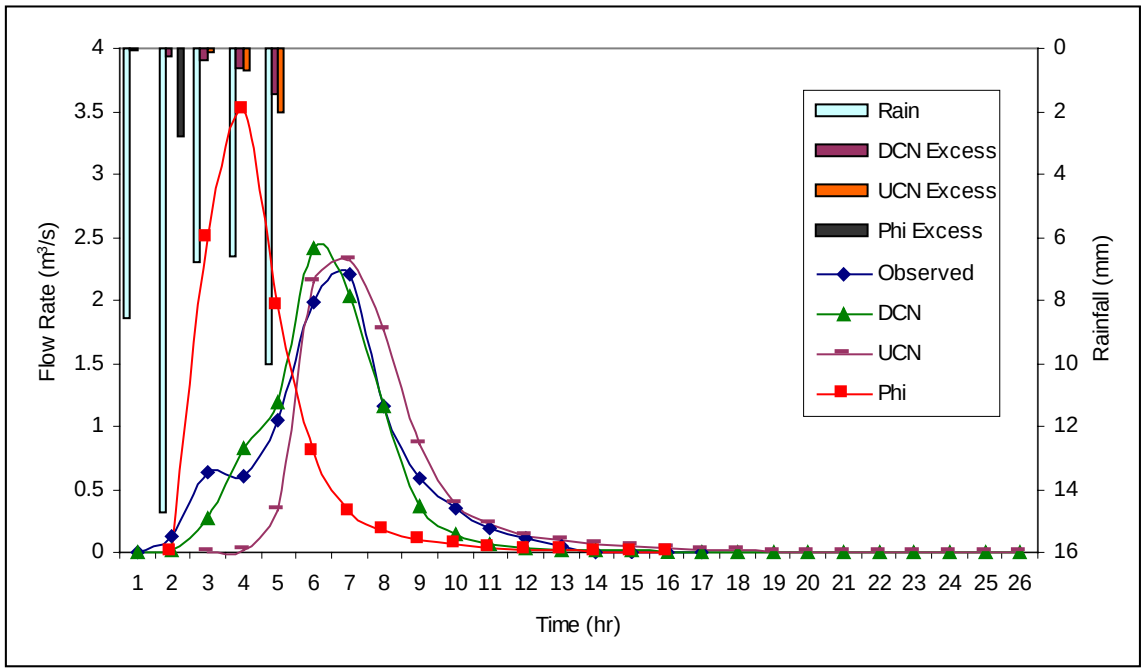

Figure B.14. Storm #14 (September 17-18, 1991)

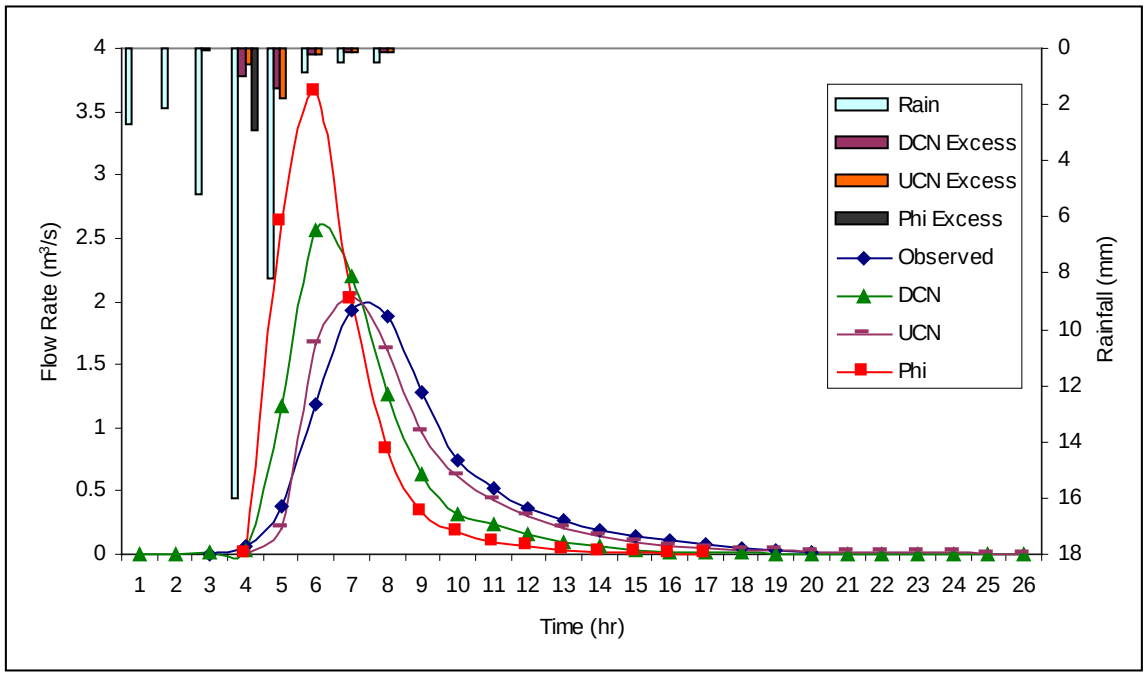

Figure B.15. Storm #15 (September 24, 1991)

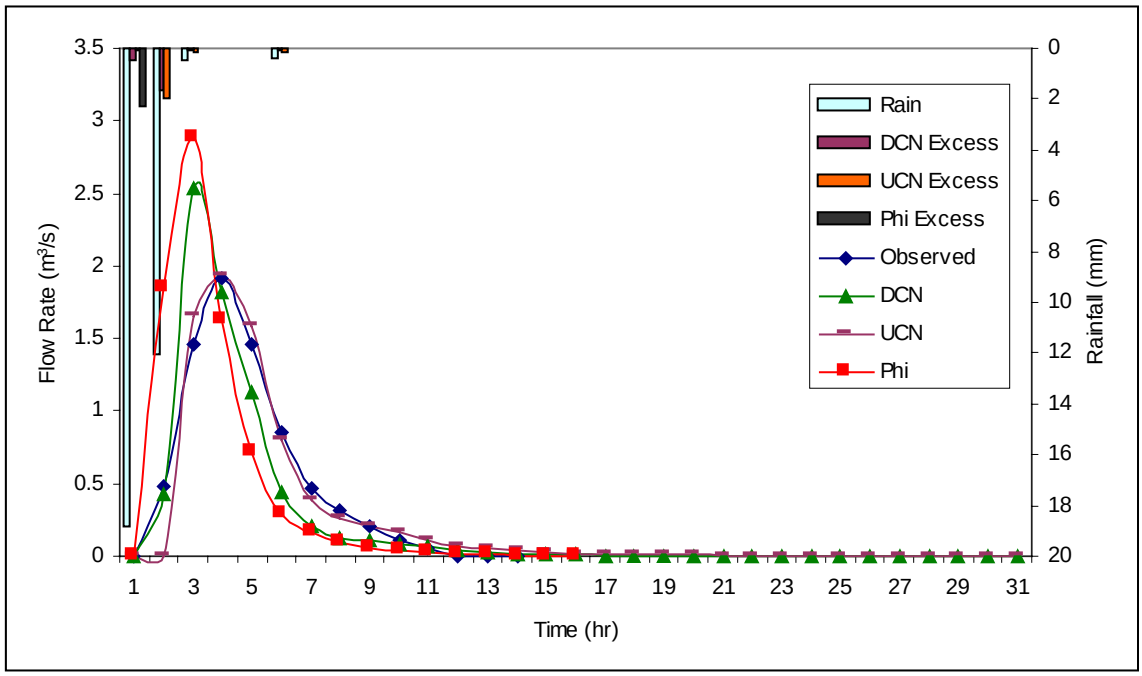

Figure B.16. Storm #16 (October 5-6, 1991)

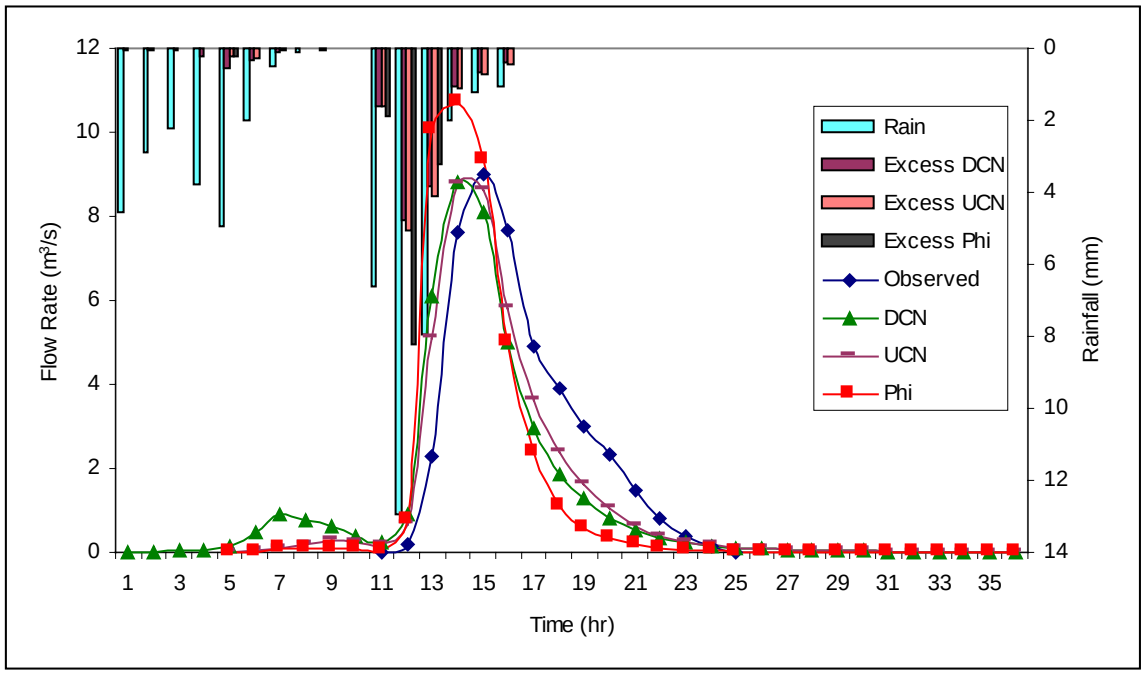

Figure B.17. Storm #17 (April 21, 1992)

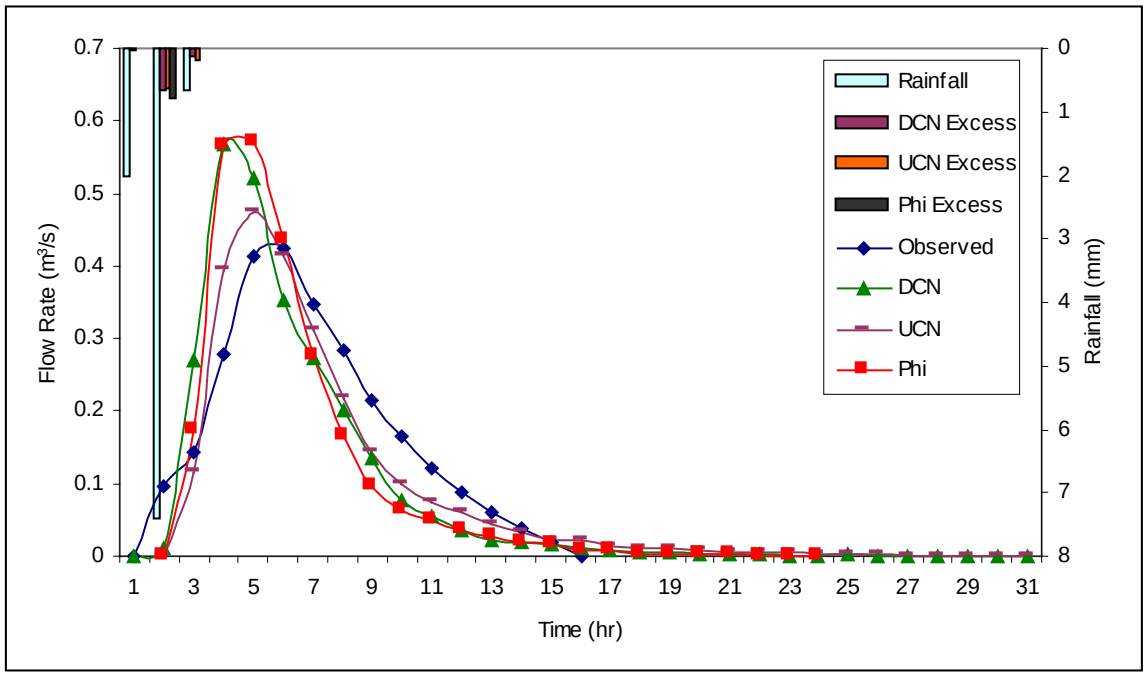

Figure B.18. Storm #18 (May 8, 1992)

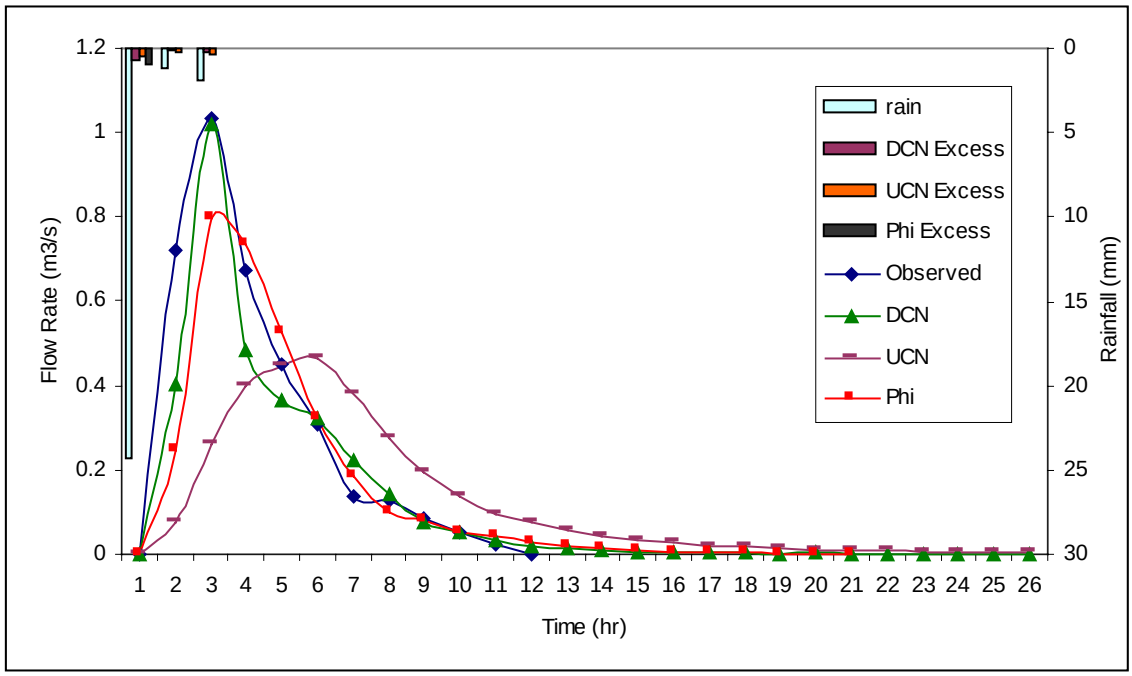

Figure B.19. Storm #19 (June 30, 1992)

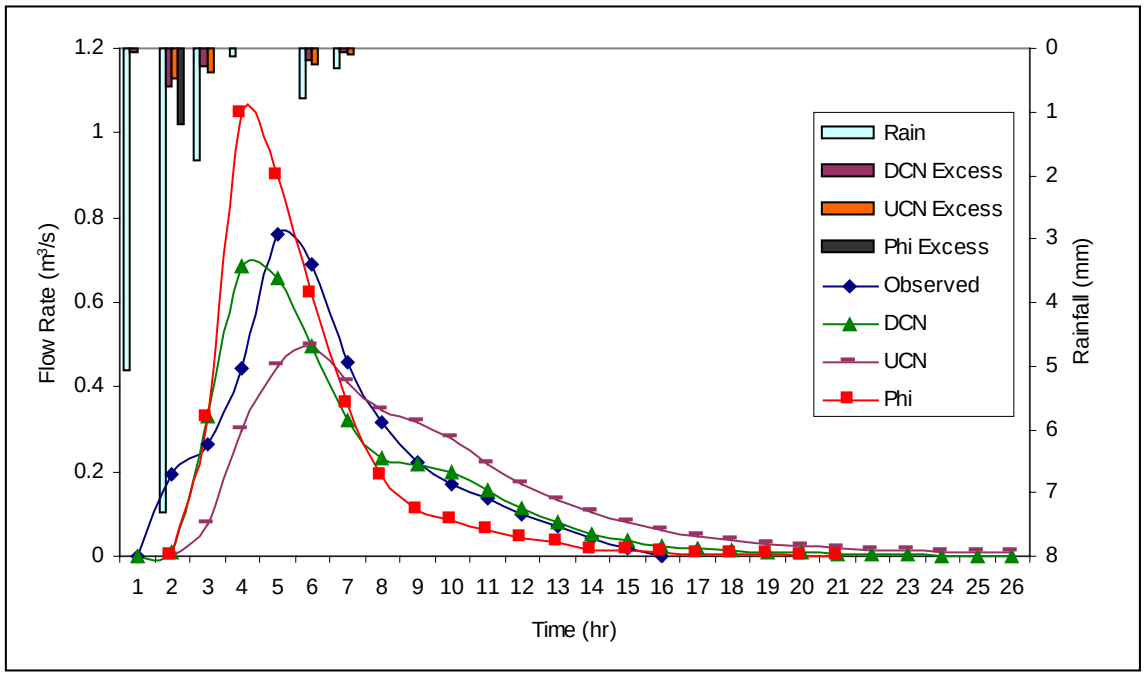

Figure B.20. Storm #20 (July 3-4, 1992)

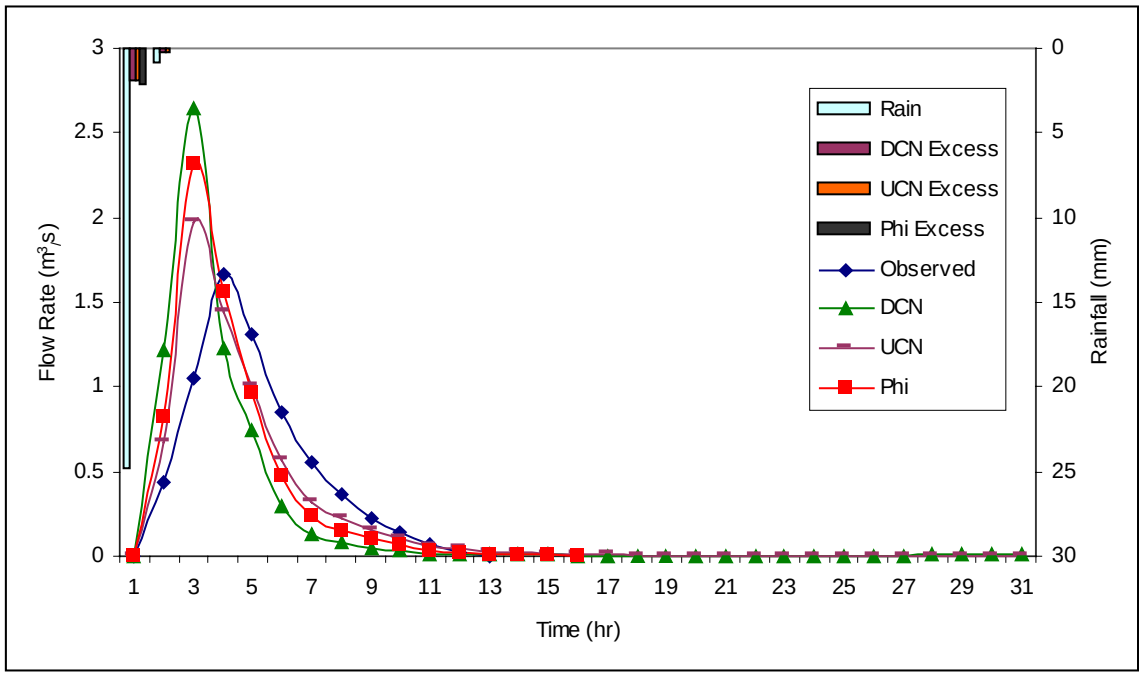

Figure B.21. Storm #21 (July 24, 1992)

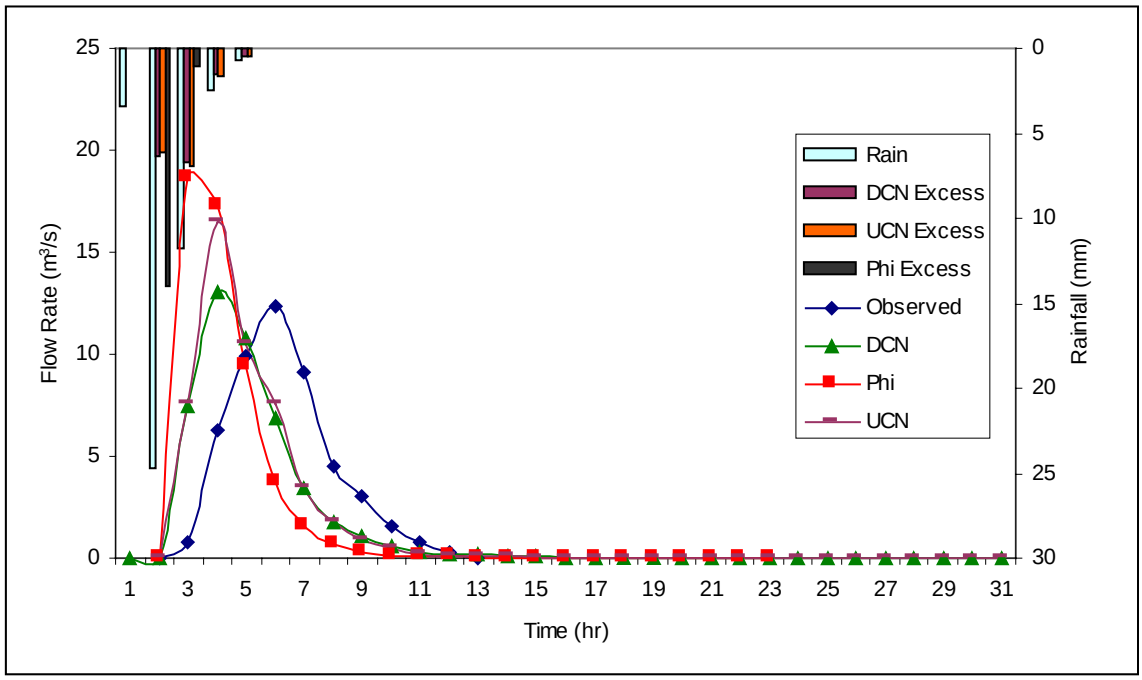

Figure B.22. Storm #22 (July 27, 1992)

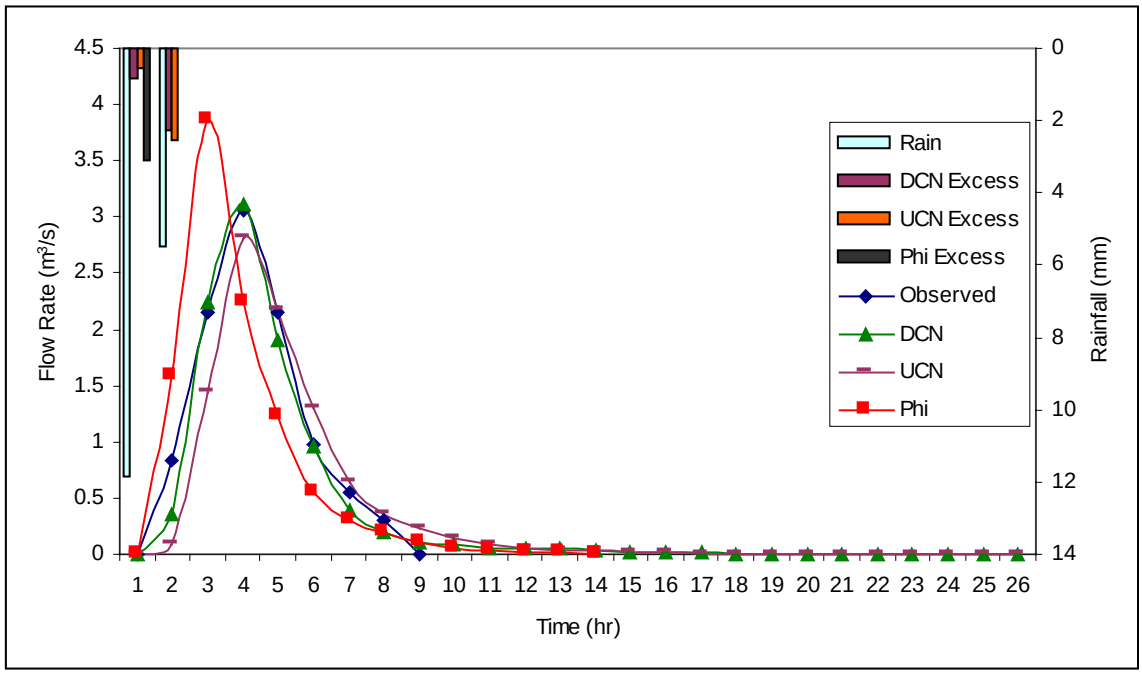

Figure B.23. Storm #23 (July 31, 1992)

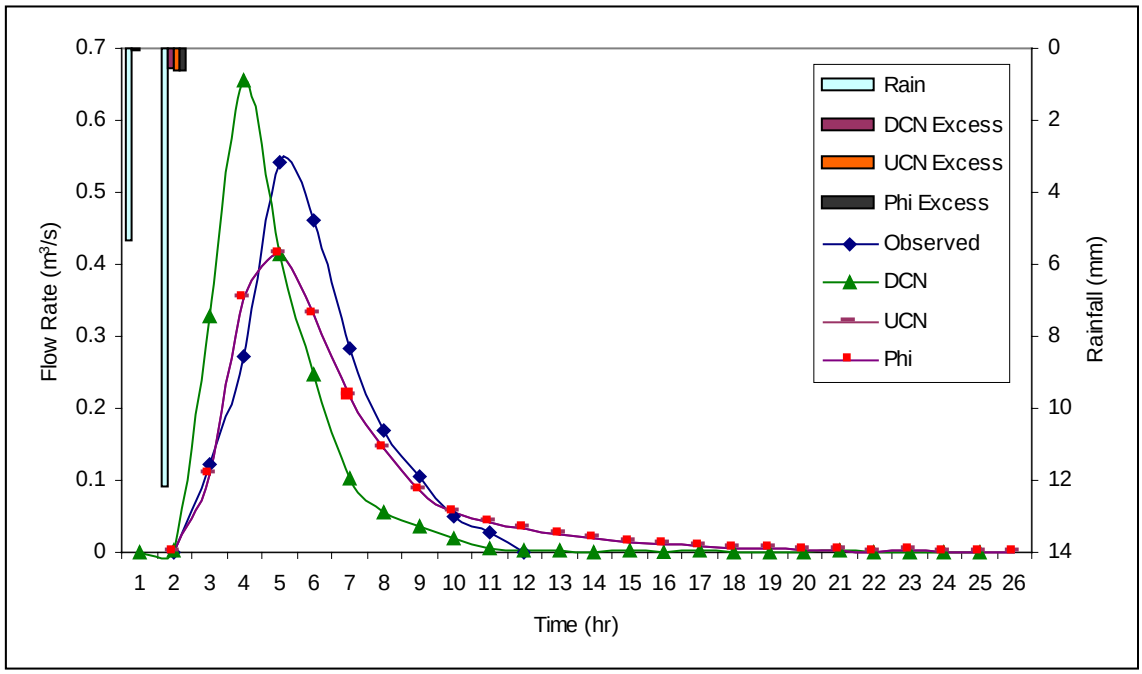

Figure B.24. Storm #24 (August 4, 1992)

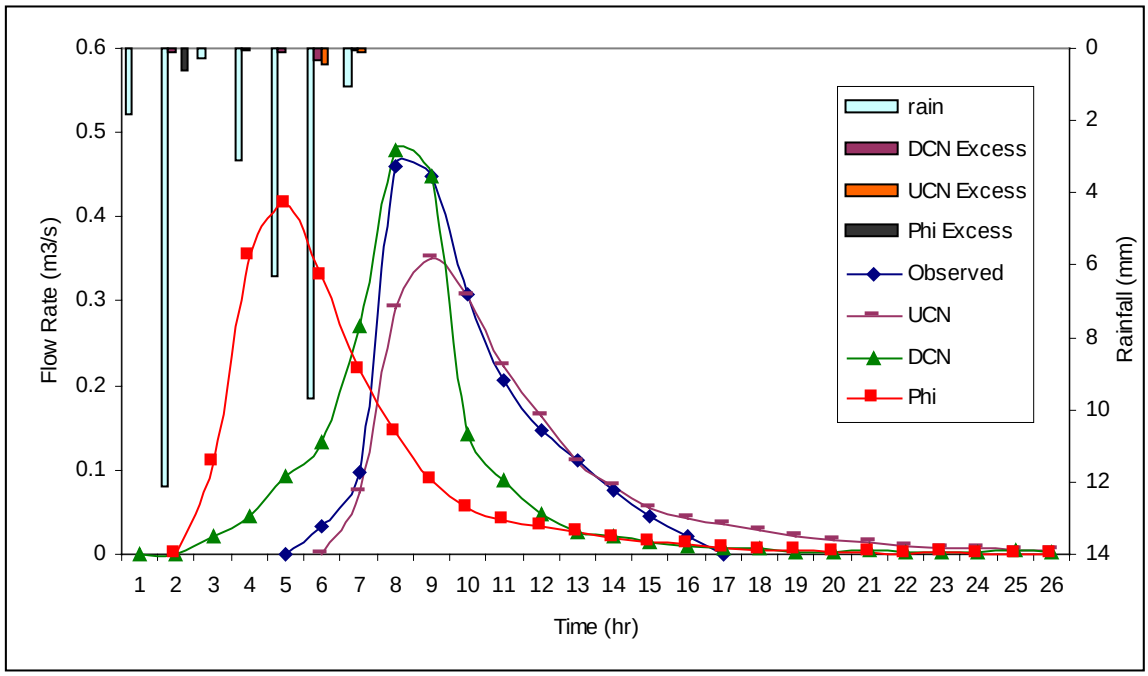

Figure B.25. Storm #25 (September 2, 1992)

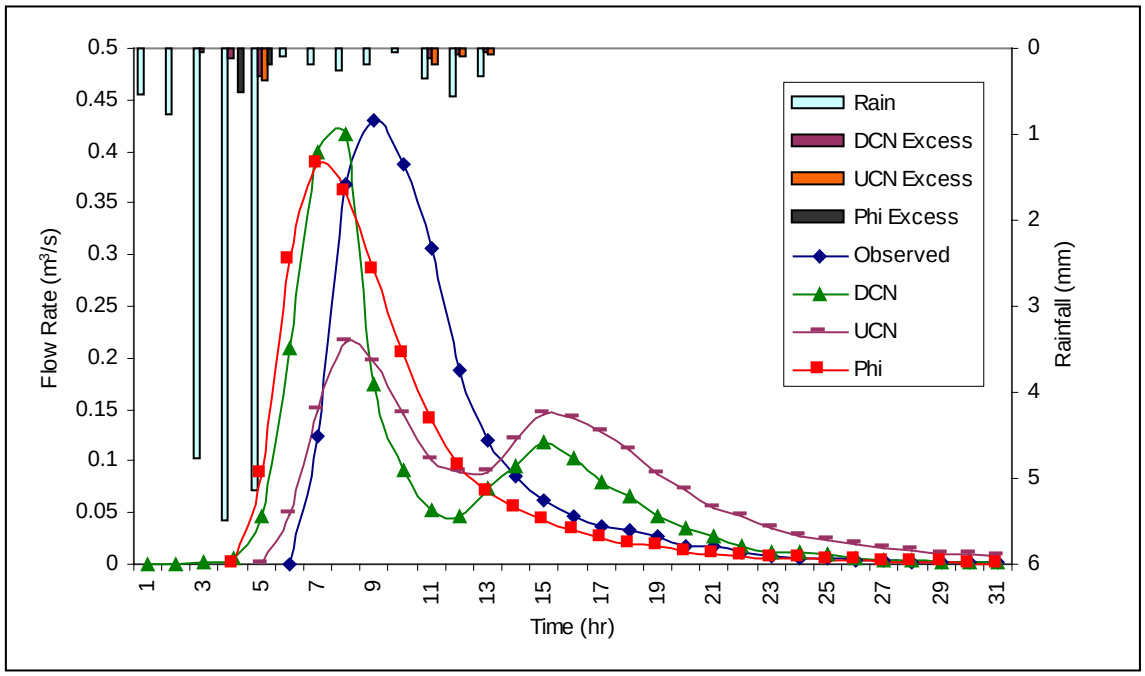

Figure B.26. Storm #26 (September 5-6, 1992)

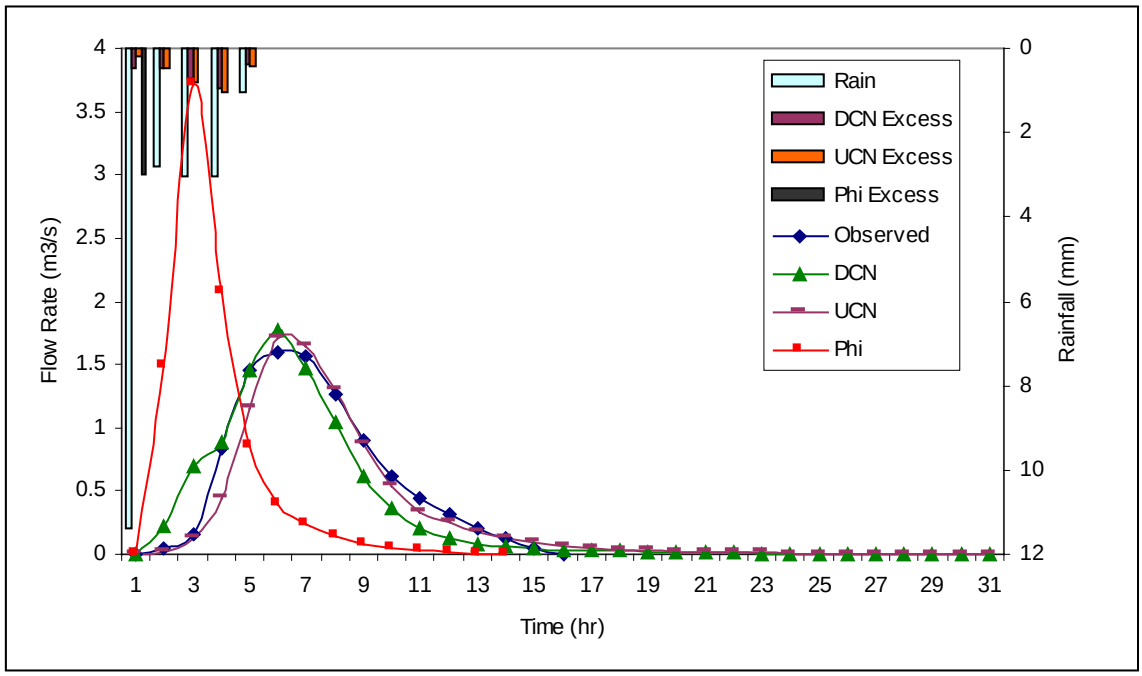

Figure B.27. Storm #27 (September 10-11, 1992)

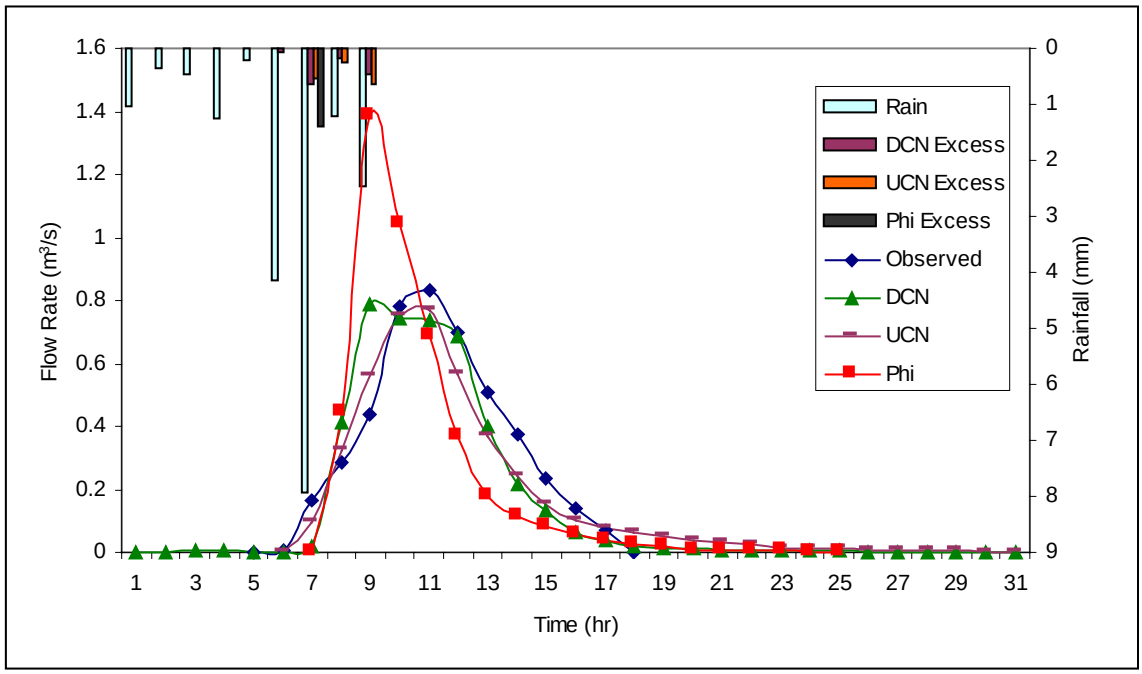

Figure B.28. Storm #28 (November 2-3, 1992)

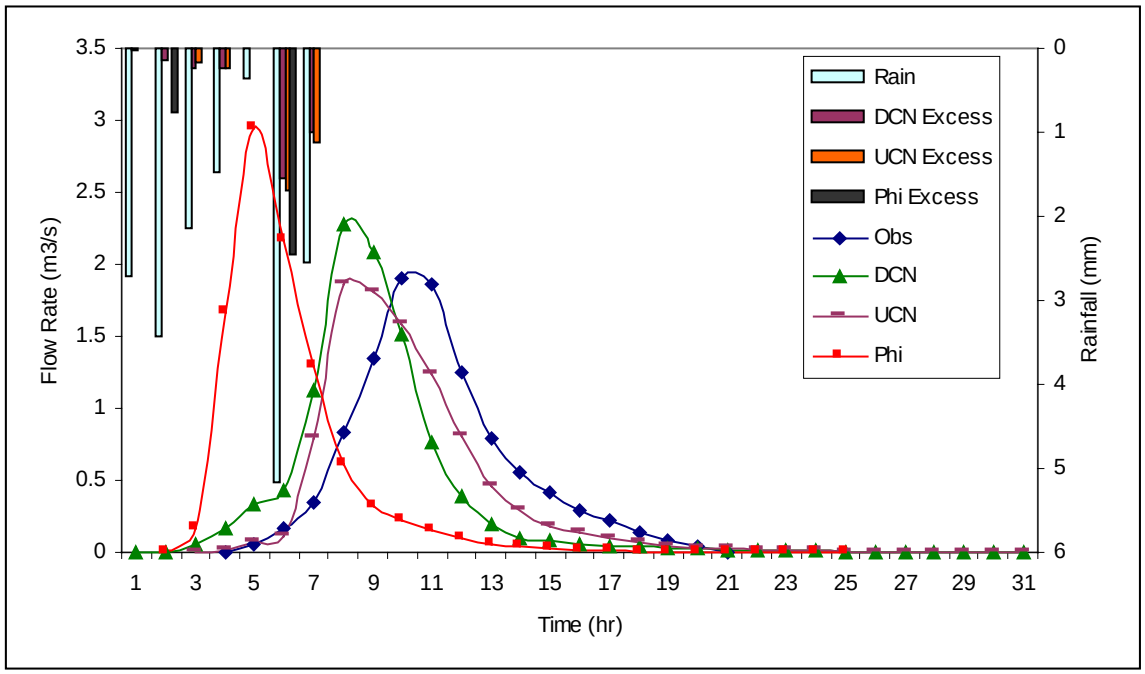

Figure B.29. Storm #29 (November 12, 1992)

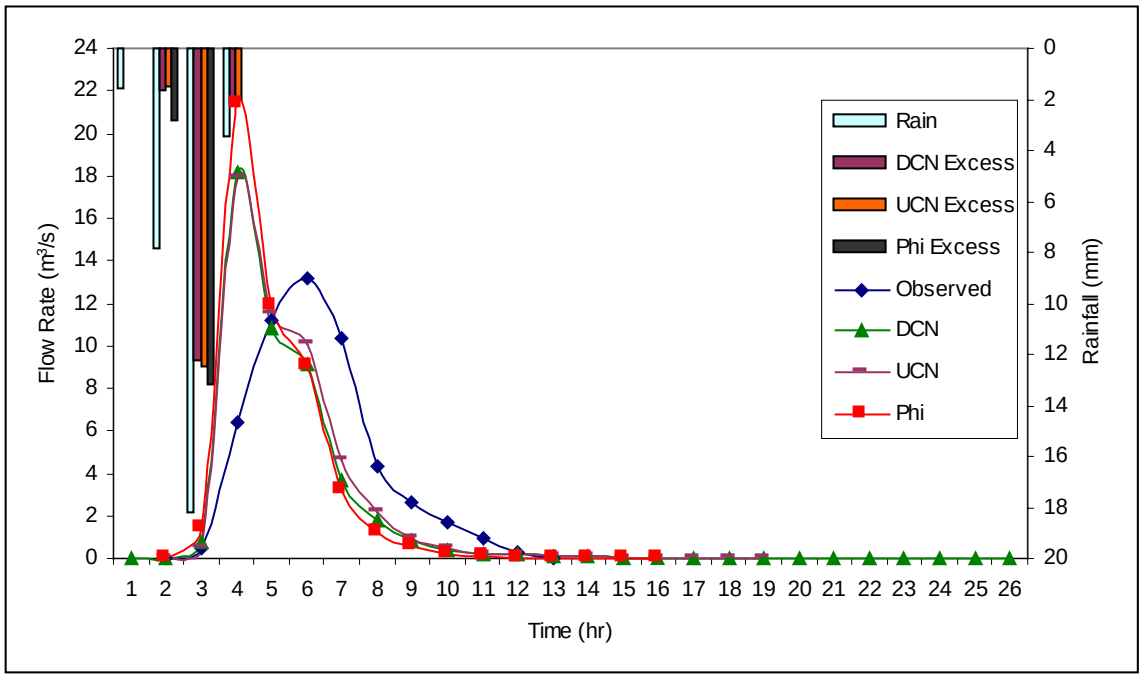

Figure B.30. Storm #30 (November 22-23, 1992)

Vita

Mohammad Al-Smadi was born on March 25, 1973 to Ahmed and Shakah Alsmadi in Ajloun, Jordan. He graduated from Ajloun High School in Ajloun, Jordan in 6/1991. Mr. Al-Smadi started his Agricultural Engineering studies at Jordan University of Science and Technology in Irbid, Jordan in 1991 and obtained his Bachelor degree in 1996. He began his graduate study at Virginia Tech in Fall/1996 working toward his Masters of Science degree in Biological Systems Engineering.